Synthesis and Characterization of Crystalline Coordination Networks Constructed From Neutral Imidazole Containing Ligand and Rigid Aromatic Carboxylate

Hirofumi Motegi

Dissertation submitted to the faculty of the
Virginia Polytechnic Institute and State University

In partial fulfillment of the requirements for the degree of

Doctor of Philosophy

In

Chemistry

Dr. Brian E. Hanson, Chair
Dr. Joseph S. Merola, Co-Chair
Dr. Karen J. Brewer
Dr. Herve Marand
Dr. David F. Cox

Date September 1st, 2010
Blacksburg, Virginia

Keywords: metal-organic frameworks, imidazole, aromatic spacer, mixed ligand,

Synthesis and Characterization of Crystalline Coordination Networks Constructed From Neutral Imidazole Containing Ligand and Rigid Aromatic Carboxylate

Hirofumi Motegi

Abstract

The work is focused on the investigation of synthesis and structure of crystalline coordination networks by combining first a row transition metal ion with one anionic and one neutral bridging ligand. In the field of crystalline coordination networks, the goal is to synthesize porous 3D crystalline coordination networks with molecular sized cavities. The materials are characterized by XRD and TGA. It is important to understand the structural topologies to develop practical applications, such as gas storage, gas separation, and catalysis.

The bi- and tetra- dentate flexible imidazole ligands, 9,10-bis(imidazol-1-ylmethyl)anthracene (Chapter 2) and 1, 2, 4, 5-tetrakis(imidazol-1ylmethyl)benzene (Chapter 3), are synthesized and used as linkers to construct 1D, 2D, and 3D crystalline coordination networks with cobalt(II) or zinc(II) cations and H_3BTC anions under solvothermal conditions.

Two 1D chain networks, $[M(HBTC^{2-})(C_{22}H_{18}N_4)(H_2O)_2]\cdot H_2O$, are constructed from M(Zn(II) or Co(II)), H_3BTC, and 9,10-bis(imidazol-1-ylmethyl)anthracene (Compound **2.1** and **2.2**). These two 1D zigzag chains are linked into infinite 2D sheets by inter-chain π···π stacking and hydrogen bonding.

Two 2D and one 3D cobalt(II) coordination networks are constructed from the tetradentate imidazole ligand and H_3BTC. Compound **3.1** has a 2D corrugated sheet structure

that is linked by inter-layer π···π stacking and hydrogen bonding. Compound **3.2** has a 2D sheet structure. These sheets are interconnected by hydrogen bonds at the free acid group of the $HBTC^{2-}$ ligand. Compound **3.3** forms a two fold interpenetrated 3D network structure. Void spaces in the structure are filled with six water molecules.

Six 3D cobalt (II) coordination networks are constructed with bidentate rigid imidazole containing neutral ligands, 1,4-bis(imidazol-1-yl)benzene(**L1**), 1,4-bis(imidazol-1-yl)naphthalene(**L2**), and 9,10-bis(imidazol-1-yl)anthracene(**L3**), and H_2BDC or H_3BTC anion (Chapter 4). In **4.1**-**4.3**, **L1**-**L3** affects on degree of interpenetrations constructed with H_2BDC ligand. In **4.1** and **4.2** are interpenetrating 3D networks with no accessible void space. In **4.3**, void spaces of 3D networks are filled with 2D sheets. Compounds **4.4**-**4.6** are prepared by different concentrations of starting materials and different solvents. In **4.4**-**4.6**, **L3** serves as a pillar building block to construct 3D networks by applying with H_3BTC ligand. The solvent exchange experiment for **4.4** is further discussed.

Acknowledgements

I would like to thank to Dr. Brian E. Hanson for his supervision over the course of my Ph.D. studies. He has been a great help and guidance to discuss about research and laboratory technique. I am very grateful to work in his lab and I have learned so many things in the past five years.

I also thank to my committee members, Drs. Karen J. Brewer, Joseph S. Merola, Herve Marand, and David F. Cox, for their great scientific knowledge and guidance throughout the completion of my study and development of my research.

For Virginia Tech Crystallography groups, Drs. Ross J. Angel, Carla Slebodnick, Elinor C. Spencer, I would like to say thank to all of the members and helping me solving the difficult structures and giving me great advise in science.

My lab members and friends in chemistry department: I had a great time sharing knowledge and everyday research. They are my friends and I am very thankful to them for helping me to complete this degree. I have so many friends to thank for but especially, Liang-ming Hu, Robbie Hull, Brian Hickory, Hunter Champion, Joan Zapitor, Paula Weiss, and Jessica Lu. I had really great discussions about science and life over going out to eat.

I am deeply thankful to my parents and younger sister, Kazuo Motegi, Kimi Motegi, and Chika Motegi as well as grandmother Kiku Kitamura, my uncle, Saburo, and aunt, Michiko Wakabayashi. Being away from Japan, they are always there for me to support everyday from such a long distance. I could not do this work without their strong supports.

I would like to thank to all of my friends from Columbus, Georgia, where I can definitely call as the second home in my life. I would like to say thanks to everyone who has been impacted

me so many times but I would like to say some special friends in here; Sammie Saxon, Gary Hart, Miguel Godoy, Rutvig Vaid, Christopher Williams, and Pam and Robert Knight, Dylan and Alex.

My story started back in 2001 with extremely difficult conditions when I came to the United State. Sleeping in the closet at night because my neighbor and roommates were so loud almost every night, without any friends, car, everything was started over as if I became a baby again in my life when I came to the US. All my hope was to get a degree and then going back to Japan.

This was a long journey of my life time experience with meeting lots of great people I have met in my life. At the same time, I may not be able to meet again, which is how my life is about, we walk and work together once but at some point of life time, we will walk separately in the end. Dance company of Virginia Tech (DCVT) members, especially Onica Patalive and Heather Leeper. Member of FMDS, Branble Trionfo is such a great person to introduce me to the society and Jordan Lobik and other executive members from 2007 I would like to thank them all being great friends! Kid Dangerous crews of Virginia Tech, Mandy Teehan and Julie Karrafa are my great friends and Steve Nanino the president from L.A., I will never forget. At the very last great memories in my Ph.D. life, I met the special group of dancers, Contemporary Dance Ensemble (CDE), I would like to say thank for them and I really had so many memories over the past two semesters. Especially, Jamie Gurubba who was a student director of CDE and if she did not respond my email, I would have never met all of the great friends! The last photo project with Kaitlin Cannavo was definitely my best time. Her friendship and passion in dance through this project gave me so many positive energies. I will miss working with such a talented person in my life. There are so many friends I would like to name here and show my appreciation but I will do it when I get back to JAPAN and whenever they come to visit me.

Table of Contents

List of Figures

List of Schemes

List of Tables

Preface

All of the works in this dissertation is done by the author except the following crystallographic data collection and structural analyses.

Dr. Brian E. Hanson is my major adviser who gave me suggestions and helpful discussions towards my work.

Manuscript 1 (Chapter 2)

Dr. Liangming Hu collected a crystallographic data and solved the crystal of 9,10-bis(imidazole-1-ylmethyl)anthracene (**L**)

Manuscript 3 (Chapter 4)

Dr. Carla Slebodnick collected five crystallographic data sets and solved the structures of the following compounds:

1,4-bis(1-imidazolyl)naphthalene **(L2)**, 9,10-bis(1-imidazolyl)anthracene (**L3**), compound 4.3, compound 4.5, compound 4.6.

Chapter 1

1. Introduction

1.1 Metal-Organic Frameworks or Porous Coordination Polymers

Crystalline coordination networks, also known as Metal Organic Frameworks (MOFs) or Porous Coordination Polymers (PCPs), are a new class of porous materials, which have been a rapidly growing research topic over the past two decades.[1-15] The design of these materials has been extensively studied by applying knowledge of atomic and molecular geometry of both metal ions and ligands which serve as building blocks. These building blocks are used to construct extended networks.[16-20] The variety of potential structures is endless and ability to predict structure is limited. These new porous solids have attracted much attention because of their well defined, highly ordered, and tunable structures. The combination of building blocks can lead to a variety of molecular topologies; one dimensional (1D), two dimensional (2D), or three dimensional (3D) network structures (Figure 1.1). Several MOFs have been examined for various uses with high impact, such as selective gas separation, small gas molecule storage, and catalysis.[6, 21-28]

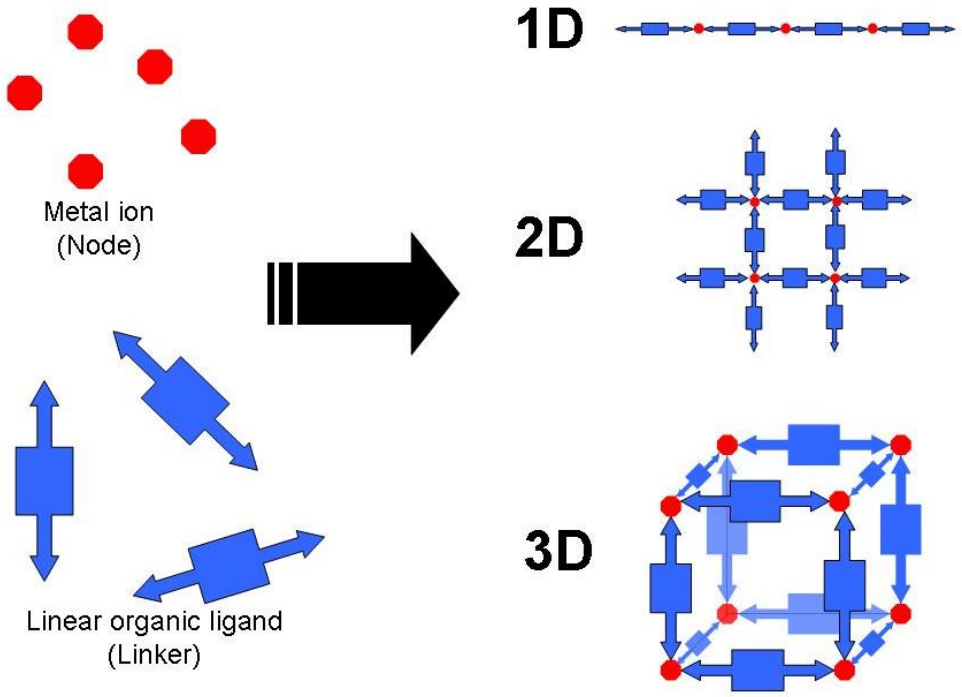

Figure 1.1 A general schematic representation for MOFs; organic ligands with more than two coordination sites to metal ions require to form extended networks.

O.M.Yaghi and co-workers reported the first covalently bonded 3D framework with high surface area and retention of porosity after removal of solvent molecules in the cavity in 1999. The compound, known as MOF-5, has a 15 Å pore diameter with a surface area greater than 3000 m^2g^{-1} after removal of solvent molecules.[29] Yaghi's group introduced and developed the concept of reticular chemistry. i.e. the chemistry of networks, using divalent zinc cations and bifunctional linear carboxylate ligands to form a variety of porous 3D frameworks.[30-32]

Reticular chemistry defines Secondary Building Units (SBUs) built from primary building blocks of metals and ligands. In the case of MOF-5, the SBU, $[Zn_4O(COO^-)_6]$, forms octahedral joints and organic linkers to construct a 3D framework structure. A

variety of bifunctional linear carboxylate groups link the octahedral SBU to construct a series of 3D porous materials of similar connectivity (Figure 1.2). This synthetic method is defined as "reticular synthesis" by Yaghi, within his series of structures the 3D network can be predicted. In Yaghi's definition, the related structures in a series are termed isoreticular metal-organic frameworks (IRMOF-n). Over two hundred 3D frameworks have been constructed and characterized in Yaghi's lab(Figure 1.2).[33] These porous materials have been investigated extensively in the past decade and have had major impact in the field of small molecular storage materials, such as hydrogen storage and carbon dioxide storage.[34]

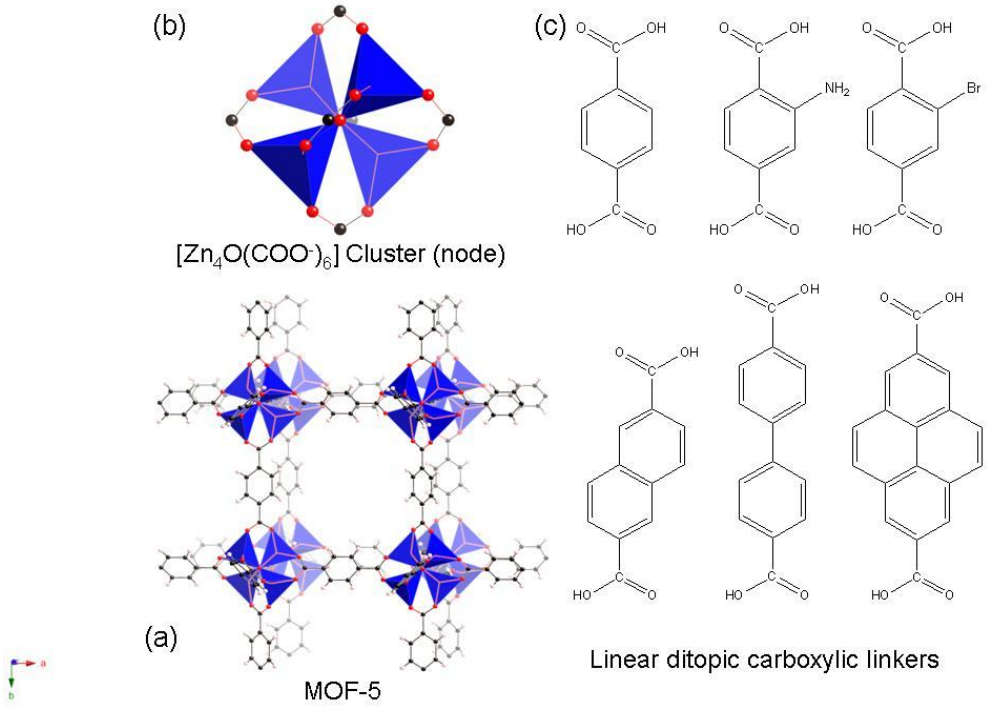

Figure 1.2 (a) The crystallographic structure of MOF-5 and (b) zinc carboxylate clusters are used as nodes. (c) The examples of linear dicarboxylate linkers are used for IRMOF-n series. These figures are modified and generated from reference 29.

Organic ligands which have more than one donor groups are required for construction of these extended networks. The choice of the organic ligands plays an important role in constructing the network architecture. The ligand is used as a spacer and may incorporate a specific functionality. Unlike conventional zeolite materials, MOFs can be tuned to yield functionalized pores by carefully choosing a specific ligand. For example, several MOFs have been studied and used for enantioselective catalysis or post-synthetic modification of organic linkers in order to add functionality for a specific application.[35-44] The research field of post-synthetic modification of MOFs was developed by S.M.Cohen's group, such as pore walls of amine functionality in MOF-3 is reacted via hydrolysis reactions with different reagents.[45, 46]

In many cases, functionalized porous MOFs have been directly synthesized by solvothermal conditions. Optimization of porous MOFs in rational and systematic synthesis remains a challenge because it is difficult to construct desired porous MOFs with functionalities. The synthesis of MOFs is affected by many reaction variables, such as time, temperature, concentration of reactants, pH, and preparation method. This makes prediction of the resulting framework topology complicated when only considering the geometry of the metal ion and organic ligand.

Applications of MOFs often rely on two features, (1) unsaturated metal centers and (2) organic functional group on linkers. Since conventional MOF syntheses typically employ solvothermal conditions over 100 °C and elevated pressure, researchers are often forced to construct novel MOFs by trial and error.

Carboxylate groups coordinate to metal ions in many different coordination modes (Figure 1.3). Because we can not control the formation of coordination bonds at

desired positions, the direct synthesis of MOFs are limited by the directionality of the organic ligands and the number of coordination bonding sites. This makes it impossible to give an exact structural design scheme for construction of a novel MOF that has two different coordination sites. Synthetic conditions for constructing MOFs are often derived from the outcome of preliminary experimental results. They are usually determined by comparing the empirical formula at assumed neutral charge to results of a single crystal X-ray diffraction study.

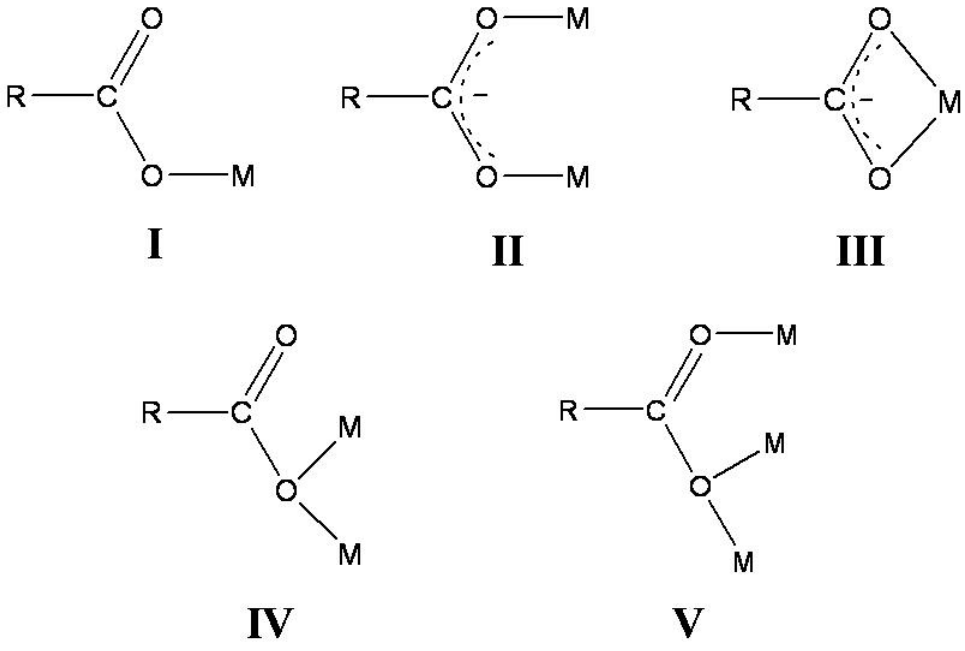

Figure 1.3 Five coordination modes of carboxylic group. (M: metal cation)

1.2 Applications of MOF materials

The properties of ordered pore walls, high surface area, tunable pore walls, and high thermal stability give MOFs a strong advantage over typical zeolite and carbon materials. Once crystalline materials are produced, X-ray diffraction technique can yield

detailed structural information. After obtaining the structural information of the porous materials, synthesis can be improved accordingly for desired applications. In this section two of these applications are described.

1.2.1 Gas Storage

Gas storage in porous materials is an emerging technology for transporting fuels or capturing carbon dioxide emissions in industry. The most remarkable features of MOFs are high surface area with ordered pore walls that are maintained after removal of solvent molecules. Although zeolite and carbon materials are known to be highly porous materials as well, MOFs have the advantage of tunable pore size and shape through the addition of functionality to the pore walls. These properties of MOFs make them good candidates for storing or separating gas molecules. Porous MOF materials have therefore been studied for gas storage for a variety of gases including hydrogen, carbon dioxide, and methane.

Hydrogen storage is a major goal for porous materials due to demand for an alternative energy sources in recent years. Porous MOF solids have attracted many researchers due to their distinct properties. One way to capture hydrogen molecules requires coordinatively unsaturated metal centers in frameworks. For example, manganese metal is exposed on the pore walls of the 3D framework, $Mn_3[(Mn_4Cl)_3(btt)_8(CH_3OH)_{10}]_2$, (btt= 1,3,5-benzenetristetrazolate), as noted by J.R. Long's group. Hydrogen uptake for this material is 6.9 wt% at 77K (90 bar).[47-49]

A major issue with storing hydrogen molecules stems from the structure of the molecule itself. Both electrons within the hydrogen molecule are used for the bonding and only weak interactions, van der Waals forces, can be used to attract hydrogen. The

bonding pair of electrons is available for donation only to very electrophilic metal centers. A smaller pore size could be preferred for storing hydrogen molecules since pore walls are the ones that have weak interactions rather than having a large cavity. Hydrogen storage project continues to be ongoing research area in this field of chemistry.

Recent environmental concerns have created demands to reduce carbon dioxide (CO_2) emissions in industry. The high surface area in porous MOF materials has proven useful for capturing carbon dioxide at ambient conditions. Recently, MOF-200 and 210 have showed the highest surface area of any MOFs to date, 6500 m^2g^{-1}, and high CO_2 sorption capacity.[50]

1.2.2 Catalysis

MOF materials can be constructed to include specific functionality on organic ligands, which are the pore walls of frameworks. Typical MOF materials have high thermal stability, often over 300 °C, and chemical stability, such as insoluble in common organic solvent. With these properties of MOFs, several enantiopure ligands have been used to construct chiral 3D MOFs.[51, 52] One of the examples of enantioselective catalysis with a chiral MOF was reported by K. Kim.[53] Kim's group constructed the first homochiral framework with enantiopure ligand to perform asymmetric catalysis.

In principle, catalytic active site can be designed at coordinatively unsaturated metal center, chiral ligand, or metalloligand for porous MOF materials. Controlling the size and shape of pores as well as immobilization of catalytically active metal center may affect on improving the recyclable heterogeneous catalysis with porous MOF materials in the future.

1.3 Synthetic Methods of Crystalline Coordination Networks

Crystalline MOF materials are produced using several crystallization techniques, such as the slow evaporation, the bilayer solvent method, and hydro- or solvo- thermal synthesis.

Solvothermal synthesis is typically applied in this field of research to produce crystalline coordination networks in a mild temperature range of 65 to 180 °C. Solvents such as water, ethanol, methanol, dimethylformaldehyde (DMF), diethylformaldehyde (DEF), or acetonitrile are generally used to dissolve the framework components. This method is widely used in synthesis of zeolite materials as well because crystallization occurs at high temperature. It is important to find the best reaction conditions for each reaction container, such as heavy walled glass test tubes, screw top glass vials, or Teflon lined acid digestion steel bombs.

1.3.1 Solvothermal synthesis in a glass tube and a steel (Acid Digestion) bomb

Crystalline coordination network solids are commonly synthesized by using a sealed heavy walled glass tube or a Teflon lined acid digestion steel bomb (Parr instruments) in our lab. The maximum volume for these reaction containers are 10 mL for a glass test tube and 23 mL for a steel bomb. Each reaction container has a different maximum temperature and a total amount of sample loading. 130 °C and 200 mg for a glass tube and 180 °C and 1.00 g for a Teflon lined steel bomb are performed.

In the literature, crystal formation is typically observed and reported while lowering the temperature after heating in an oven for two to seven days. In this research, crystals are often formed at elevated temperature with a solvothermal synthesis in a

sealed glass test tube. After cooling, the crystalline products are collected by gravitational filtration and washed with water several times and dried in air.

1.4 Characterization Method

1.4.1 Thermogravimetric Analysis

Thermogravimetric analysis (TGA) technique allows us to measure changes in mass of the samples as a function of temperature or time. It is often used to analyze volatile molecules and decomposition temperature of the solid materials. This information gives us to analyze the thermal stability and to predict the chemical compositions based on thermal degradation of materials in quantitative manner. The TGA measurement is carried out under air or nitrogen atmosphere with linear heating rates, 5 to 10 °C/min. The solid samples are measured from room temperature to 800 °C. A minimum amount of samples are required at least 5 to 10 mg for a reliable quantitative measurement, particularly measuring absorbed volatile molecules. For crystalline porous materials, it is very useful technique to measure the quantity of absorbed water or solvent molecules inside the pores. It also gives us information about thermal stability of coordination networks, which is corruption of network architecture.

1.4.2 Fourier Transform Infrared (FTIR) Spectroscopy

Infrared spectroscopy technique is to measure molecular vibrations by absorbing infrared light. It is used to identify a functional group of a compound. The spectra also give information of the symmetry and shapes of simple molecules. Fourier transform infrared (FTIR) spectroscopy technique is commonly used in these days because of high sensitivity and fast data processing. FTIR spectrometer uses interference effects between

two rays from a broad band source. It detects an interferogram, a signal at the detector that oscillates in time. The mathematical tool of Fourier transformation converts the interferogram into an absorption spectrum as a function of frequency. The spectrum is usually recorded as percentage transmission against wavenumber. In this research, solid state samples are prepared with KBr disks.

1.4.3 Elementral Analysis

Elemental analysis is used to determine a bulk sample for any new synthesized materials. Typically combustion method is employed to identify composition of carbon, hydrogen, and nitrogen in a olid sample. This technique is typically performed by combustion method under excess amount of oxygen. Then, resulting products, such as carbon dioxide, water, and nitric oxide, are collected and calculated. The amount od samples is required about 2.5 mg scale. Proof of purity of the sample is required for new compounds, which are produced, by reporting this information. The deviation of bulk sample for each elemental composition should be within a range of ± 0.4%.

Thesis statement

The goal of my work is to construct 3D networks with void spaces by using a mixed ligand system. Three kinds of neutral bridging ligands are selected and synthesized in order to use as linkers for this study. It is proposed that flexible linkers may pack more efficiently to fill void spaces by adopting different conformation modes. Additionally, rigid linkers with restricted conformations may fill space less efficiently, which will lead to permanent void spaces in the crystal lattice.

1.5 References

1. Eddaoudi, M.; Moler, D. B.; Li, H.; Chen, B.; Reineke, T. M.; O'Keeffe, M.; Yaghi, O. M., *Acc. Chem. Res.* **2001,** *34*, 319-330.
2. Farha, O. K.; Hupp, J. T., *Acc. Chem. Res. 43*, 1166-1175.
3. Fischer, R. A.; Woell, C., *Angew. Chem., Int. Ed.* **2008,** *47*, 8164-8168.
4. James, S. L., *Chem. Soc. Rev.* **2003,** *32*, 276-288.
5. Kitagawa, S.; Matsuda, R., *Coord. Chem. Rev.* **2007,** *251*, 2490-2509.
6. Lee, J. Y.; Farha, O. K.; Roberts, J.; Scheidt, K. A.; Nguyen, S. B. T.; Hupp, J. T., *Chem. Soc. Rev.* **2009,** *38*, 1450-1459.
7. Perry, J. J. I. V.; Perman, J. A.; Zaworotko, M. J., *Chem. Soc. Rev.* **2009,** *38*, 1400-1417.
8. Tranchemontagne, D. J.; Mendoza-Cortes, J. L.; O'Keeffe, M.; Yaghi, O. M., *Chem. Soc. Rev.* **2009,** *38*, 1257-1283.
9. Yaghi, O. M., *Nat. Mater.* **2007,** *6*, 92-93.
10. Kitagawa, S.; Kitaura, R.; Noro, S.-i., *Angew. Chem., Int. Ed.* **2004,** *43*, 2334-2375.
11. Kitagawa, S.; Noro, S.-i.; Nakamura, T., *Chem. Commun. (Cambridge, U. K.)* **2006**, 701-707.
12. Ferey, G., *Stud. Surf. Sci. Catal.* **2007,** *170A*, 66-86.
13. Cheetham, A. K.; Rao, C. N. R.; Feller, R. K., *Chem. Commun. (Cambridge, U. K.)* **2006**, 4780-4795.
14. Moulton, B.; Zaworotko, M. J., *Chem. Rev. (Washington, D. C.)* **2001,** *101*, 1629-1658.
15. Zaworotko, M. J., *Angew. Chem., Int. Ed.* **1998,** *37*, 1211-1213.
16. Chen, B.; Ockwig, N. W.; Fronczek, F. R.; Contreras, D. S.; Yaghi, O. M., *Inorg. Chem.* **2005,** *44*, 181-183.
17. Furukawa, H.; Kim, J.; Ockwig, N. W.; O'Keeffe, M.; Yaghi, O. M., *J. Am. Chem. Soc.* **2008,** *130*, 11650-11661.
18. Batten, S. R.; Robson, R., *Angew. Chem., Int. Ed.* **1998,** *37*, 1461-1494.
19. Batten, S. R.; Robson, R., *Mol. Catenanes, Rotaxanes Knots* **1999**, 77-106.
20. Robson, R., *Dalton* **2000**, 3735-3744.
21. Li, J.-R.; Kuppler, R. J.; Zhou, H.-C., *Chem. Soc. Rev.* **2009,** *38*, 1477-1504.
22. Czaja, A. U.; Trukhan, N.; Muller, U., *Chem. Soc. Rev.* **2009,** *38*, 1284-1293.
23. Ma, S.; Zhou, H.-C., *Chem. Commun. (Cambridge, U. K.) 46*, 44-53.
24. Hinks, N. J.; McKinlay, A. C.; Xiao, B.; Wheatley, P. S.; Morris, R. E., *Microporous Mesoporous Mater.* **2009,** *129*, 330-334.
25. Qiu, S.; Zhu, G., *Coord. Chem. Rev.* **2009,** *253*, 2891-2911.
26. Hong, D.-Y.; Hwang, Y. K.; Serre, C.; Ferey, G.; Chang, J.-S., *Adv. Funct. Mater.* **2009,** *19*, 1537-1552.
27. Farrusseng, D.; Mirodatos, C., *Des. Heterog. Catal.* **2009**, 161-194.
28. Farrusseng, D.; Aguado, S.; Pinel, C., *Angew. Chem., Int. Ed.* **2009,** *48*, 7502-7513.
29. Li, H.; Eddaoudi, M.; O'Keeffe, M.; Yaghi, M., *Nature (London)* **1999,** *402*, 276-279.

30. Ockwig, N. W.; Delgado-Friedrichs, O.; O'Keeffe, M.; Yaghi, O. M., *Acc. Chem. Res.* **2005,** *38*, 176-182.
31. O'Keeffe, M.; Peskov, M. A.; Ramsden, S. J.; Yaghi, O. M., *Acc. Chem. Res.* **2008,** *41*, 1782-1789.
32. Tranchemontagne, D. J.; Ni, Z.; O'Keeffe, M.; Yaghi, O. M., *Angew. Chem., Int. Ed.* **2008,** *47*, 5136-5147.
33. Rowsell, J. L. C.; Yaghi, O. M., *Microporous Mesoporous Mater.* **2004,** *73*, 3-14.
34. Banerjee, R.; Furukawa, H.; Britt, D.; Knobler, C.; O'Keeffe, M.; Yaghi, O. M., *J. Am. Chem. Soc.* **2009,** *131*, 3875-3877.
35. Wang, Z.; Cohen, S. M., *Chem. Soc. Rev.* **2009,** *38*, 1315-1329.
36. Burrows, A. D.; Frost, C.; Mahon, M. F.; Richardson, C., *Angew. Chem., Int. Ed.* **2008,** *47*, 8482-8486.
37. Gadzikwa, T.; Lu, G.; Stern, C. L.; Wilson, S. R.; Hupp, J. T.; Nguyen, S. T., *Chem. Commun. (Cambridge, U. K.)* **2008**, 5493-5495.
38. Morris, W.; Doonan, C. J.; Furukawa, H.; Banerjee, R.; Yaghi, O. M., *J. Am. Chem. Soc.* **2008,** *130*, 12626-12627.
39. Song, Y.-F.; Cronin, L., *Angew. Chem., Int. Ed.* **2008,** *47*, 4635-4637.
40. Wang, Z.; Cohen, S. M., *J. Am. Chem. Soc.* **2009,** *131*, 16675-16677.
41. Garibay, S. J.; Wang, Z.; Tanabe, K. K.; Cohen, S. M., *Inorg. Chem. (Washington, DC, U. S.)* **2009,** *48*, 7341-7349.
42. Tanabe, K. K.; Cohen, S. M., *Angew. Chem., Int. Ed.* **2009,** *48*, 7424-7427, S7424/1-S7424/15.
43. Wu, C.-D.; Hu, A.; Zhang, L.; Lin, W., **2005,** *127*, 8940-8941.
44. Wu, C.-D.; Lin, W., **2007,** *46*, 1075-1078.
45. Wang, Z.; Cohen, S. M., *Angew. Chem., Int. Ed.* **2008,** *47*, 4699-4702.
46. Wang, Z.; Cohen, S. M., *J. Am. Chem. Soc.* **2007,** *129*, 12368-12369.
47. Dinca, M.; Dailly, A.; Liu, Y.; Brown, C. M.; Neumann, D. A.; Long, J. R., *J. Am. Chem. Soc.* **2006,** *128*, 16876-16883.
48. Dinca, M.; Long, J. R., *J. Am. Chem. Soc.* **2007,** *129*, 11172-11176.
49. Murray, L. J.; Dinca, M.; Long, J. R., *Chem. Soc. Rev.* **2009,** *38*, 1294-1314.
50. Furukawa, H.; Ko, N.; Go, Y. B.; Aratani, N.; Choi, S. B.; Choi, E.; Yazaydin, A. O.; Snurr, R. Q.; O'Keeffe, M.; Kim, J.; Yaghi, O. M., *Science (Washington, DC, U. S.) 329*, 424-428.
51. Evans, O. R.; Manke, D. R.; Lin, W., *Chem. Mater.* **2002,** *14*, 3866-3874.
52. Ouyang, X.; Chen, Z.; Liu, X.; Yang, Y.; Deng, M.; Weng, L.; Zhou, Y.; Jia, Y., *Inorg. Chem. Commun.* **2008,** *11*, 948-950.
53. Seo, J. S.; Whang, D.; Lee, H.; Jun, S. I.; Oh, J.; Jeon, Y. J.; Kim, K., *Nature (London)* **2000,** *404*, 982-986.

Chapter 2

Synthesis and Structure of Two New Cobalt(II) and Zinc(II) Crystalline Coordination Networks Constructed with 1,3,5-Benzene Tricarboxylate and 9,10-bis(imidazol-1-ylmethyl) Anthracene

Name of author and affiliation: Hirofumi Motegi, Liangming Hu, Carla Slebodnick, Brian E. Hanson* (tel.:001-540-231-7206, hanson@vt.edu) Department of Chemistry, Virginia Polytechnic Institute and State University, Blacksburg, VA 24061, USA

Abstract:

Two new cobalt and zinc(II) coordination networks constructed from an anthracene based bis imidazole ligand, 9,10-bis(imidazol-1-ylmethyl)anthracene ligand (**L**) are reported. The compounds { [Co ($HBTC^{2-}$) (**L**) $(H_2O)_2]\cdot H_2O$ }$_\infty$(**2.1**) and {[Zn ($HBTC^{2-}$) (**L**) $(H_2O)_2]\cdot H_2O$}$_\infty$(**2.2**) were synthesized under solvothermal conditions and structurally characterized by single X-ray diffraction analysis and thermogravimetric analysis. Both **2.1** and **2.2** have a one-dimensional covalently bonded (1D) zigzag chain structure that is linked into infinite two-dimensional (2D) sheets by inter-chain π···π stacking and hydrogen bonding.

Keywords:

Metal-organic framework, Anthracene, Solvothermal synthesis, Imidazole ligand, π···π stacking

This work is published in Microporous and Mesoporous Materials Volume 129, Issue 3, 15 April 2010, Pages 360-365

2.1 Introduction

The rational design of functional porous coordination networks based on transition metal ions and organic bridging ligands is of interest because of the interesting topologies and potential applications possible with the new materials.[1] One strategy for the construction of coordination networks is to employ appropriate bridging ligands that are capable of binding to two or more metal ions through coordination bonds, and to choose metal ions with the a coordination geometry that allows for the formation of an extended network.[2] Through this strategy researchers in the field have prepared thousands of new structures. Nonetheless, the synthesis of networks is rarely rational; that is although a prediction may be made based on the likely geometries of the components the bonding capabilities of multidentate organic ligands and metal ions often lead to an unexpected structure.[3] The carboxylate group is a widely used anionic bridging ligand for constructing interesting porous structures; notably with di- and tri-carboxylates coordinate to metal ions to form extended structures that have potential use as gas storage materials.[4] The versatility of this group as a ligand is illustrated by the variety of its coordination modes when it acts as a bridge in framework architectures.[5]

Metal organic coordination networks with anthracene based bridging ligands have not been explored extensively. This is likely due to the poor solubility of the polycyclic aromatic ligand under solvothermal reaction conditions and the difficulty in packing the anthracene moiety efficiently in a network solid. This led us to speculate that anthracene based ligands, if successfully incorporated into a crystalline solid may lead to materials with permanent porosity. There are only a few reports of studies on the coordination networks with anthracene based neutral ligands[6], such as 9,10-bis(triazol-1-

ylmethyl)anthracene[7], 9,10-bis(N-benzimidazolyl)anthracene[8], and 9,10-bis(4-pyridyl)anthracene[6c] in the literature. As shown in Scheme 2.1, we have synthesized bifunctional flexible anthracene and imidazole containing ligand, 9,10-bis(imidazol-1-ylmethyl)anthracene (**L**).

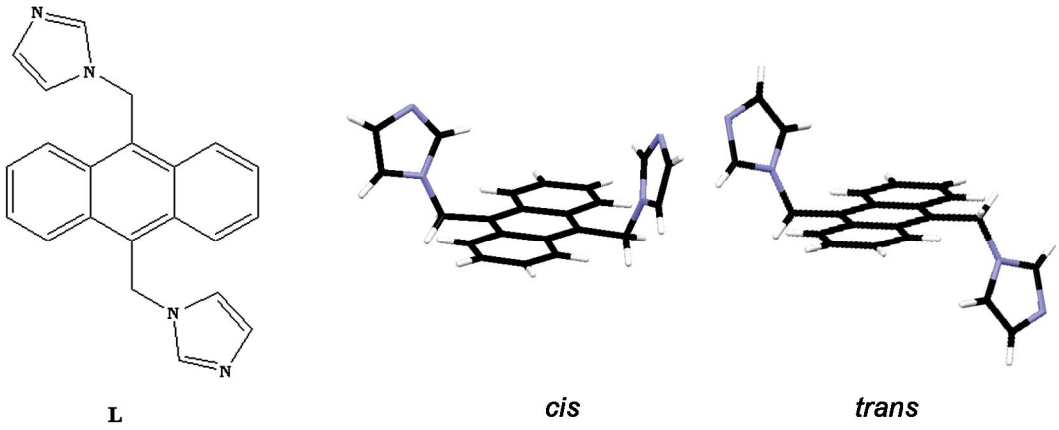

Scheme 2.1 Schematic drawings of anthracene based imidazole containing ligand(**L**) and two conformations.

Herein, we report the synthesis and crystal structure of two novel cobalt(II) and zinc(II) anthracene containing coordination networks incorporating the 1,3,5-benzene tricarboxylate (H_3BTC) anionic ligand and the neutral ligand, **L**, $[Co(C_9H_4O_6)(C_{22}H_{18}N_4)(H_2O)_2]\cdot H_2O$ (**2.1**) and $[Zn(C_9H_4O_6)(C_{22}H_{18}N_4)(H_2O)_2]\cdot H_2O$ (**2.2**). Compounds **2.1** and **2.2** consist of 1D chains constructed from cobalt(II) ion, one $HBTC^{2-}$, one **L** ligand, and one lattice water molecule.

2.2 Experimental

2.2.1 Materials and General Procedure

All commercially available chemicals are of reagent grade and used as received without further purification except 1,4-dioxane that was purified over sodium metal and benzophenone and then distilled prior to the synthesis. 9,10-Bis(chloromethyl)anthracene was synthesized by a previously reported procedure.[9]

2.2.2 Physical Measurements

Elemental Analyses of C, H, and N were performed by Galbraith Laboratories, Inc. Thermogravimetric analysis (TGA) measurements were performed on a TGA Q500 thermal analyzer under flowing N_2 stream with the heating rate of 10 °C min^{-1}. The anthracene based neutral Bridging Ligand (**L**) was synthesized according to modified literature procedures.[10]

2.2.3 9,10-bis(imidazol-1-ylmethyl)anthracene (**L**)

A freshly distilled 1,4-dioxane solution of imidazole (0.991 g, 14.6 mmol) was added to a suspension of sodium hydride (0.349 g, 14.6 mmol) in 1,4-dioxane (100 mL) and the mixture was stirred for 1 h at 90 °C. A 1,4-dioxane (50 mL) solution of 9,10-bis(chloromethyl)anthracene (2.00 g, 7.28 mmol) was added dropwise to the above solution.[10] The mixture was stirred and refluxed for 24 h to give a brown solution with tanned yellow precipitate. The solvent was reduced by a rotary evaporator and distilled water (300 mL) was added to the residue. Then, the solution was extracted with CH_2Cl_2 (3 × 50 mL). The methylene chloride solution was dried with anhydrous $MgSO_4$. Removal of the solvent yielded a yellow solid which was recrystallized from CH_2Cl_2/diethyl ether to give a yellow powder of **L**. Yield 1.12 g, 50 %. Melting point:

310 °C - 315 °C. ^{1}H NMR (400 MHz, DMSO-d^{6}): δ=8.58 (dd, 4H), 7.68(s, 2Hs), 7.62 (m, 4H), 6.87 (s, 2H), 6.72 (s,2H), 6.24 (s, 4H). ESI-MS($C_{22}H_{18}N_4$): m/z = 339 $[L-H]^+$

2.2.4 Synthesis of Complexes

Our synthetic protocol for the preparation of hybrid materials is to charge a heavy-walled glass tube (0.15 × 15 cm) with the solid precursors for the desired hybrid and 6 mL of a water/acetonitrile mixture. The tube is then frozen, evacuated, and sealed with a flame. The sealed tube is placed in an oven at 130 °C for up to 7 days. Upon cooling, the tubes are examined and crystalline product is collected by filtration. The crystalline product is washed with distilled water several times and dried at room temperature.

2.2.4.1 $[Co(HBTC^{2-})(L)(H_2O)_2]\cdot H_2O$ (2.1)

Solvothermal treatment of cobalt(II) chloride hexahydrate (24 mg, 0.10 mmol), **L** (34 mg, 0.10 mmol), benzenetricarboxylate(H_3BTC) (21 mg, 0.10 mmol), acetonitrile (1.0 mL), and distilled water (5.0 mL) for 7 days at 130 °C yielded a brown crystalline product. The crystalline product was collected by filtration and washed with distilled water. Yield 20 mg, 83 % based on cobalt. Anal. Calc (%). For $C_{31}H_{28}N_4O_9Co$: C, 56.46; H, 4.28; N, 8.50. Found (%): C, 56.59; H, 4.21; N, 8.43.

2.2.4.2 $[Zn(HBTC^{2-})(L)(H_2O)_2]\cdot H_2O$ (2.2)

Solvothermal treatment of zinc(II) nitrate hexahydrate (29 mg, 0.10 mmol), **L** (34 mg, 0.10 mmol), benzenetricarboxylate(H_3BTC) (21 mg, 0.10 mmol), acetonitrile (1.0 mL), and distilled water (5.0 mL) for 7 days at 130 °C yielded a light yellow crystalline product. The crystalline product was collected by filtration and washed with distilled

water. Yield 20 mg, 69 % based on zinc. Anal. Calc (%). For $C_{31}H_{28}N_4O_9Zn$: C, 56.46; H, 4.28; N, 8.50. Found (%): C, 56.56; H, 4.23; N, 8.41.

2.3 X-ray crystallography

Single crystals of ligand **L** (yellow needle, 0.71 × 0.09 × 0.08), compound **2.1** (brown rectangle, 0.35 × 0.10 × 0.09 mm^3), and compound **2.2** (light yellow rectangle, 0.35 × 0.07 × 0.05 mm^3) were selected and centered on the goniometer of an Oxford Diffraction Gemini A Ultra diffractometer operating with MoKα radiation (λ = 0.7107 Å) and at 100 K. The data collection routine, unit cell refinement, and data processing were carried out with the program CrysAlisPro.[11] The Laue symmetries of the diffraction patterns for the compounds were consistent with monoclinic (**L**, **2.1,** and **2.2**) crystal systems. The systematic absences were consistent with the monoclinic space group $P2_1/n$ for **L**, **2.1**, and **2.2**. Structure solution and refinement were performed with the graphical user interface WinGX.[12] The structures were solved by direct methods using SIR92[13] and refined by full matrix least squares analysis using SHELXL-97.[14] The final refinement models included anisotropic displacement parameters for all non-hydrogen atoms, and a riding model for all hydrogen atoms of the framework. In both structures of the compounds, one water molecule co-crystallized in the lattice. In compounds **2.1** and **2.2**, one strong residual electron density peak remained unaccounted for after the network structure had been located. This peak was assigned as a water oxygen atom and the hydrogen atoms of this water molecule were located in the residual electron density map. The crystal parameters, data collection, and refinement results for ligand **L**, compounds **2.1**, and **2.2** are summarized in Table 2.1. The program package ORTEP-3 was used for molecular graphics generation.[15]

Table 2.1 Crystallographic data and structure refinement details for **L**, **2.1,** and **2.2**.

	L	**2.1**	**2.2**
Empirical formula	$C_{22}H_{18}N_4$	$C_{31}H_{28}CoN_4O_9$	$C_{31}H_{28}ZnN_4O_9$
Formula weight	338.40	659.50	665.94
Temperature (K)	100(2)	100(2)	100(2)
Space group	$P2_1/n$	$P2_1/n$	$P2_1/n$
a (Å)	4.467(3)	14.1301(2)	14.223(4)
b (Å)	18.042(9)	12.2524(2)	12.201(3)
c (Å)	10.283(5)	17.0920(3)	17.077(4)
α (°)	90	90	90
β (°)	91.24(6)	105.285(2)	105.72(3)
γ (°)	90	90	90
Volume ($Å^3$)	828.6(8)	2854.42(8)	2852.6(9)
Z	2	4	4
Density (mg/m^3)	1.356	1.535	1.551
Absorption coefficient (mm^{-1})	0.083	0.666	0.926
F(000)	356	1364	1376
Reflections collected	8238	17589	26709
Independent reflections	2413	5056	8377
R_{int}	0.0634	0.0400	0.0705
GOF	0.873	0.960	0.777
R_1/wR_2 [I>2sigma(I)]	0.0536/0.1215	0.0299/0.0623	0.0435/0.0734

Rint: internal-R value from averaging the reflections in point group -1. GOF: goodness of fit value should converge to 1.0 for a very good structure at the end of refinement.

R_1/wR_2: These values are all standard algorithms for presenting the quality of the agreement for observed data.

2.4 Results and Discussion

2.4.1 Description of 9,10-bis(imidazol-1-ylmethyl)anthracene (**L**)

The structure of **L** with atom numbering scheme is shown in Figure 2.1. The ligand crystallizes in a *trans* conformation. The dihedral angle between the imidazole group and the anthracene group is 112.22°.

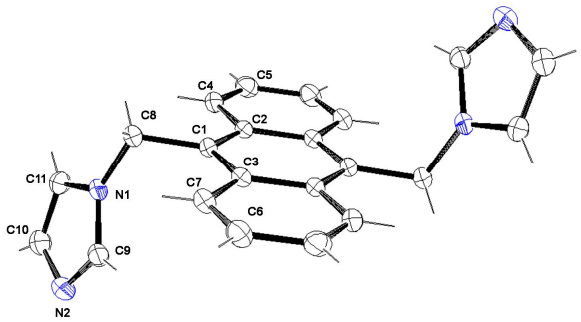

Figure 2.1 Molecular structure of ligand **L** with the ellipsoids drawn at the 30 % probability level.

2.4.2 Structural description of $[Co(C_9H_4O_6)(C_{22}H_{18}N_4)(H_2O)_2]\cdot H_2O$ (**2.1**)

The structure of **2.1** with atom numbering scheme is shown in Figure 2.2. Selected bond length and angles are summarized in Table 2.2. The asymmetric unit of **2.1** contains one octahedral cobalt(II) ion, one $HBTC^{2-}$ ligand, one **L** ligand, two coordinated water molecules, and one lattice water molecule. The distorted octahedral cobalt atom is coordinated to two oxygen atoms of a chelating carboxylate group (Co-O: 2.141(1) and 2.291(1) Å) from one $HBTC^{2-}$ anion, two water molecules (Co-O: 2.046(2) and 2.050(2) Å), and two nitrogen atoms (Co-N: 2.123(2) and 2.108(2) Å) from one **L** ligand.

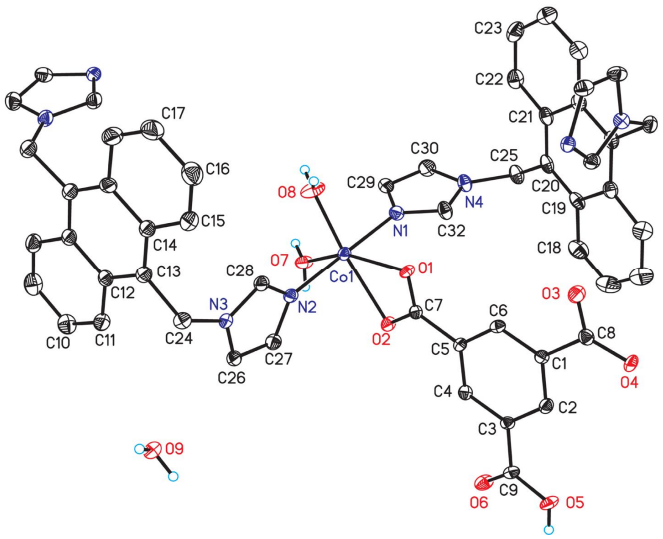

Figure 2.2 Coordination environment of cobalt(II) ion in **2.1** with the ellipsoids drawn at the 30 % probability level.

Since there are no ionic species in the network cavities, the crystalline coordination network must be neutral. Therefore, two carboxylate groups on the BTC ligand must be deprotonated to balance the total charge of the network. As the cobalt(II) atom is coordinated to one chelating carboxylate group that has a negative charge, one of the other two carboxylate groups bound to this ion must also have a negative charge. The crystallographic study reveals that O3 and O4 of one carboxylate group of the $HBTC^{2-}$ ligand have a delocalized negative charge based on the equivalent bond distances of C8-O3 (1.265 (2) Å) and C8-O4 (1.253 (2) Å). The third carboxylate group on the $HBTC^{2-}$ ligand is neutral and the hydrogen atom of this group was located in the residual electron density map. In order to confirm which oxygen atom is bonded to the hydrogen atom, the bond distances between the carbon and oxygen atoms were analyzed. The

crystallographic study showed that C9-O5 is 1.327 (2) Å (Table 2.2), which is consistent with a C-O single bond, and C9-O6 is 1.222 (2) Å (Table 2.2), which is indicative of a double bond. Therefore, the hydrogen atom of this carboxylate group is bound to atom O5.

Table 2.2 Selected bond distances (Å) and angles (°) for compound **2.1**.

Bond Distance	**(Å)**
Co(1)-N(2)	2.1075(17)
Co(1)-N(1)	2.1229(18)
Co(1)-O(1)	2.1413(13)
Co(1)-O(2)	2.2910(14)
O(7)-Co(1)	2.0464(16)
O(8)-Co(1)	2.0501(17)
O(1)-C(7)	1.271(2)
O(2)-C(7)	1.267(2)
O(3)-C(8)	1.265(2)
O(4)-C(8)	1.253(2)
O(5)-C(9)	1.327(2)
O(6)-C(9)	1.222(2)
Bond Angles	**(°)**
O(7)-Co(1)-O(8)	101.16(8)
O(7)-Co(1)-N(2)	90.88(7)

O(8)-Co(1)-N(2)	89.50(7)
O(7)-Co(1)-N(1)	89.77(7)
O(8)-Co(1)-N(1)	90.79(7)
N(2)-Co(1)-N(1)	179.23(6)
O(7)-Co(1)-O(1)	153.44(7)
O(8)-Co(1)-O(1)	105.12(7)
N(2)-Co(1)-O(1)	93.03(6)
N(1)-Co(1)-O(1)	86.21(6)
O(7)-Co(1)-O(2)	94.84(6)
O(8)-Co(1)-O(2)	163.49(7)
N(2)-Co(1)-O(2)	86.17(6)
N(1)-Co(1)-O(2)	93.35(6)
O(1)-Co(1)-O(2)	59.29(5)
O(6)-C(9)-O(5)	123.87(19)
O(2)-C(7)-O(1)	119.85(18)
O(4)-C(8)-O(3)	124.96(19)

The conformation of **L** in compound **2.1** is *cis*; two nitrogen atoms on the imidazole groups of **L** are connected to two cobalt atoms along the (010) direction to give 1D zigzag chain (Figure 2.3).

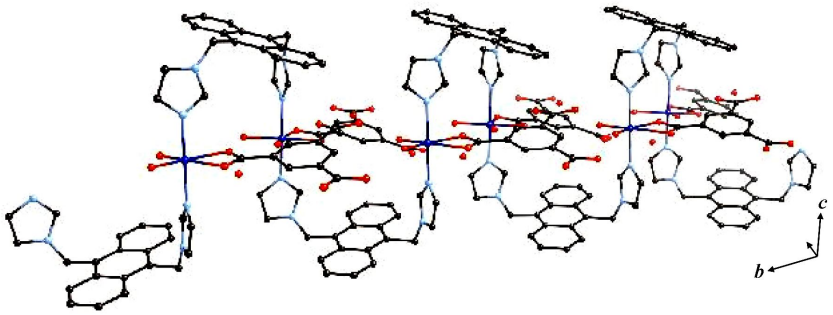

Figure 2.3 1D zigzag chain in compound **2.1**.

The 1D zigzag chains observed in compound **2.1** are linked via hydrogen bonds to form an extended 2D sheet structure; this hydrogen bond linkage involves two uncoordinated carboxylate groups and coordinated water molecules on the chains, and lattice water molecules (Figure 2.4). Hydrogen bond distances between lattice water molecules and neighboring atoms are summarized in Table 2.3.

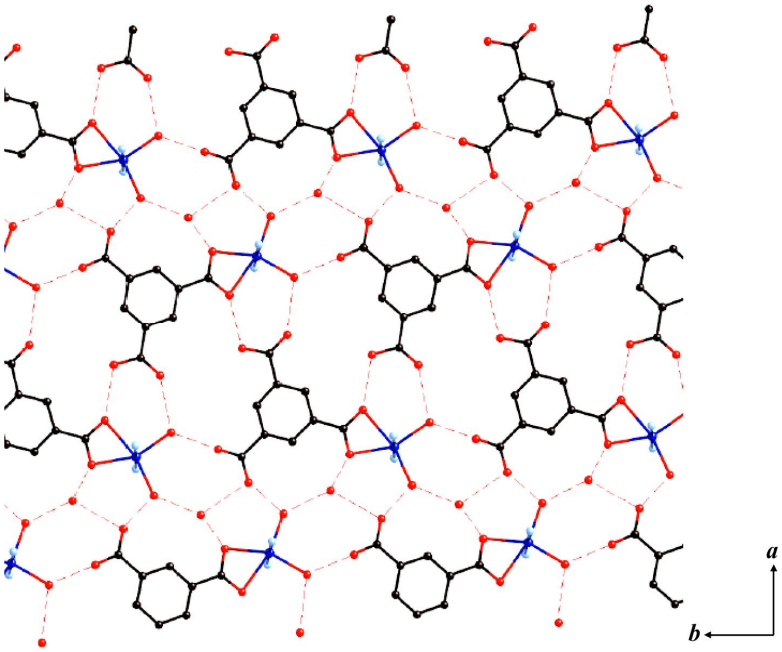

Figure 2.4 A 2D sheet is connected via hydrogen bond in **2.1**. Neutral ligand (**L**) is omitted.

Table 2.3 Hydrogen bond distances between lattice water molecules and neighboring atoms in compound **2.1**.

D-H···A	D···A (Å)
O5-H5···O2	2.632(2)
O9-H9A···O3	2.753(2)
O9-H9B···O1	2.767(2)
O7-H7A···O6	2.759(2)
O8-H8A···O3	2.680(2)
O8-H8B···O9	2.669(2)
O7-H7B···O4	2.647(2)

Furthermore, these 2D sheets are linked into 3D network by inter-sheet π···π stacking interactions between the aromatic anthracene ring of one sheet and a benzene ring of a BTC in adjacent sheets (Figure 2.5). The selected π···π interactions shown in Figure 2.5 are within the range of 3.750 - 3.966 Å, which reveals the existence of face-face π···π interactions in compound **2.1.**[16]

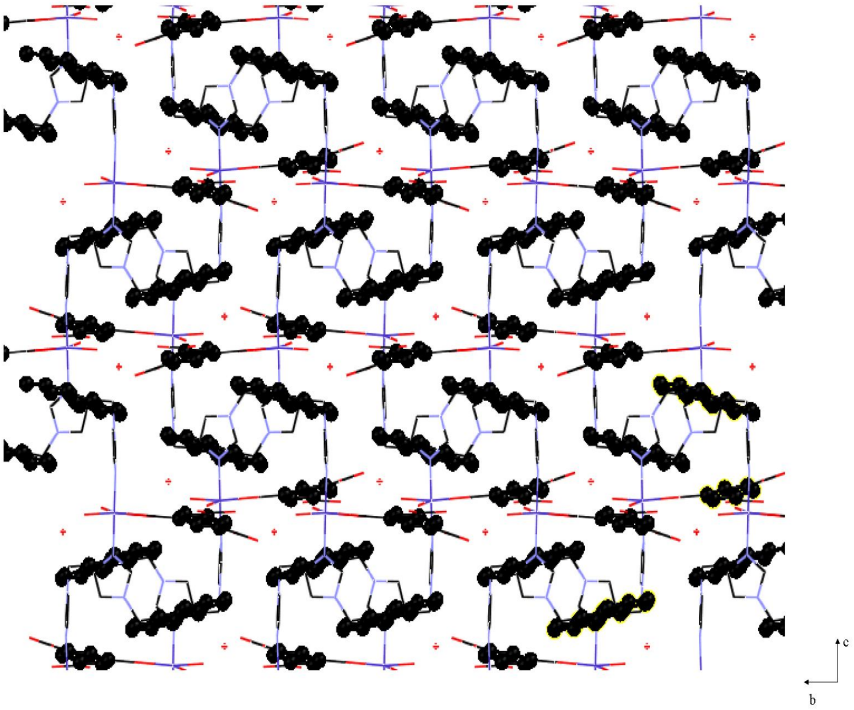

Figure 2.5 In **2.1,** inter-sheet π···π stacking interactions between the aromatic anthracene rings of one sheet and benzene rings of $HBTC^{2-}$ in adjacent sheets.

2.4.3 Structural description of $[Zn(C_9H_4O_6)(C_{22}H_{18}N_4)(H_2O)_2]\cdot H_2O$ (2.2)

The structure of **2.2** with atom numbering scheme is shown in Figure 2.6. Selected bond length and angles are summarized in Table 2.4. The compound **2.2** is isostructural with compound **2.1** except metal ion is zinc(II). The asymmetric unit of **2.2** contains one octahedral zinc(II) ion, one $HBTC^{2-}$ ligand, one **L** ligand, two coordinated

water molecules, and one lattice water molecule. Like the compound **2.1**, compound **2.2** is neutral. The distorted octahedral zinc atom is coordinated to two oxygen atoms of a chelating carboxylate group (Zn-O: 2.141(2) and 2.447(2) Å) from one $HBTC^{2-}$ anion, two water molecules (Zn-O: 2.016(2) and 2.053(2) Å), and two nitrogen atoms (Zn-N: 2.092(2) and 2.108(2) Å) from one $\mathbf{L_2}$ ligand.

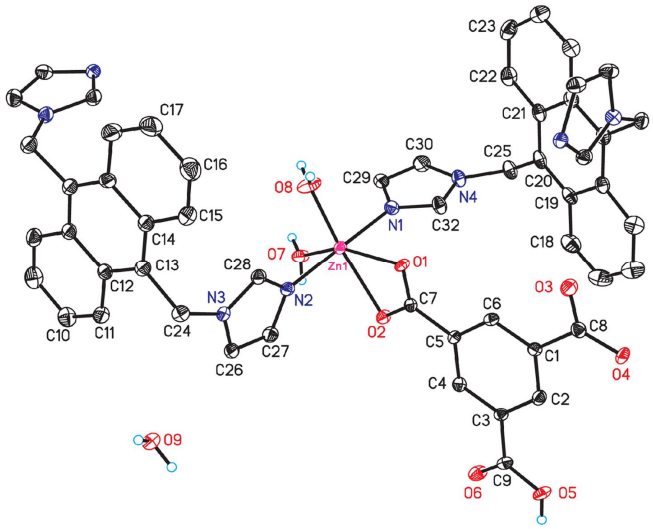

Figure 2.6 Coordination environment of zinc(II) ion in **2.2** with the ellipsoids drawn at the 30 % probability level.

Again, the hydrogen atom on the free carboxylate group is located by careful crystallographic analysis. Two carboxylate groups on the BTC ligand must be deprotonated to balance the total charge of the network. As the zinc(II) ion is coordinated to one chelating carboxylate group (O1 and O2) that has a negative charge, one of the other two carboxylate groups must have a negative charge. The crystallographic study reveals that O3 and O4 of one carboxylate group of the BTC ligand have a delocalized negative charge based on the equivalent bond distances of C9-O3 (1.264 (3) Å) and C9-O4 (1.255 (3) Å). The third carboxylate group on the BTC ligand is neutral and the

hydrogen atom of this group was located in the residual electron density map. The crystallographic study showed that C8-O5 is 1.320 (3) Å (Table 2.4), which is consistent with a C-O single bond, and C9-O6 is 1.224 (3) Å (Table 2.4), which is indicative of a double bond. Therefore, the hydrogen atom of this carboxylate group is bound to atom O5.

Table 2.4 Selected Bond distances (Å) and angles (°) for compound **2.2**.

Bond Distance	**(Å)**
N(1)-Zn(1)	2.0917(18)
N(3)-Zn(1)	2.1076(18)
O(1)-Zn(1)	2.4470(16)
O(2)-Zn(1)	2.1408(15)
O(7)-Zn(1)	2.0531(16)
O(8)-Zn(1)	2.0161(17)
C(7)-O(1)	1.261(2)
C(7)-O(2)	1.271(2)
C(8)-O(6)	1.224(3)
C(8)-O(5)	1.320(3)
C(9)-O(4)	1.250(3)
C(9)-O(3)	1.264(3)
Bond Angles	**(°)**
O(1)-C(7)-O(2)	120.6(2)
O(6)-C(8)-O(5)	123.7(2)
O(4)-C(9)-O(3)	124.9(2)
O(8)-Zn(1)-O(7)	106.84(7)
O(8)-Zn(1)-N(1)	92.81(8)
O(7)-Zn(1)-N(1)	90.53(7)
O(8)-Zn(1)-N(3)	90.72(8)
O(7)-Zn(1)-N(3)	89.08(7)
N(1)-Zn(1)-N(3)	176.41(7)
O(8)-Zn(1)-O(2)	107.15(7)
O(7)-Zn(1)-O(2)	146.00(6)
N(1)-Zn(1)-O(2)	87.00(7)
N(3)-Zn(1)-O(2)	91.33(6)
O(8)-Zn(1)-O(1)	163.02(6)
O(7)-Zn(1)-O(1)	89.41(6)
N(1)-Zn(1)-O(1)	91.89(7)
N(3)-Zn(1)-O(1)	84.54(6)
O(2)-Zn(1)-O(1)	56.83(5)

The conformation of **L** in compound **2.2** has been shown as a *cis* conformation. Two nitrogen atoms on the imidazole group of **L** are connected to two zinc atoms along the (010) direction to give 1D zigzag chain. It is interesting to note that the 1D zigzag chains observed in compound **2.2** are linked via hydrogen bonds to form an extended 2D sheet structure; this hydrogen bond linkage involves two uncoordinated carboxylate groups and coordinated water molecules on the chains, and lattice water molecules. Hydrogen bond distances between lattice water molecules and neighboring atoms are summarized in Table 2.5.

Table 2.5 Hydrogen bond distances between lattice water molecules and neighboring atoms in compound **2.2**.

D-H···A	D···A (Å)
O5-H5···O1	2.632(2)
O9-H9A···O3	2.753(2)
O9-H9B···O1	2.767(2)
O7-H7A···O6	2.759(2)
O8-H8A···O3	2.680(2)
O8-H8B···O9	2.669(2)
O7-H7B···O4	2.647(2)

2.5 Thermogravimetric analysis

Thermogravimetric analysis (TGA) was performed under a flowing nitrogen stream with the heating rate of 10 °C min^{-1} on a crystalline sample of compounds **2.1** and **2.2**. TGA curve of compound **2.1** displays the first weight loss starts after 100 °C to give a total weight loss of 8.55%, corresponding to the loss of the one uncoordinated and two

coordinated water molecules (calculated, 8.20%) (Figure 2.7 (Green)). The second weight loss starts at 300 °C, and corresponds to the release of ligand, **L**, and the compound **2.1** begins to decompose. TGA curve of compound **2.2** displays the similar weight loss as compound **2.1**. The first weight loss starts after 100 °C to give a total weight loss of 8.10%, corresponding to the loss of the one uncoordinated and two coordinated water molecules (calculated, 8.20%) (Figure 2.7 (Red)).

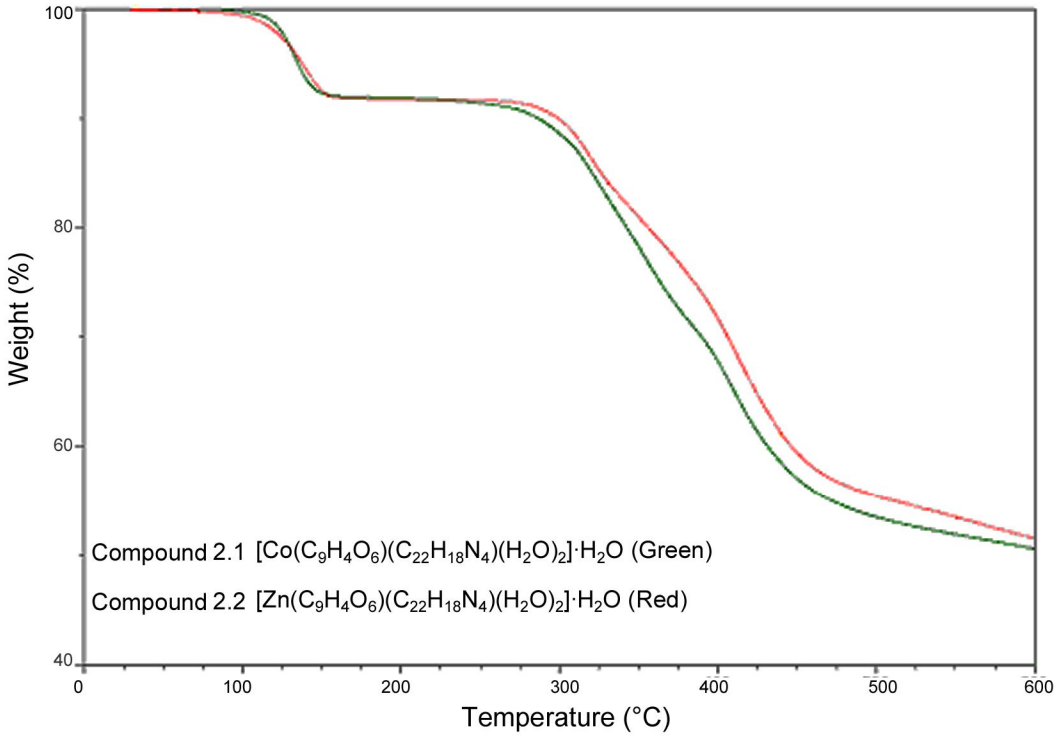

Figure 2.7 TGA plots of compounds **2.1** (Green) and **2.2** (Red).

2.6 Conclusions

In conclusion, we have synthesized and characterized cobalt(II) and zinc(II) coordination networks with the neutral anthracene based flexible bridging ligand (**L**). Both of the crystalline coordination networks exhibited that the $HBTC^{2-}$ anion that has

two deprotonated carboxylate groups and *cis* conformation of **L** generates a 1D chain structure.

2.7 References

1. (a) O.M. Yaghi, M. O'Keeffe, N.W. Ockwig, H.K. Chae, M. Eddaoudi, J. Kim, Nature 423, (2003), 705

(b) S. Kitagawa, R. Kitaura, S. Noro, Angew. Chem. Int. Ed. 43, (2004), 2334

(c) G. Férey, Chem. Soc. Rev. (2008), *37*, 191

(d) D. Bradshaw, J.B. Claridge, E.J. Cussen, T.J. Prior, M.J. Rosseinsky, Acc. Chem. Res. 38, (2005), 273

(e) S.L. James, Chem. Soc. Rev. 32, (2003), 276.

(f) C. Janiak, Dalton Trans. (2003), 2781.

2. (a) M. Eddaoudi, D.B. Moler, H.L. Li, B.L. Chen, T.M. Reineke, M. O'Keeffe, O.M. Yaghi, Acc. Chem. Res. 34, (2001), 319

(b) M.J. Zaworotko, Chem. Commun. (2001), p. 1.

(c) Batten, S. R.; Robson, R. *Angew. Chem., Int. Ed.* **1998**, *37*, 1460.

3. (a)K. Koh, A. G. Wong-Foy, A. J. Matzger, Angew. Chem., Int. Ed. (2008), 47, 677

(b) A. K. Cheetham, C. N. R. Rao, R. K. Feller, Chem. Commun. (2006), 4780

4. (a) A. G. Wong-Foy, A. J. Matzger, O. M. Yaghi, J. Am. Chem. Soc. (2006), 128, 3494

(b) S. Ma, D. Sun, J. M. Simmons, C. D. Collier, D. Yuan, H.-C. Zhou, J. Am. Chem. Soc. (2008), 130, 1012

5. (a) B.H. Ye, M.L. Tong, X.M. Chen, Coord. Chem. Rev. 249, (2005), 545

(b) Y.Y. Liu, J.F. Ma, J. Yang, Z.M. Su, Inorg. Chem. 46, (2007), 3027

(c) Qi, Y.; Luo, F.; Che, Y. X.; Zheng, J. M. Cryst. Growth Des. (2008), 8, 606

6. (a) T. Sawaki, T. Dewa, Y. Aoyama, J. Am. Chem. Soc. 120, (1998), 8539

(b) K. Biradha, M. Fujita, Chem. Commun. (2001), 15

(c) G. Marin, M. Andruh, A. M. Madalan, A. J. Blake, C. Wilson, N. R. Champness, M. Schröder. Cryst. Growth Des. (2008), 8, 964

(d) T. M. Fasina, J. C. Collings, D. P. Lydon, D. Albesa-Jove, A. S. Batsanov, J. A. K. Howard, P. Nguyen, M. Bruce, A. J. Scott, W. Clegg, S. W. Watt, C. Viney, T. B. Marder, J. Mater. Chem. (2004), 14, 2395

(e) J.-R. Li, Y. Tao, Q. Yu, X.-H. Bu, Chem. Commun. (2007) 1527

7. D. Z. Wang, C. S. Liu, J. R. Li, L. Li, Y. F. Zeng , X. H. Bu, CrystEngComm. (2007), 9, 289

8. L. Li, T. L.Hu, J. R.Li, , D. Z.Wang, Y. F.Zeng , X. H.Bu, CrystEngComm. (2007), 9, 412

9. M. W. Miller, R. W. Amidon, P. O. Tawney, J. Am. Chem. Soc. (1955), 77**,** 2845

10. Q.-X. Liu, F.-B. Xu, Q.-S. Li, X.-S. Zeng, X-B. Leng, Y.L. Chou, Z-Z. Zhang, Organometallics (2003), 22, 309.

11. CrysAlisPro v171.32, Oxford Diffraction: Wroclaw, Poland, 2008

12. L. J. Farrugia, "WinGX: An Integrated System of Windows Programs for the Solution, Refinement, and Analysis of Single Crystal X-ray Diffraction Data" J.Appl.Cryst.**,** (1999)**,** 32, 837

13. A. Altomare, G. Cascarano, C. Giacovazzo, A. J. Guagliardi, Appl. Cryst. (1993), 26, 343-350.

14. G. M. Sheldrick, "A short history of SHELX". Acta Cryst. A64, (2008), 112-122.

15. L. J. Farrugia, J. Appl. Cryst (1997), 30, 565

16. C. A. Hunter, K. R. Lawson, J. Perkins, C. J. Urch, J. Chem. Soc., Perkin Trans. 2, 2001, 651

Chapter 3

Solvothermal Synthesis of Cobalt(II) Coordination Networks Based on Tetradentate Neutral Ligand and 1,3,5-Benzenetricarboxylate Anion

Name of author and affiliation: Hirofumi Motegi, Carla Slebodnick, Brian E. Hanson* (tel.:001-540-231-7206, hanson@vt.edu) Department of Chemistry, Virginia Polytechnic Institute and State University, Blacksburg, VA 24061, USA

Abstract:

Three new cobalt (II) coordination networks constructed from the tetradentate imidazole ligand, 1, 2, 4, 5-tetrakis(imidazol-1ylmethyl)benzene (**L**) and from 1,3,5-benzenetricarboxylate (H_3BTC), are reported. The compounds, $[Co(HBTC)(\mathbf{L})_{0.5}(H_2O)]\cdot H_2O$ (**3.1**), $[Co(HBTC)(\mathbf{L})_{0.5}]\cdot 1.72H_2O$ (**3.2**), and $[Co_3(BTC)_2(L)(H_2O)_4]\cdot 6H_2O$ (**3.3**), were synthesized under solvothermal conditions and characterized by single crystal X-ray diffraction analysis and thermogravimetric analysis. Compound **3.1** has a two-dimensional (2D) covalently bonded corrugated sheet structure that is linked by inter-layer π···π stacking and hydrogen bonding. Compound **3.2** has a 2D covalently bonded sheet structure in which the sheets are connected by hydrogen bonds at the free acid group of $HBTC^{2-}$. Compound **3.3** forms an interpenetrated three-dimensional (3D) covalently bonded framework structure. Void spaces in the structure are filled with six water molecules.

Keywords:

Metal-organic framework, Mixed ligand, Solvothermal synthesis, Tetradentate, imidazole, Benzenetricarboxylate

This paper will be submitted to crystal growth and design.

3.1 Introduction

The use of flexible multifunctional ligands remains a challenge in the synthesis of crystalline coordination networks.[54-56] Because of the conformational diversity exhibited by the flexible groups in this class of ligands, the topology of the final products is difficult to predict based solely on the concepts of ligand directionality and metal coordination geometry. Recently, there have been a number of studies of flexible ligands that contain terminal imidazole groups[57-63] and coordination networks incorporating bidentate and tridentate terminal imidazole ligands have been reported.[59-63] The use of neutral tetradentate ligands in the synthesis of coordination networks is relatively rare and only a few examples have been reported.[64-71] Recently, cadmium(II) metal ion networks with 1,2,4,5-tetrakis(imidazol-1-ylmethyl)benzene, **L**, and a variety of anions were reported and the result showed that 2D and 3D frameworks were constructed. One of these showed reversible anion exchange properties.[68]

We describe the formation of networks with the flexible tetradentate ligand, **L**, and the rigid multifunctional anions derived from 1,3,5-benzenetricarboxylic acid, H_3BTC. The ligand **L** can adopt a variety of conformations due to the flexibility of the methylene connection between the imidazole and benzene rings and the orientation of imidazole ring. Deprotonation of H_3BTC gives anions of -1, -2, or -3 charge and can link several metal ions in a network.[72-76] Some of the possible conformations of **L** and bridging possibilities of BTC^{3-} are shown schematically below.

In the case of **L**, four conformations have previously been described[68]; an H configuration in which the nitrogen donor atoms are as close to coplanar with the benzene ring as possible (I, Scheme 3.1), "up, up, down, down" configuration in which the

imidazole rings are oriented in a pinwheel fashion (IIa, Scheme 3.1). “up, down, down, up” also has a similar configuration as IIa, pinwheel shape, although the positions of imidazole groups are different than IIa (IIb, Scheme 3.1). “up, down” configuration in which diagonally positioned imidazole groups are oriented in plane (III, Scheme 3.1). The diversity of linkages that can be formed by this ligand in a network is derived from the conformational flexibility and the fact that the ligand can bind one, two, three, or four metals in the network.

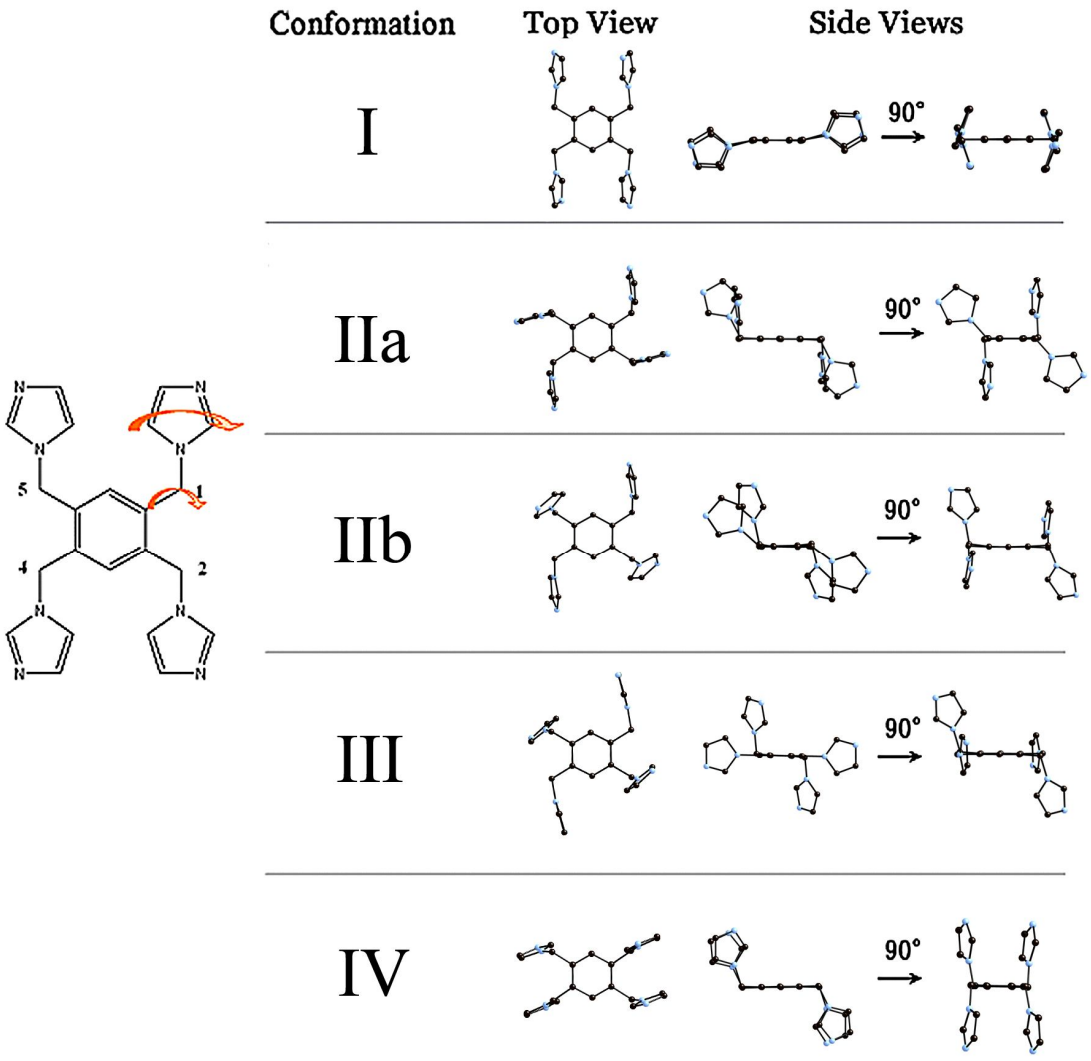

Scheme 3.1 Four different coordination modes of **L.**

Carboxylate groups in network structures can bond to a single metal ion in an η-1 or η-2 fashion or bridge two metal ions. Thus, the ligand HBTC and its related anions can connect to one, two, three, or more metal ions depending on the charge and coordination mode. Several connectivity patterns for $H_{3-x}BTC^{x-}$ are shown in Scheme 2. The H_3BTC derived anions also balance the charge of the network structures.[63, 77-85] Clearly, the structural variety of networks derived from two multifunctional ligands such as **L** and H_3BTC is immense.

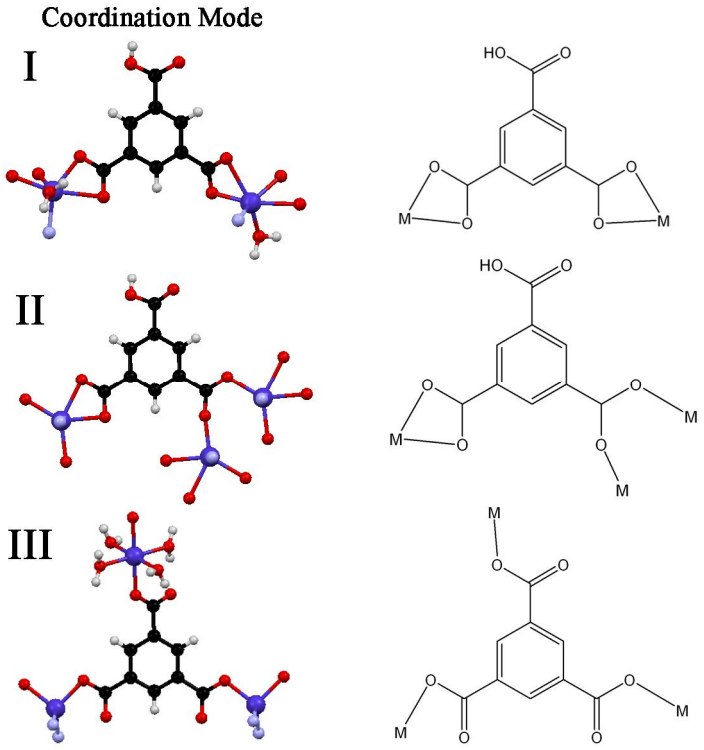

Scheme 3.2 Three coordination modes of H_3BTC anion.

We describe the synthesis and crystal structures of three compounds, $[Co(HBTC^{2-})(\mathbf{L})_{0.5}(H_2O)]\cdot H_2O$ (**3.1**), $[Co(HBTC^{2-})(\mathbf{L})_{0.5}]\cdot 1.72H_2O$ (**3.2**), and $[Co_3(BTC^{3-})_2(\mathbf{L})(H_2O)_4]\cdot 6H_2O$ (**3.3**). The crystal structure of those compounds, thermal stability,

and coordination modes of H_3BTC and **L** as they relate to the frameworks will be discussed.

3.2 Experimental Section

3.2.1 Materials and Physical measurements

All commercially available starting materials are of reagent grade and used as received without further purification except imidazole, which was dried under vacuum overnight. The ligand (**L**) was prepared by a modified procedure that is detailed below.[86] FT-IR spectra were recorded in the range 4000.0 – 400.0 cm^{-1} on a Perkin Elmer FT-IR Spectrum One spectrometer using KBr disks. Thermogravimetric analysis (TGA) measurements were performed on a TGA Q500 thermal analyzer under flowing N_2 stream with a heating rate of 10 °C min^{-1} for all measurements.

3.2.2 X-ray Crystallography

Compound **3.1** (purple rectangle, 0.03 × 0.07 × 0.09 mm^3), compound **3.2** (light pink rectangle, 0.04 × 0.08 × 0.11 mm^3), and compound **3.2** (purple rod, 0.12 × 0.13 × 0.36 mm^3) were crystallized from a mixture of water and acetonitrile by solvothermal synthesis at 85-130 °C. The chosen crystals were centered on the goniometer of an Oxford Diffraction Gemini A Ultra diffractometer operating with MoKα radiation (λ = 0.7107 Å) and at 100 K. The data collection routine, unit cell refinement, and data processing were carried out with the program CrysAlis.[87] The Laue symmetry and systematic absences for compound **3.1** were consistent with the monoclinic space group $P2_1/n$. The Laue symmetry for compounds **3.2** and **3.3** was consistent with the triclinic space groups *P1* and *P-1*; In both cases, *P-1* was chosen based on E-statistics. Structure solution and refinement were performed with the graphical user interface WinGX.[88] The

structures were solved by direct methods using SIR92[89] and refined by full matrix least squares analysis using SHELXL-97.[90] Anisotropic displacement parameters were refined for all non-hydrogen atoms. A riding model was used for all hydrogen atoms except the hydrogen atoms of water molecules. In compound **3.1**, after locating the network structure, one strong residual electron density peak was assigned as the oxygen of a water molecule. The hydrogen atom positions on this water molecule were located in the residual electron density map and refined with restraints. In compound **3.2**, five strong residual electron density peaks remained, but were too close to be fully occupied waters. Thus, a two position disorder model was used. With this model, O7 and O8 occupancies refined to 0.565(12) and the O7 ··· O8 distances is 2.741 Å. The occupancies of O9 and O10 refined to 0.435(12) with an O9 ··· O10 distance of 2.855 Å. The hydrogen atoms on the water molecules could not be located in the residual electron density map and were not included in the refinement. In compound **3.3**, three strong residual electron density were located 2.60-2.75 Å from neighboring electron donors and were assigned as the oxygen atoms of water molecules. The hydrogen atoms on the water molecules could not be located in the residual electron density map and were not included in the refinement. The crystal parameters, data collection, and refinement results for compounds **3.1**, **3.2**, and **3.3** are summarized in Table 3.1.

Table 3.1 Crystallographic data and structure refinement details for **3.1**, **3.2**, and **3.3**.

	3.1	**3.2**	**3.3**
Empirical formula	$C_{20}H_{19}CoN_4O_8$	$C_{20}H_{15}CoN_4O_{7.72}$	$C_{40}H_{48}Co_3N_8O_{22}$
Formula weight	502.32	493.77	1169.65
Temperature (K)	100(2)	100(2)	100(2)
Space group	$P2_1/n$	P -1	P -1
a (Å)	11.005(4)	10.0336(19)	10.1402(18)
b (Å)	11.881(3)	10.549(2)	11.076(2)
c (Å)	16.085(4)	11.371(2)	11.888(3)
α (°)	90	93.177(16)	115.05(2)
β (°)	94.97(3)	110.770(17)	99.747(17)
γ (°)	90	111.222(19)	95.652(16)
Volume ($Å^3$)	2095.2(11)	1025.4(3)	1170.3(4)
Z	4	2	1
Density (mg/m^3)	1.592	1.605	1.66
Absorption coefficient (mm^{-1})	0.876	0.896	1.144
F(000)	1032	503	601
Reflections collected	18309	11305	7429
Independent reflections	3691	4715	4049
R_{int}	0.1127	0.0649	0.0333
GOF	1.027	0.96	1.06
R_1/wR_2 [I>2sigma(I)]	0.0673/0.0949	0.0676/ 0.1165	0.0521/0.1483

Rint: internal-R value from averaging the reflections in point group -1. GOF: goodness of fit value should converge to 1.0 for a very good structure at the end of refinement.

R_1/wR_2: These values are all standard algorithms for presenting the quality of the agreement for observed data.

3.3.3 Synthesis of 1, 2, 4, 5-tetrakis(imidazol-1-ylmethyl)benzene (L)

L was synthesized using a modified literature procedure.[86] To a reaction mixture of imidazole (1.30 g, 19.0 mmol) in dry THF (100 mL) was added NaH (0.475 g, 19.0 mmol) at 0 °C. After the reaction mixture was stirred for three hours at 0 °C, the color of the solution turned to a light tan color. 1, 2, 4, 5-tetrakis(bromomethyl)benzene (1.00 g, 2.23 mmol) was added and the solution was allowed to warm to room temperature. After stirring for 24 h at room temperature, distilled water (30 mL) was added to the reaction mixture. The reaction mixture was concentrated under reduced pressure. The product was crystallized by adding ethyl acetate and cooled overnight to yield a light tan crystalline product separated. (0.800 g, 80 % yield) The ^{1}H-NMR and unit cell parameters were consistent with those reported in the literature.[68]

3.3.4 Synthesis of [Co ($HBTC^{2-}$)(**L**)$_{0.5}$(H_2O)]·H_2O (**3.1**)

A mixture of $CoCl_2 \cdot 6H_2O$ (0.024g, 0.10mmol), H_3BTC (0.021 g, 0.10 mmol), and **L** (0. 20 g, 0.05 mmol) in acetonitrile (2.0 mL) and water (6.0 mL) was heated at 130 °C for 3 days. After the mixture was cooled to room temperature, rectangular shaped purple crystals of **3.1** were obtained. Yield: 70%. Anal. for $C_{20}H_{19}N_4O_8Co$. Calc (%): C, 47.82; H, 3.81; N, 11.15. Found (%): C, 47.90; H, 3.66; N, 11.11.FT-IR (cm^{-1}): 3478 (m), 3281 (m), 3130 (m), 1608 (s), 1552 (s), 1431 (s), 1386 (s), 1243 (m), 1181 (m), 1097 (s), 952 (w), 837 (m), 766 (m), 737 (s), 712 (m), 654 (m), 636 (m), 515 (w).

3.3.5 Synthesis of [Co($HBTC^{2-}$)(**L**)$_{0.5}$]·1.72H_2O (**3.2**)

A mixture of $Co(NO_3)_2 \cdot 6H_2O$ (0.029g, 0.10 mmol), H_3BTC (0.021 g, 0.10 mmol), and **L** (0.020 g, 0.05 mmol) in dimethylformaldehyde (DMF) (7.0 mL) was heated at 85 °C for 6 days. After the mixture was cooled to room temperature, a mixture of

compound **3.1** and rectangular shaped light pink crystals of **3.2** were obtained. Yield: 40%. Anal. for $C_{20}H_{18.44}N_4O_{7.72}Co$. Calc (%): C, 49.47; H, 3.07; N, 12.35. Found (%): C, 49.84; H, 3.18; N, 12.16. FT-IR (cm^{-1}): 3125 (w), 1717 (m), 1626 (s), 1555 (s), 1519 (m), 1450 (m), 1388 (s), 1342 (s), 1235 (m), 1148 (m), 1111 (s), 1029 (w), 940 (m), 759 (m), 726 (s), 662 (m).

3.3.6 Synthesis of $[Co_3 (BTC^{3-})_2(\mathbf{L})(H_2O)_4] \cdot 6H_2O$ (**3.3**)

A mixture of $CoCl_2 \cdot 6H_2O$ (0.072 g, 0.30mmol), H_3BTC (0.042 g, 0.20 mmol), NaOH (0.024 g, 0.60 mmol), and **L** (0.39 g, 0.10 mmol) in CH_3CN (4.0 mL) and water (4.0 mL) was heated at 130 °C for 5 days. After the mixture was cooled to room temperature, rod shaped purple crystals of **3.3** were obtained. Yield: 40%. Anal. for $C_{20}H_{24}N_4O_{11}Co_{1.5}$. Calc (%): C, 41.07; H, 4.14; N, 9.58. Found (%): C, 40.68; H, 3.75; N, 9.38. FT- IR (cm^{-1}): 3446 (w), 3112 (s), 1638 (s), 1619(s), 1576 (m), 1520 (m), 1436 (m), 1386 (s), 1357 (s), 1111 (m), 1098 (m), 1029 (w), 935 (w), 823(m), 774 (s), 731 (m), 660 (m).

3.4 Structural Description

3.4.1 $[Co(HBTC^{2-})(\mathbf{L})_{0.5}(H_2O)] \cdot H_2O$ (**3.1**)

The cobalt metal coordination environment of **3.1** with atom numbering scheme is shown in figure 1. The asymmetric unit contains one octahedral cobalt(II) ion, $HBTC^{2-}$ anion, one coordinated water molecule, a half of a **L** ligand that uses only two imidazole groups, and a lattice water molecule. Compound **3.1** forms a two-dimensional(2D) neutral network that consists of cobalt(II), $HBTC^{2-}$, and **L**. The cobalt(II) ion (Co1) has distorted octahedral geometry formed by the coordination of two η^2-$HBTC^{2-}$, a water

oxygen atom, and an imidazole nitrogen atom from **L** (Figure 3.1). Selected bond distances for compound **3.1** are given in Table 3.2.

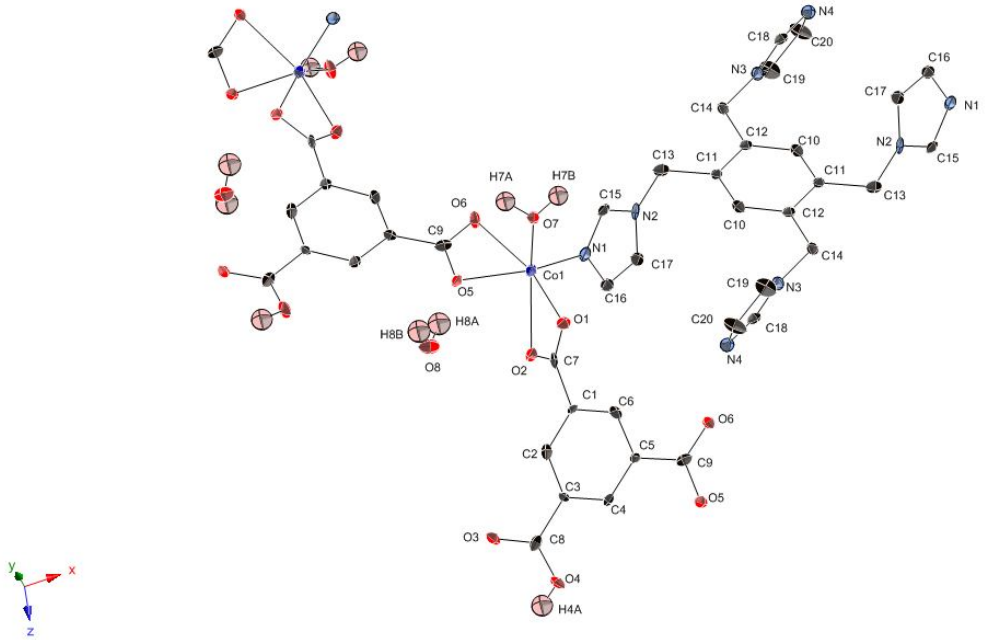

Figure 3.1 Coordination environment of cobalt (II) ion in **3.1** with the ellipsoids drawn at the 50 % probability level.

Table 3.2 Selected bond distances (Å) and angles (°) for compound **3.1.**

Bond distances	(Å)
N(1)-Co(1)	2.031(4)
O(1)-Co(1)	2.043(3)
O(2)-Co(1)	2.405(3)
O(7)-Co(1)	2.031(3)
Co(1)-O(5)#	2.056(3)
Co(1)-O(6)#	2.391(3)
Bond angles	(°)
N(1)-Co(1)-O(7)	105.71(16)
N(1)-Co(1)-O(1)	101.29(14)
O(7)-Co(1)-O(1)	95.47(13)
N(1)-Co(1)-O(5)#	142.53(14)

O(7)-Co(1)-O(5)#	94.97(13)
O(1)-Co(1)-O(5)#	107.54(13)
N(1)-Co(1)-O(6)#	90.79(13)
O(7)-Co(1)-O(6)#	87.99(12)
O(1)-Co(1)-O(6)#	165.98(13)
O(5)#-Co(1)-O(6)#	58.55(12)
N(1)-Co(1)-O(2)	91.32(13)
O(7)-Co(1)-O(2)	151.84(12)
O(1)-Co(1)-O(2)	58.66(11)
O(5)#-Co(1)-O(2)	83.90(12)
O(6)#-Co(1)-O(2)	114.52(11)

Symmetry transformations used to generate equivalent atoms: #; x+1/2,-y+1/2,z+1/2

The network architecture of **3.1**, can be described as 2D corrugated sheet: It is constructed from an $HBTC^{2-}$ ligand in coordination mode I (Scheme 3.2-(I)) and a bridging mode I of **L** ligand (Scheme 3.1-(I)). The octahedral cobalt ion and chelating $HBTC^{2-}$ groups link to make 1D chains. The $[Co(HBTC^{2-})]_n$ chains are linked in a second dimension by two imidazole nitrogen atoms of a single ligand, **L.** The remaining two imidazole nitrogen atoms of **L** remain uncoordinated. The 2D sheet motif is severely corrugated with an acute dihedral angle of 45.1° (Figure 3.2a).

(a)

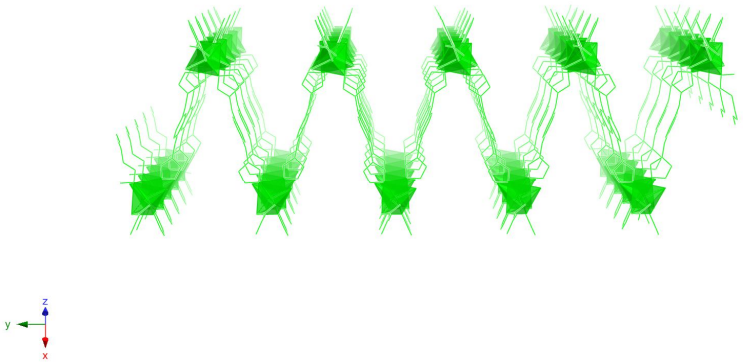

Figure 3.2 (a) A schematic representation of the 2D zigzag sheet of compound **3.1**. The acute dihedral angle is 45.1°.

(b)

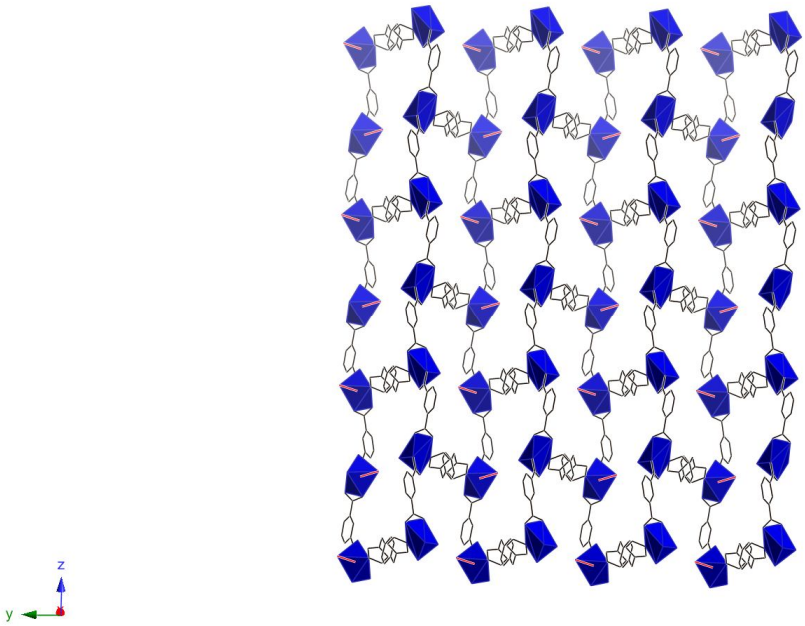

Figure 3.2 (b) A schematic representation of the 2D network of **3.1**. Polyhedral represents Co(II) and $HBTC^{2-}$ and **L** are shown as sticks.

The 2D zigzag sheets are layered to form like a zipper-like structure when viewed on Figure 3.3; hydrogen bonds between the free acid groups of $HBTC^{2-}$ from one layer to the uncoordinated imidazole nitrogen atom from an adjacent layer connect the layers. Interlayer water molecules are also involved in the hydrogen bonding.

(a)

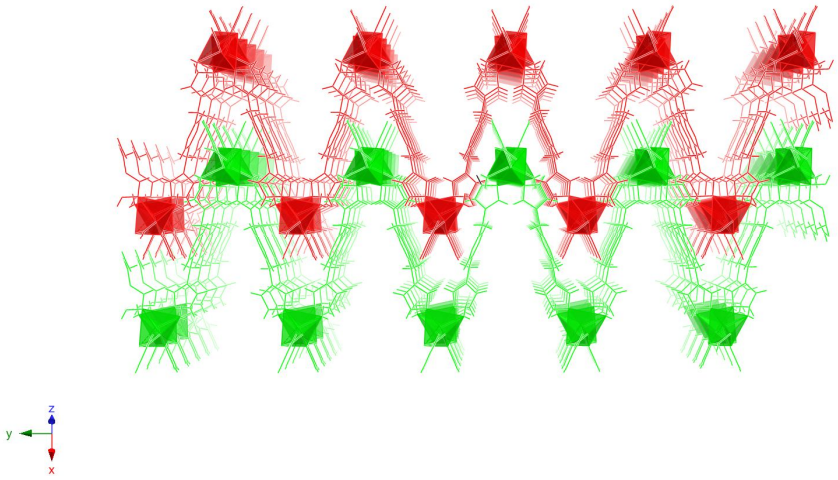

(b)

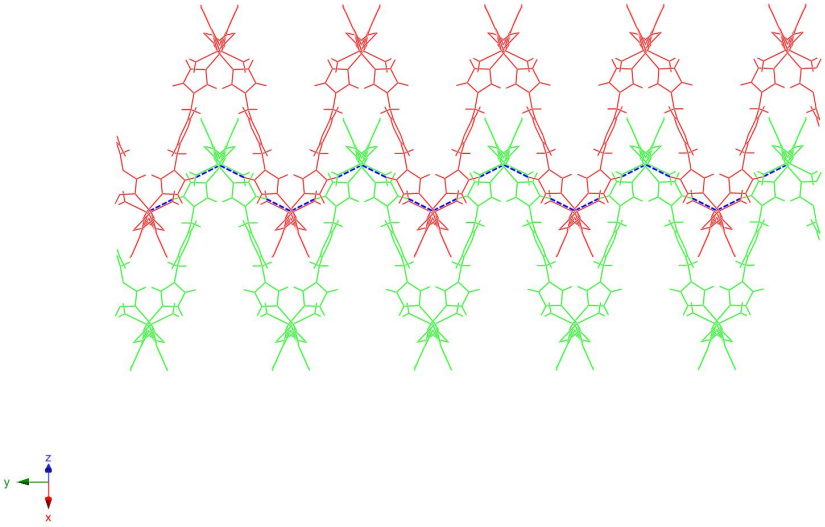

Figure 3.3 (a) Corrugated shape of extended networks of **3.1**. (b) 2D sheets of compound **3.1** are interlinked via hydrogen bonds to have a zipper-like structure. Hydrogen bonds are shown in blue dotted lines.

3.4.2 $[Co(HBTC^{2-})(\mathbf{L})_{0.5}]\cdot 1.72H_2O$ (**3.2**)

The cobalt metal coordination environment of **3.2** with atom numbering scheme is shown in figure 3.4. Selected bond length and angles are given in Table 3.3.

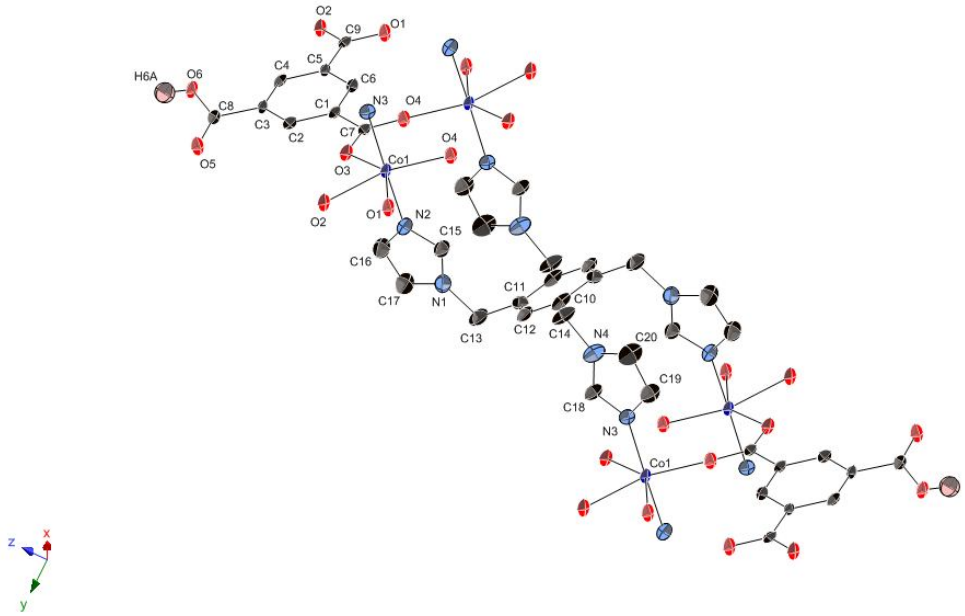

Figure 3.4 Coordination environment of cobalt (II) ion in **3.2** with the ellipsoids drawn at the 50 % probability level. Partially occupied lattice water molecules are omitted for clarity.

Table 3.3 Selected bond distances (Å) and angles (°) for compound **3.2.**

Bond distances	(Å)
N(2)-Co(1)	2.086(3)
N(3)-Co(1)	2.098(3)
O(1)-Co(1)	2.167(3)
O(2)-Co(1)	2.284(3)
O(3)-Co(1)	2.048(2)
O(4)-C(7)#	1.244(5)
O(4)-Co(1)	2.042(3)

C(7)-O(3)	1.260(4)
C(8)-O(5)	1.202(5)
C(8)-O(6)	1.335(4)
C(9)-O(1)	1.250(5)
C(9)-O(2)	1.275(4)
Bond angles	(°)
O(4)-Co(1)-O(3)	127.29(11)
O(4)-Co(1)-N(2)	89.65(13)
O(3)-Co(1)-N(2)	88.37(12)
O(4)-Co(1)-N(3)	90.05(13)
O(3)-Co(1)-N(3)	87.89(11)
N(2)-Co(1)-N(3)	175.07(13)
O(4)-Co(1)-O(1)	88.30(11)
O(3)-Co(1)-O(1)	144.40(11)
N(2)-Co(1)-O(1)	91.43(12)
N(3)-Co(1)-O(1)	93.48(12)
O(4)-Co(1)-O(2)	146.86(10)
O(3)-Co(1)-O(2)	85.73(10)
N(2)-Co(1)-O(2)	94.59(12)
N(3)-Co(1)-O(2)	88.34(12)
O(1)-Co(1)-O(2)	58.79(9)

Symmetry transformations used to generate equivalent atoms: #;-x+1,-y,-z

The asymmetric unit contains one octahedral cobalt(II) ion, one $HBTC^{2-}$ anion, half of the tetradentate imidazole ligand, **L**, and 1.72 lattice water molecules. Compound **3.2,** like **3.1**, forms a neutral 2D network that consists of cobalt(II) ion, $HBTC^{2-}$, and **L**. The ligand **L** uses all four imidazole groups in the construction of the network adopting the geometry show in Scheme1, conformation mode IV. The cobalt(II) ion (Co1) has a distorted octahedral geometry; two nitrogen atoms from imidazole groups of **L** are coordinated in *trans* positions and four oxygen atoms from three different $HBTC^{2-}$ anions form a distorted square plane. The oxygen atoms (O1 and O2) from one carboxylate group form a chelate with Co1 and the other two oxygen atoms (O3 and O4)

are from two symmetry related monodentate carboxylate groups. The 2D sheets are made from two "double" chains linked by a carboxylate bridged cobalt dimer. The Co-$HBTC^{2-}$ double chain is shown in Figure 3.5a and 3.5b.

(a)

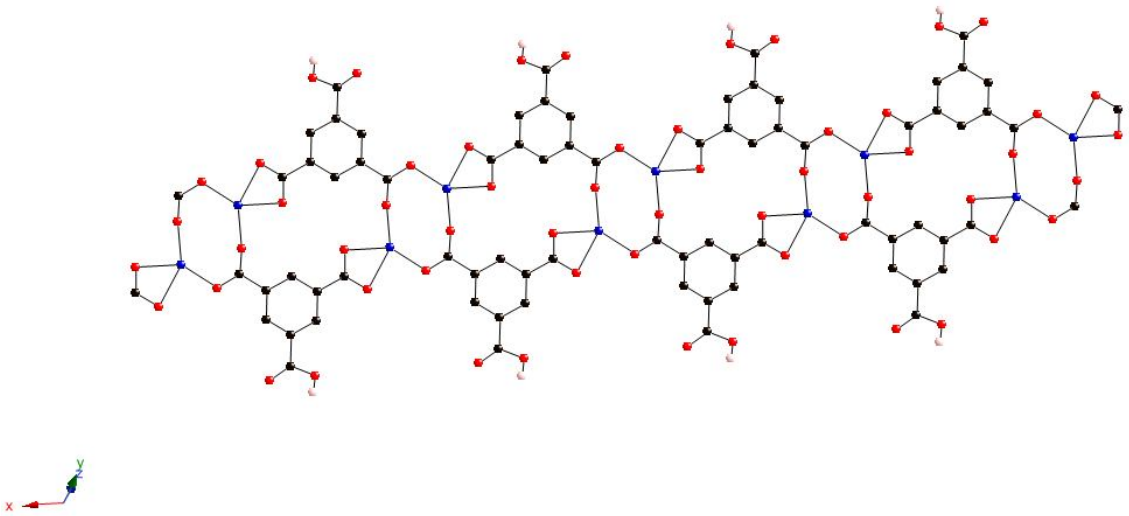

(b)

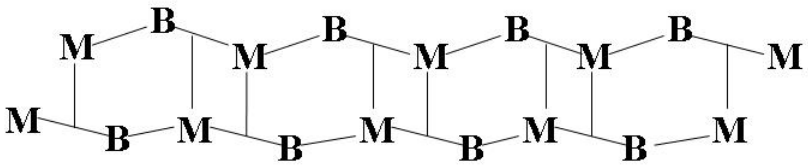

Figure 3.5 (a) In compound **3.2**, the two octahedral Co1(II) ions are coordinated with two independent $HBTC^{2-}$ ligand, which create a neutral 1D chain: cobalt(blue), oxygen(red), carbon(black), and hydrogen(pink). (b) Schematic representation of a neutral 1D chain. **M** represents Co(II) metal ion and **B** represents $HBTC^{2-}$.

The second dimension consists of Co-**L** chains as seen in Figure 3.6. The resulting sheet is relatively planar. The 2D layers are connected in the third dimension via hydrogen bonds between protonated carboxylate groups (O6-H6A···O2:2.615(2) Å) (Figure 3.6). The interlayer void spaces in compound **3.2** are filled with 1.72 water molecules, which are modeled as being disordered and showing partial occupancy.

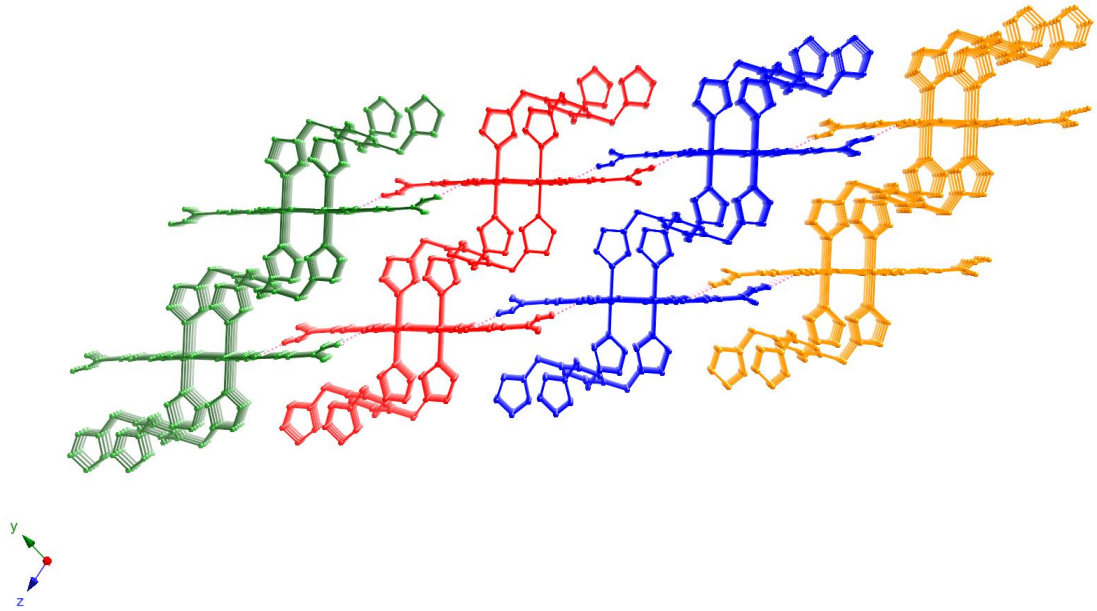

Figure 3.6 The 2D layers of compound **3.2** are interlinked via hydrogen bonds to form extended 3D networks. Each sheet is colored differently.

3.4.3 $[Co_3(BTC^{3-})_2(\mathbf{L})(H_2O)_4]\cdot 6H_2O$ (**3.3**)

Compound **3.3** is a covalently bonded two-fold interpenetrating 3D neutral framework. The cobalt metal coordination environment of **3.3** with atom numbering scheme is shown in Figure 3.7. Selected bond length and angles are given in Table 3.4.

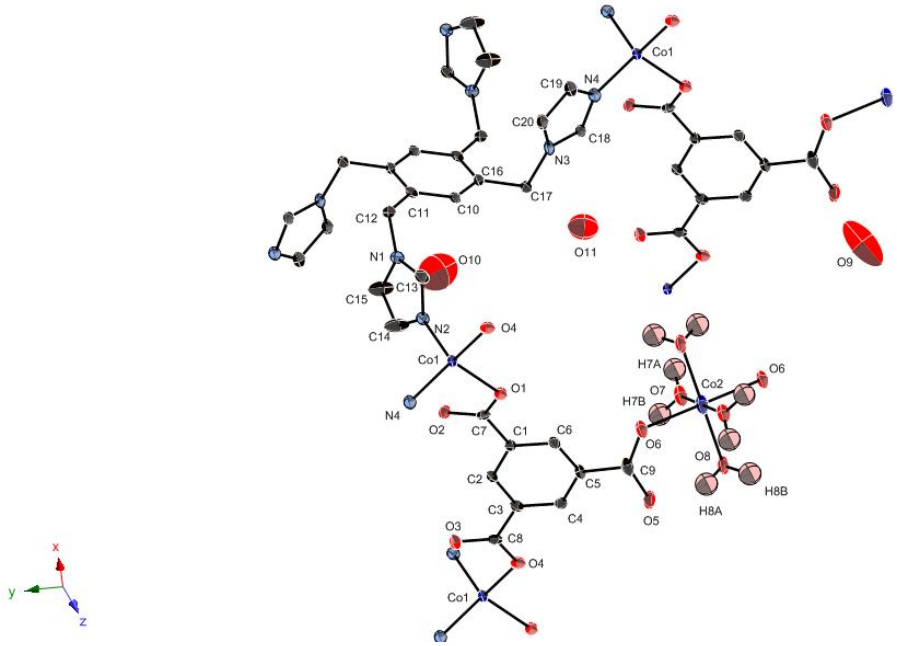

Figure 3.7 Coordination environment of cobalt (II) ion in **3.3** with the ellipsoids drawn at the 50 % probability level.

Table 3.4 Selected bond distances (Å) and angles (°) for compound **3.3**.

Bond distances	(Å)
N(2)-Co(1)	2.004(4)
N(4)-Co(1)#1	2.049(4)
O(1)-Co(1)	2.010(3)
O(4)-Co(1)#2	1.996(3)
O(6)-Co(2)	2.105(3)
O(7)-Co(2)	2.081(4)
O(8)-Co(2)	2.097(3)

Bond angles	(°)
O(4)#3-Co(1)-N(2)	106.05(13)
O(4)#3-Co(1)-O(1)	96.48(12)
N(2)-Co(1)-O(1)	116.78(14)
O(4)#3-Co(1)-N(4)#4	114.71(14)
N(2)-Co(1)-N(4)#4	111.60(15)
O(1)-Co(1)-N(4)#4	110.44(14)
O(7)#5-Co(2)-O(7)	180.000(1)
O(7)#5-Co(2)-O(8)#5	89.32(15)
O(7)-Co(2)-O(8)#5	90.68(15)
O(8)#5-Co(2)-O(8)	180.000(1)
O(7)#5-Co(2)-O(6)	87.22(13)
O(7)-Co(2)-O(6)	92.78(13)
O(8)#6-Co(2)-O(6)	90.12(13)
O(8)-Co(2)-O(6)	89.88(13)

Symmetry transformations used to generate equivalent atoms:

#1; x,y+1,z+1, #2; x+1,y,z, #3; x-1,y,z, #4; x,y-1,z-1, #5; -x+2,-y+2,-z+2

The asymmetric unit consists of one and a half cobalt(II) ions, one BTC^{3-} anion, half of **L**, and five water molecules. Co1 has tetrahedral geometry with two nitrogen atoms from **L** and two oxygen atoms from BTC^{3-} completing the coordination sphere. The octahedral Co2 sits on an inversion center and has four coordination sites in a square plane occupied by water and carboxylate groups from BTC^{3-} in axial positions. All of the three carboxylates of BTC^{3-} are coordinated η-1 and bridges two tetrahedral Co1 ions and one octahedral Co2 to form 1D ladders running parallel to the *a*-axis. An octahedral Co2 with the trans-coordinated BTC^{3-} ions forms the rungs of the ladder. The tetrahedral Co1 links each rung of the ladder via the remaining coordination sites of BTC^{3-} to form the sides of the ladder (Figure 3.8c). The tetradentate **L** links the four tetrahedral Co1 ions to form a 3D network. The conformation of **L** is the key in accommodating the 3D network.

L adopts the pinwheel conformation of IIa (Scheme 3.1). Figure 3.8 depicts the many rings and channels present in a single 3D network of **3.3**.

(a)

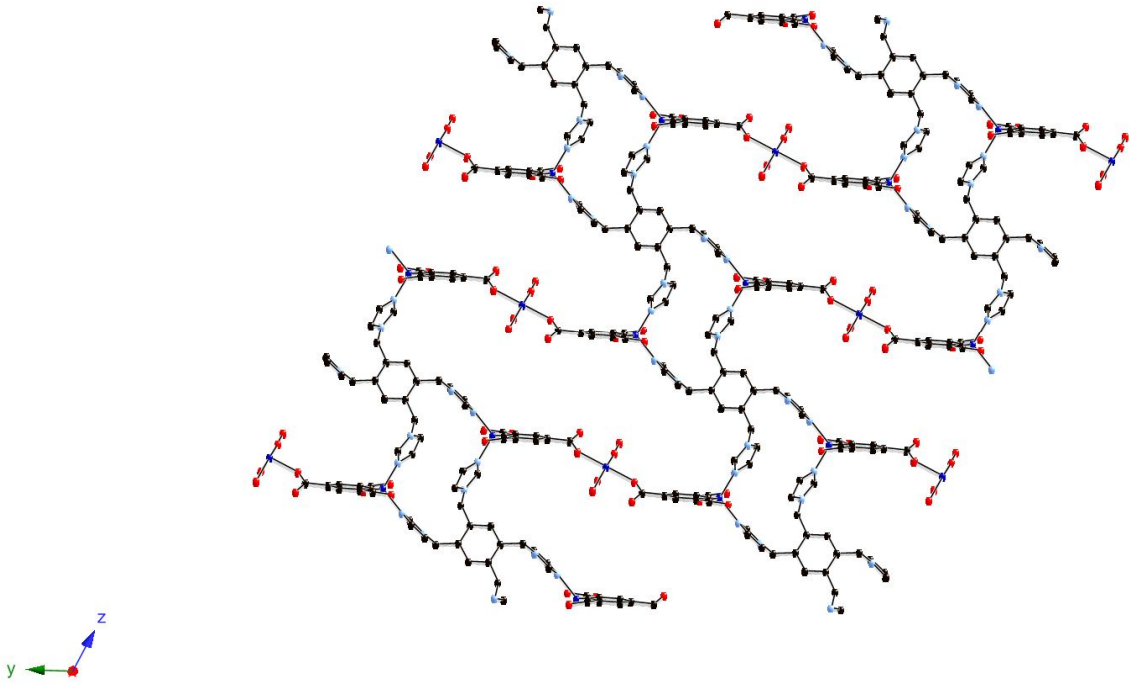

Figure 3.8 (a) Large channels and cages are formed with two octahedral cobalt ions, four tetrahedral cobalt ions, four BTC^{3-}, and two **L** ligands on y-z plane.

(b)

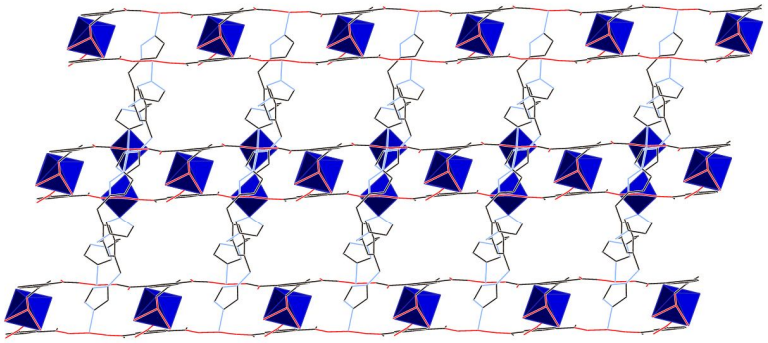

(c)

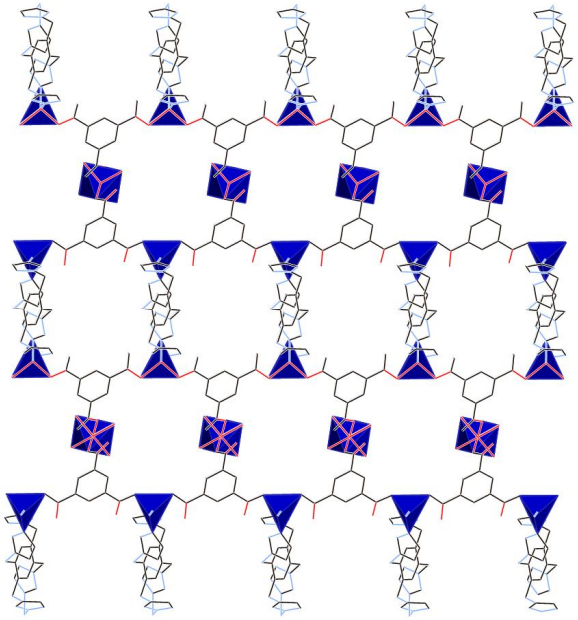

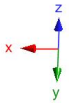

Figure 3.8 (b) View down [010] showing 1D channels. Lattice water molecules are omitted due to clarity. (c) View down [011]. The ladder structure formed by the Co(II) ions and the bridging BTC^{3-} ions is running parallel to the *a*-axis; the ligand **L** links the ladders to form a 2D network.

A mutual 3D network is interpenetrated to form a two fold 3D network structure. The interpenetrating networks fill most of the apparent voids shown in Figure 3.8, as illustrated in Figure 3.9. The large rings shown in Figure 8a are blocked by the adjacent network (Figure 3.9a). The channels parallel to the *b*-axis, however, are retained (Figure 3.8b versus Figure 3.9b). The 1D channels have a cross section of 5.4 Å × 7.4 Å. Three lattice water molecules are located in the channels; these are hydrogen bonded to the oxygen atoms of carboxylate groups from BTC^{3-} and coordinated water molecules on octahedral cobalt metal ions. The covalently bonded 3D framework of **3.3** is unique among the structures described here in that both BTC^{3-} and **L** are fully connected in the structure.

(a)

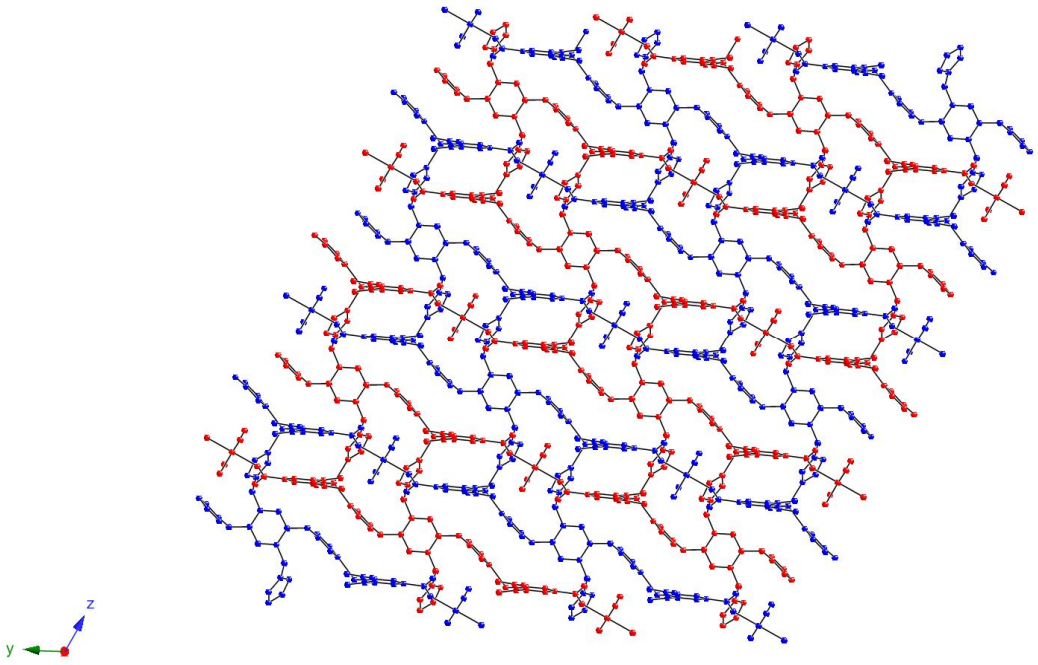

Figure 3.9 (a) View down [100] depicting how the interpenetrating networks fill the large channels and cages of the individual 3D networks shown in Figure 8a. Lattice water molecules are omitted clarity.

(b)

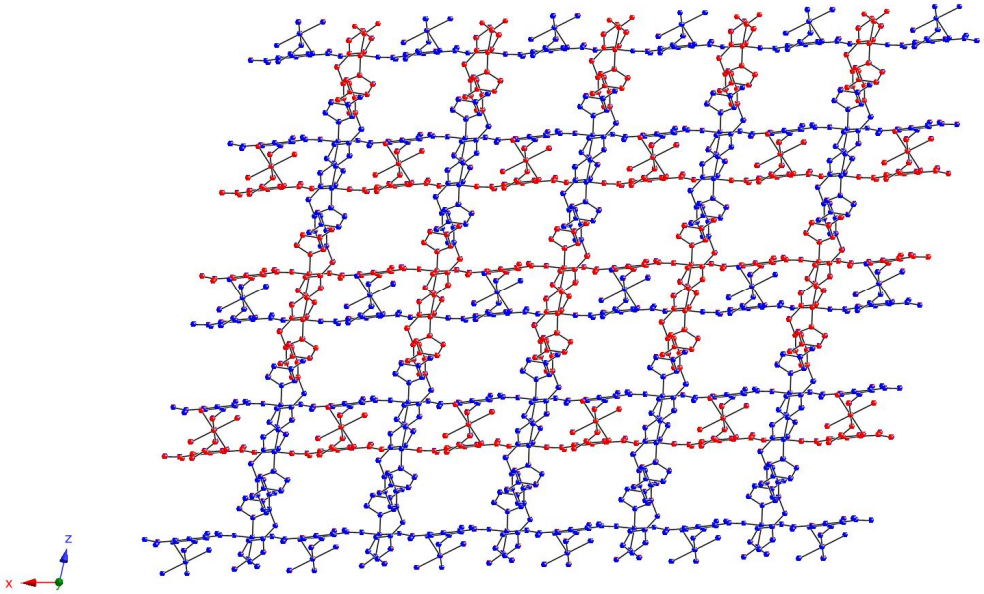

Figure 3.9 (b) View down [010] showing how the 1D channel depicted in Figure 8b is retained in the interpenetrating structure. Lattice water molecules are omitted clarity.

3.5 Thermogravimetric analysis (TGA)

TGA plots for crystalline samples of **3.1**, **3.2**, and **3.3** are shown in Figure 3.10a, 10b, and 10c, respectively. The TGA of compound **3.1** displays a weight loss of 4.0% from room temperature to 100 °C, which corresponds to the loss of the one uncoordinated lattice water molecules (calculated, 3.6%). An additional weight loss of 4.0% occurs between 130 °C to 180 °C, corresponding to the release of one coordinated water molecules (calculated, 3.6%). Decomposition begins at 250 °C.

(a)

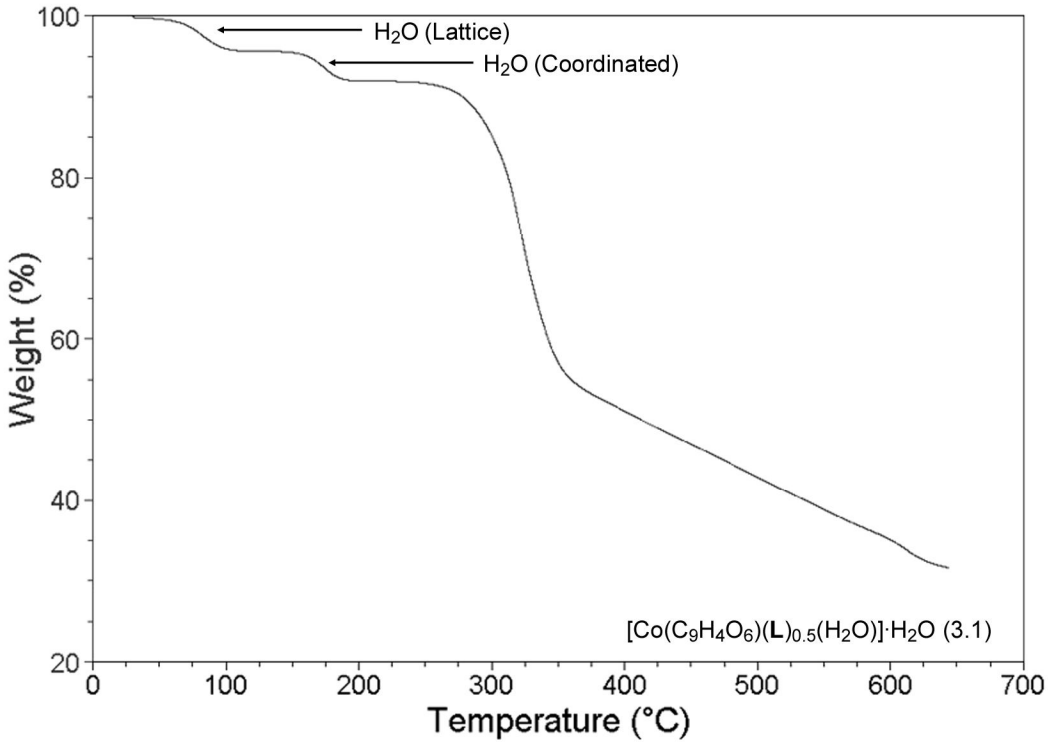

Figure 3.10 (a) The TGA plot of compound **3.1.**

The TGA of **3.2**, which has disordered lattice water molecules, displays a weight loss of 4.1% from the room temperature to 100 °C, which corresponds to the loss of most of the uncoordinated water molecules (calculated, 6.2%). Compound **3.2** begins to decompose around 320 °C.

(b)

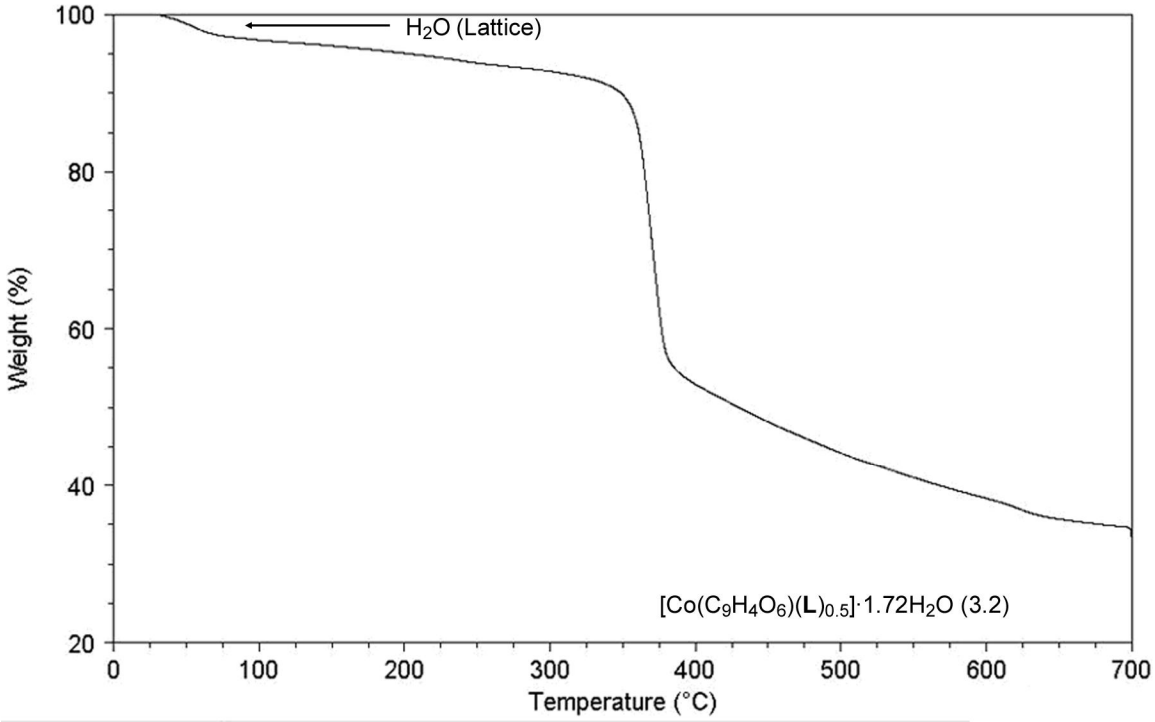

Figure 3.10 (b) The TGA plot of compound **3.2.**

The TGA of **3.3** displays a weight loss of 8.8% from room temperature to 95 °C: This corresponds to the loss of the six uncoordinated lattice water molecules (calculated, 9.2%). Subsequent weight loss of 5.5% from 100 °C to 160 °C corresponds to the release of four coordinated water molecules (calculated, 6.2%). Compound **3.3** begins to decompose at 280 °C.

(c)

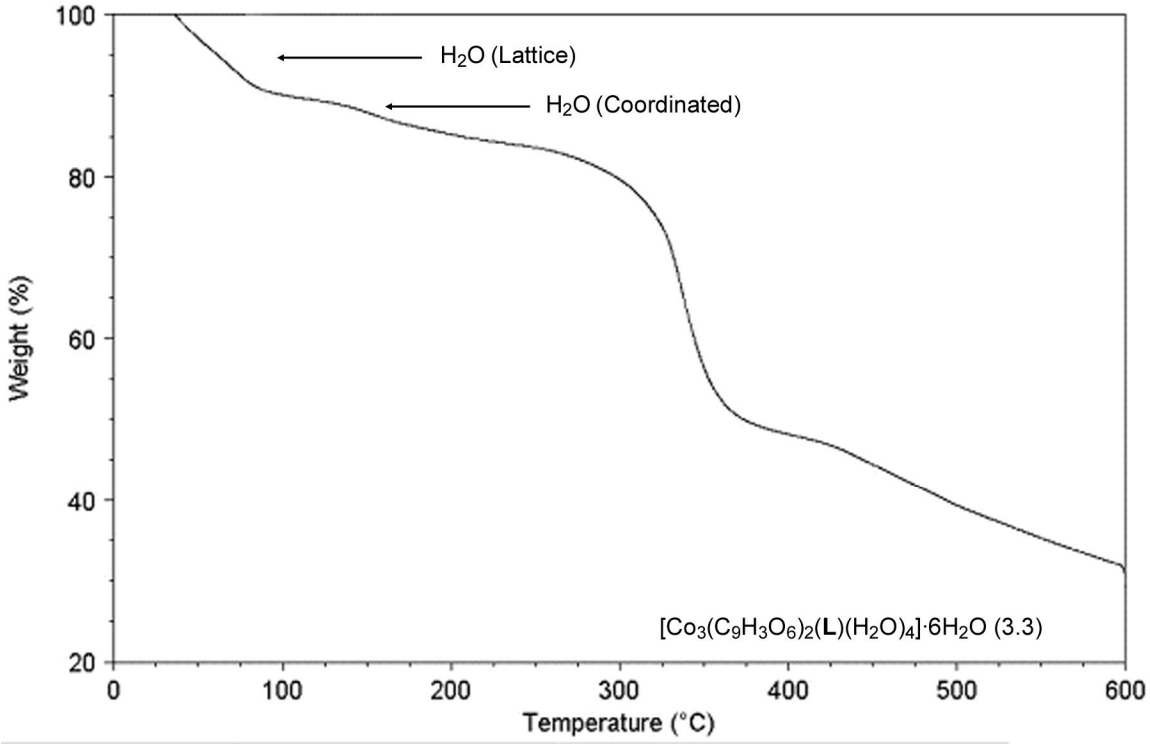

Figure 3.10 (c) The TGA plot of compound **3.3.**

The decomposition of compounds, **3.1** and **3.3**, which contain coordinated water molecules, occurs at somewhat lower temperatures than compound **3.2**. It is hypothesized that the lower stability of **3.1** and **3.3** is due to the loss of coordinated water molecules on cobalt(II). The cobalt metal ion with one or more vacant sites in the metal coordination

sphere is not sufficiently stable to keep the structure intact. In compound **3.2**, the octahedral coordination sphere on cobalt metal is coordinated to either oxygen atom of carboxylate group or nitrogen atom of imidazole ring. As a result the thermal stability for compound **3.2** is moderately increased.

3.6 Discussion

3.6.1 Coordination mode of H_3BTC

The $H_{3-x}BTC^{x-}$ anionic ligand shows different coordination modes in compounds **3.1**, **3.2**, and **3.3**. These are shown in Scheme 3.2. The $HBTC^{2-}$ adopts coordination mode I in **3.1**, II in **3.2**, and BTC^{3-} adopts III in **3.3**. Clearly, there are additional coordination modes that $H_{3-x}BTC^{x-}$ could adopt. Coordination mode I in **3.1** leads to $[Co^{2+}(HBTC^{2-})]$ neutral zig-zag chains (Figure 3.2-a). Coordination mode II in **3.2** leads to a "double" chain motif (Figure 3.5-b). The fully connected mode III in **3.3** gives a ladder motif (Figure 3.8c).

3.6.2 Coordination mode of L

In compound **3.1**, only the imidazole groups in positions 1 and 4 of **L** are coordinated to cobalt metal centers of $[Co(HBTC^{2-})]$ chains. The four methylene groups of **L** are positioned in plane so that conformation I (Scheme 3.1) is adopted. The two uncoordinated imidazole groups occupy interlayer space and hydrogen bond to the adjacent layer. In compound **3.2**, all four imidazole groups are coordinated to four cobalt ions with **L** in the chair conformation IV (Scheme 3.1). This leads to Co-**L** double chains to complete 2D sheets with Co-$HBTC^{2-}$ double chains. In compound **3.3**, **L** has the

pinwheel coordination IIa (Scheme 3.1). The pinwheel motif leads to the more complicated network connection observed in **3.3**. The shape and conformation of **L** plays an important role in constructing 3D networks. When **L** has a conformation IIa, IIb, or III, which has two diagonally positioned imidazole groups, L forms an intersection for four rods connected on the benzene ring. Thus, **L** can act as either a linear rod (1D building block) or diagonally crossed rods (2D building block).

3.6.3 Stability in crystalline network solids

The compounds **3.1** and **3.3** have coordinated water molecules on cobalt(II) metal center. When those water molecules are removed, it creates open coordination sites on cobalt metal. The loss of coordinated water molecules results in a slightly lower stability in these compared to **3.2**, which has fully coordinated cobalt in the network. Coordinatively unsaturated cobalt is inherently more reactive than fully coordinated cobalt; this is very likely the origin of the lower stability.

3.7 Conclusion

In this paper, we report the synthesis and structural analyses of three different structures of crystalline coordination networks that were prepared using a mixed ligand system that includes an anionic ligand $H_{3-x}BTC^{x-}$ and a neutral ligand with four imidazole groups, **L**. The coordination variability of both H_3BTC and **L** appears to be the key factor in the production of different topologies. Since all of the compounds are prepared under similar conditions, the difference in temperature and choice of solvents also influences the resulting crystalline product. This work contributes to the development of materials for synthesis with a mixed ligand system.

3.8 References

1. Eddaoudi, M.; Moler, D. B.; Li, H.; Chen, B.; Reineke, T. M.; O'Keeffe, M.; Yaghi, O. M., *Acc. Chem. Res.* **2001,** *34*, 319-330.
2. Farha, O. K.; Hupp, J. T., *Acc. Chem. Res. 43*, 1166-1175.
3. Fischer, R. A.; Woell, C., *Angew. Chem., Int. Ed.* **2008,** *47*, 8164-8168.
4. James, S. L., *Chem. Soc. Rev.* **2003,** *32*, 276-288.
5. Kitagawa, S.; Matsuda, R., *Coord. Chem. Rev.* **2007,** *251*, 2490-2509.
6. Lee, J. Y.; Farha, O. K.; Roberts, J.; Scheidt, K. A.; Nguyen, S. B. T.; Hupp, J. T., *Chem. Soc. Rev.* **2009,** *38*, 1450-1459.
7. Perry, J. J. I. V.; Perman, J. A.; Zaworotko, M. J., *Chem. Soc. Rev.* **2009,** *38*, 1400-1417.
8. Tranchemontagne, D. J.; Mendoza-Cortes, J. L.; O'Keeffe, M.; Yaghi, O. M., *Chem. Soc. Rev.* **2009,** *38*, 1257-1283.
9. Yaghi, O. M., *Nat. Mater.* **2007,** *6*, 92-93.
10. Kitagawa, S.; Kitaura, R.; Noro, S.-i., *Angew. Chem., Int. Ed.* **2004,** *43*, 2334-2375.
11. Kitagawa, S.; Noro, S.-i.; Nakamura, T., *Chem. Commun. (Cambridge, U. K.)* **2006**, 701-707.
12. Ferey, G., *Stud. Surf. Sci. Catal.* **2007,** *170A*, 66-86.
13. Cheetham, A. K.; Rao, C. N. R.; Feller, R. K., *Chem. Commun. (Cambridge, U. K.)* **2006**, 4780-4795.
14. Moulton, B.; Zaworotko, M. J., *Chem. Rev. (Washington, D. C.)* **2001,** *101*, 1629-1658.
15. Zaworotko, M. J., *Angew. Chem., Int. Ed.* **1998,** *37*, 1211-1213.
16. Chen, B.; Ockwig, N. W.; Fronczek, F. R.; Contreras, D. S.; Yaghi, O. M., *Inorg. Chem.* **2005,** *44*, 181-183.
17. Furukawa, H.; Kim, J.; Ockwig, N. W.; O'Keeffe, M.; Yaghi, O. M., *J. Am. Chem. Soc.* **2008,** *130*, 11650-11661.
18. Batten, S. R.; Robson, R., *Angew. Chem., Int. Ed.* **1998,** *37*, 1461-1494.
19. Batten, S. R.; Robson, R., *Mol. Catenanes, Rotaxanes Knots* **1999**, 77-106.
20. Robson, R., *Dalton* **2000**, 3735-3744.
21. Li, J.-R.; Kuppler, R. J.; Zhou, H.-C., *Chem. Soc. Rev.* **2009,** *38*, 1477-1504.
22. Czaja, A. U.; Trukhan, N.; Muller, U., *Chem. Soc. Rev.* **2009,** *38*, 1284-1293.
23. Ma, S.; Zhou, H.-C., *Chem. Commun. (Cambridge, U. K.) 46*, 44-53.
24. Hinks, N. J.; McKinlay, A. C.; Xiao, B.; Wheatley, P. S.; Morris, R. E., *Microporous Mesoporous Mater.* **2009,** *129*, 330-334.
25. Qiu, S.; Zhu, G., *Coord. Chem. Rev.* **2009,** *253*, 2891-2911.
26. Hong, D.-Y.; Hwang, Y. K.; Serre, C.; Ferey, G.; Chang, J.-S., *Adv. Funct. Mater.* **2009,** *19*, 1537-1552.
27. Farrusseng, D.; Mirodatos, C., *Des. Heterog. Catal.* **2009**, 161-194.
28. Farrusseng, D.; Aguado, S.; Pinel, C., *Angew. Chem., Int. Ed.* **2009,** *48*, 7502-7513.
29. Li, H.; Eddaoudi, M.; O'Keeffe, M.; Yaghi, M., *Nature (London)* **1999,** *402*, 276-279.

30. Ockwig, N. W.; Delgado-Friedrichs, O.; O'Keeffe, M.; Yaghi, O. M., *Acc. Chem. Res.* **2005,** *38*, 176-182.
31. O'Keeffe, M.; Peskov, M. A.; Ramsden, S. J.; Yaghi, O. M., *Acc. Chem. Res.* **2008,** *41*, 1782-1789.
32. Tranchemontagne, D. J.; Ni, Z.; O'Keeffe, M.; Yaghi, O. M., *Angew. Chem., Int. Ed.* **2008,** *47*, 5136-5147.
33. Rowsell, J. L. C.; Yaghi, O. M., *Microporous Mesoporous Mater.* **2004,** *73*, 3-14.
34. Banerjee, R.; Furukawa, H.; Britt, D.; Knobler, C.; O'Keeffe, M.; Yaghi, O. M., *J. Am. Chem. Soc.* **2009,** *131*, 3875-3877.
35. Wang, Z.; Cohen, S. M., *Chem. Soc. Rev.* **2009,** *38*, 1315-1329.
36. Burrows, A. D.; Frost, C.; Mahon, M. F.; Richardson, C., *Angew. Chem., Int. Ed.* **2008,** *47*, 8482-8486.
37. Gadzikwa, T.; Lu, G.; Stern, C. L.; Wilson, S. R.; Hupp, J. T.; Nguyen, S. T., *Chem. Commun. (Cambridge, U. K.)* **2008**, 5493-5495.
38. Morris, W.; Doonan, C. J.; Furukawa, H.; Banerjee, R.; Yaghi, O. M., *J. Am. Chem. Soc.* **2008,** *130*, 12626-12627.
39. Song, Y.-F.; Cronin, L., *Angew. Chem., Int. Ed.* **2008,** *47*, 4635-4637.
40. Wang, Z.; Cohen, S. M., *J. Am. Chem. Soc.* **2009,** *131*, 16675-16677.
41. Garibay, S. J.; Wang, Z.; Tanabe, K. K.; Cohen, S. M., *Inorg. Chem. (Washington, DC, U. S.)* **2009,** *48*, 7341-7349.
42. Tanabe, K. K.; Cohen, S. M., *Angew. Chem., Int. Ed.* **2009,** *48*, 7424-7427, S7424/1-S7424/15.
43. Wu, C.-D.; Hu, A.; Zhang, L.; Lin, W., **2005,** *127*, 8940-8941.
44. Wu, C.-D.; Lin, W., **2007,** *46*, 1075-1078.
45. Wang, Z.; Cohen, S. M., *Angew. Chem., Int. Ed.* **2008,** *47*, 4699-4702.
46. Wang, Z.; Cohen, S. M., *J. Am. Chem. Soc.* **2007,** *129*, 12368-12369.
47. Dinca, M.; Dailly, A.; Liu, Y.; Brown, C. M.; Neumann, D. A.; Long, J. R., *J. Am. Chem. Soc.* **2006,** *128*, 16876-16883.
48. Dinca, M.; Long, J. R., *J. Am. Chem. Soc.* **2007,** *129*, 11172-11176.
49. Murray, L. J.; Dinca, M.; Long, J. R., *Chem. Soc. Rev.* **2009,** *38*, 1294-1314.
50. Furukawa, H.; Ko, N.; Go, Y. B.; Aratani, N.; Choi, S. B.; Choi, E.; Yazaydin, A. O.; Snurr, R. Q.; O'Keeffe, M.; Kim, J.; Yaghi, O. M., *Science (Washington, DC, U. S.) 329*, 424-428.
51. Evans, O. R.; Manke, D. R.; Lin, W., *Chem. Mater.* **2002,** *14*, 3866-3874.
52. Ouyang, X.; Chen, Z.; Liu, X.; Yang, Y.; Deng, M.; Weng, L.; Zhou, Y.; Jia, Y., *Inorg. Chem. Commun.* **2008,** *11*, 948-950.
53. Seo, J. S.; Whang, D.; Lee, H.; Jun, S. I.; Oh, J.; Jeon, Y. J.; Kim, K., *Nature (London)* **2000,** *404*, 982-986.
54. Carlucci, L.; Ciani, G.; Proserpio, D. M., *Chem. Commun. (Cambridge, U. K.)* **2004**, 380-381.
55. Lan, Y.-Q.; Li, S.-L.; Fu, Y.-M.; Xu, Y.-H.; Li, L.; Su, Z.-M.; Fu, Q., *Dalton Trans.* **2008**, 6796-6807.
56. Yang, J.; Ma, J.-F.; Liu, Y.-Y.; Ma, J.-C.; Batten, S. R., *Cryst. Growth Des.* **2008,** *8*, 4383-4393.
57. Hoskins, B. F.; Robson, R.; Slizys, D. A., *J. Am. Chem. Soc.* **1997,** *119*, 2952-2953.

58. Hoskins, B. F.; Robson, R.; Slizys, D. A., *Angew. Chem., Int. Ed. Engl.* **1997,** *36*, 2336-2338.
59. Zhao, W.; Fan, J.; Okamura, T.-a.; Sun, W.-Y.; Ueyama, N., *Microporous Mesoporous Mater.* **2005,** *78*, 265-279.
60. Fan, J.; Sun, W.-Y.; Okamura, T.-a.; Tang, W.-X.; Ueyama, N., *Inorganic Chemistry* **2003,** *42*, 3168-3175.
61. Gao, Y.; Twamley, B.; Shreeve, J. n. M., *Inorganic Chemistry* **2006,** *45*, 1150-1155.
62. Lin, J.-D.; Jia, C.-C.; Li, Z.-H.; Du, S.-W., *Inorg. Chem. Commun.* **2009,** *12*, 558-562.
63. Liu, Y.-Y.; Ma, J.-F.; Yang, J.; Su, Z.-M., *Inorg. Chem. (Washington, DC, U. S.)* **2007,** *46*, 3027-3037.
64. Cordes, D. B.; Hanton, L. R., *Inorganic Chemistry* **2007,** *46*, 1634-1644.
65. Song, L.; Du, S.-W.; Lin, J.-D.; Zhou, H.; Li, T., *Cryst. Growth Des.* **2007,** *7*, 2268-2271.
66. Weng, H.-S.; Lin, J.-D.; Long, X.-F.; Li, Z.-H.; Lin, P.; Du, S.-W., *J. Solid State Chem.* **2009,** *182*, 1408-1416.
67. Wu, J.-Y.; Lin, Y.-F.; Chuang, C.-H.; Tseng, T.-W.; Wen, Y.-S.; Lu, K.-L., *Inorg. Chem. (Washington, DC, U. S.)* **2008,** *47*, 10349-10356.
68. Xu, G.-C.; Hua, Q.; Okamura, T.-a.; Bai, Z.-S.; Ding, Y.-J.; Huang, Y.-Q.; Liu, G.-X.; Sun, W.-Y.; Ueyama, N., *CrystEngComm* **2009,** *11*, 261-270.
69. Zhao, S.-B.; Wang, R.-Y.; Wang, S., *Inorganic Chemistry* **2006,** *45*, 5830-5840.
70. Natarajan, R.; Savitha, G.; Dominiak, P.; Wozniak, K.; Moorthy, J. N., *Angew. Chem., Int. Ed.* **2005,** *44*, 2115-2119.
71. Fan, J.; Hanson, B. E., **2005,** *44*, 6998-7008.
72. Kepert, C. J.; Rosseinsky, M. J., *Chem. Commun. (Cambridge)* **1998**, 31-32.
73. Yaghi, O. M.; Davis, C. E.; Li, G.; Li, H., *J. Am. Chem. Soc.* **1997,** *119*, 2861-2868.
74. Yaghi, O. M.; Li, G.; Li, H., *Nature (London)* **1995,** *378*, 703-6.
75. Choi, H. J.; Suh, M. P., *J. Am. Chem. Soc.* **1998,** *120*, 10622-10628.
76. Livage, C.; Guillou, N.; Marrot, J.; Ferey, G., *Chem. Mater.* **2001,** *13*, 4387-4392.
77. Wen, L.-L.; Dang, D.-B.; Duan, C.-Y.; Li, Y.-Z.; Tian, Z.-F.; Meng, Q.-J., *Inorg. Chem.* **2005,** *44*, 7161-7170.
78. Qi, Y.; Luo, F.; Che, Y.; Zheng, J., *Cryst. Growth Des.* **2008,** *8*, 606-611.
79. Ma, B.-Q.; Mulfort, K. L.; Hupp, J. T., *Inorganic Chemistry* **2005,** *44*, 4912-4914.
80. Lu, J. Y.; Lawandy, M. A.; Li, J.; Yuen, T.; Lin, C. L., *Inorganic Chemistry* **1999,** *38*, 2695-2704.
81. Du, M.; Jiang, X.-J.; Zhao, X.-J., *Inorganic Chemistry* **2006,** *45*, 3998-4006.
82. Du, M.; Jiang, X.-J.; Zhao, X.-J., *Inorg. Chem. (Washington, DC, U. S.)* **2007,** *46*, 3984-3995.
83. Habib, H. A.; Sanchiz, J.; Janiak, C., *Dalton Trans.* **2008**, 1734-1744.
84. Liu, M.; Li, X.; Li, J.; Sun, W.; Yang, Z.; Gong, F.; Chen, J.; Ma, J.; Yang, G., *Transition Met. Chem. (Dordrecht, Neth.)* **2009,** *34*, 185-190.
85. Shi, Z.; Li, G.; Wang, L.; Gao, L.; Chen, X.; Hua, J.; Feng, S., *Cryst. Growth Des.* **2004,** *4*, 25-27.
86. Murai, S.; Mikoshiba, S.; Sumino, H.; Hayase, S., **2002,** *148*, 33-39.

87. *CrysAlisPro 171*, Oxford Diffraction: Wroclaw, Poland, 2004.
88. Farrugia, L. J., *J. Appl. Crystallogr.* **1999,** *32*, 837-838.
89. Altomare, A.; Cascarano, G.; Giacovazzo, C.; Guagliardi, A., *J. Appl. Crystallogr.* **1993,** *26*, 343-50.
90. Sheldrick, G. M., *Acta Crystallogr., Sect. A: Found. Crystallogr.* **2008,** *A64*, 112-122.
91. Dinca, M.; Long, J. R., *Angewandte Chemie, International Edition* **2008,** *47*, 6766-6779.
92. Mueller, U.; Schubert, M.; Teich, F.; Puetter, H.; Schierle-Arndt, K.; Pastre, J., *J. Mater. Chem.* **2006,** *16*, 626-636.
93. Rowsell, J. L. C.; Yaghi, O. M., *Angewandte Chemie, International Edition* **2005,** *44*, 4670-4679.
94. Thomas, K. M., *Dalton Trans.* **2009**, 1487-1505.
95. Shimomura, S.; Bureekaew, S.; Kitagawa, S., *Struct. Bonding (Berlin, Ger.)* **2009,** *132*, 51-86.
96. Yaghi, O. M.; O'Keeffe, M.; Ockwig, N. W.; Chae, H. K.; Eddaoudi, M.; Kim, J., *Nature (London, U. K.)* **2003,** *423*, 705-714.
97. Zaworotko, M. J., *Angewandte Chemie, International Edition* **2000,** *39*, 3052-3054.
98. Ferey, G., *Dalton Trans.* **2009**, 4400-4415.
99. Ferey, G., *Chem. Soc. Rev.* **2008,** *37*, 191-214.
100. Kitagawa, S.; Kitaura, R.; Noro, S.-i., *Angewandte Chemie, International Edition* **2004,** *43*, 2334-2375.
101. Batten, S. R., *J. Solid State Chem.* **2005,** *178*, 2475-2479.
102. Carlucci, L.; Ciani, G.; Proserpio, D. M., *Coord. Chem. Rev.* **2003,** *246*, 247-289.
103. Batten, S. R.; Robson, R., *Angewandte Chemie, International Edition* **1998,** *37*, 1461-1494.
104. Li, Z.-X.; Xu, Y.; Zuo, Y.; Li, L.; Pan, Q.; Hu, T.-L.; Bu, X.-H., *Crystal Growth & Design* **2009,** *9*, 3904-3909.
105. Li, Z.-X.; Hu, T.-L.; Ma, H.; Zeng, Y.-F.; Li, C.-J.; Tong, M.-L.; Bu, X.-H., *Crystal Growth & Design 10*, 1138-1144.
106. Yang, J.; Ma, J.-F.; Liu, Y.-Y.; Ma, J.-C.; Batten, S. R., *Crystal Growth & Design* **2008,** *8*, 4383-4393.
107. Carlucci, L.; Ciani, G.; Proserpio, D. M.; Spadacini, L., **2004,** *6*, 96-101.
108. Willans, C. E.; French, S.; Barbour, L. J.; Gertenbach, J.-A.; Junk, P. C.; Lloyd, G. O.; Steed, J. W., *Dalton Trans.* **2009**, 6480-6482.
109. Xu, G.-C.; Ding, Y.-J.; Okamura, T.-a.; Huang, Y.-Q.; Bai, Z.-S.; Hua, Q.; Liu, G.-X.; Sun, W.-Y.; Ueyama, N., *Crystal Growth & Design* **2009,** *9*, 395-403.
110. Zhang, Z.-H.; Song, Y.; Okamura, T.; Hasegawa, Y.; Sun, W.-Y.; Ueyama, N., *Inorg. Chem.* **2006,** *45*, 2896-2902.
111. Liu, Y.; Qi, Y.; Lv, Y.-Y.; Che, Y.-X.; Zheng, J.-M., *Crystal Growth & Design* **2009,** *9*, 4797-4801.
112. Yang, G.-S.; Lan, Y.-Q.; Zang, H.-Y.; Shao, K.-Z.; Wang, X.-L.; Su, Z.-M.; Jiang, C.-J., *CrystEngComm* **2009,** *11*, 274-277.
113. Qi, Y.; Che, Y.-X.; Zheng, J.-M., *Crystal Growth & Design* **2008,** *8*, 3602-3608.

114. Chu, Q.; Liu, G.-X.; Huang, Y.-Q.; Wang, X.-F.; Sun, W.-Y., *Dalton Trans.* **2007**, 4302-4311.
115. Fan, J.; Yee, G. T.; Wang, G.; Hanson, B. E., *Inorg. Chem.* **2006,** *45*, 599-608.
116. Fan, J.; Hanson, B. E., *Inorg. Chem.* **2005,** *44*, 6998-7008.
117. Li, L.; Hu, T.-L.; Li, J.-R.; Wang, D.-Z.; Zeng, Y.-F.; Bu, X.-H., *CrystEngComm* **2007,** *9*, 412-420.
118. Li, J.-R.; Tao, Y.; Yu, Q.; Bu, X.-H., *Chemical Communications (Cambridge, United Kingdom)* **2007**, 1527-1529.
119. Marin, G.; Andruh, M.; Madalan, A. M.; Blake, A. J.; Wilson, C.; Champness, N. R.; Schroeder, M., *Crystal Growth & Design* **2008,** *8*, 964-975.
120. Tanaka, D.; Horike, S.; Kitagawa, S.; Ohba, M.; Hasegawa, M.; Ozawa, Y.; Toriumi, K., *Chemical Communications (Cambridge, United Kingdom)* **2007**, 3142-3144.
121. Akimoto, K.; Kondo, Y.; Endo, K.; Yamada, M.; Aoyama, Y.; Hamada, F., *Tetrahedron Letters* **2008,** *49*, 7361-7363.
122. Ma, S.; Sun, D.; Simmons, J. M.; Collier, C. D.; Yuan, D.; Zhou, H.-C., *Journal of the American Chemical Society* **2008,** *130*, 1012-1016.
123. Nelson, A. P.; Parrish, D. A.; Cambrea, L. R.; Baldwin, L. C.; Trivedi, N. J.; Mulfort, K. L.; Farha, O. K.; Hupp, J. T., *Crystal Growth & Design* **2009,** *9*, 4588-4591.
124. Xu, L.; Choi, E.-Y.; Kwon, Y.-U., *J. Solid State Chem.* **2008,** *181*, 3185-3188.
125. Zhu, S.; Zhang, H.; Zhao, Y.; Shao, M.; Wang, Z.; Li, M., *J. Mol. Struct.* **2008,** *892*, 420-426.
126. Hu, Y.; Li, G.; Liu, X.; Hu, B.; Bi, M.; Gao, L.; Shi, Z.; Feng, S., *CrystEngComm* **2008,** *10*, 888-893.
127. Ai, W.; He, H.; Liu, L.; Liu, Q.; Lv, X.; Li, J.; Sun, D., *CrystEngComm* **2008,** *10*, 1480-1486.
128. Hao, N.; Shen, E.; Li, Y.; Wang, E.; Hu, C.; Xu, L., *Inorg. Chem. Commun.* **2004,** *7*, 510-512.
129. Bai, H.-Y.; Ma, J.-F.; Yang, J.; Zhang, L.-P.; Ma, J.-C.; Liu, Y.-Y., *Crystal Growth & Design 10*, 1946-1959.
130. Wen, L.-L.; Wang, F.; Feng, J.; Lv, K.-L.; Wang, C.-G.; Li, D.-F., *Crystal Growth & Design* **2009,** *9*, 3581-3589.
131. Yao, J.; Lu, Z.-D.; Li, Y.-Z.; Lin, J.-G.; Duan, X.-Y.; Gao, S.; Meng, Q.-J.; Lu, C.-S., *CrystEngComm* **2008,** *10*, 1379-1383.
132. Eddaoudi, M.; Li, H.; Yaghi, O. M., *Journal of the American Chemical Society* **2000,** *122*, 1391-1397.
133. Loiseau, T.; Lecroq, L.; Volkringer, C.; Marrot, J.; Ferey, G.; Haouas, M.; Taulelle, F.; Bourrelly, S.; Llewellyn, P. L.; Latroche, M., *Journal of the American Chemical Society* **2006,** *128*, 10223-10230.
134. Kepert, C. J.; Prior, T. J.; Rosseinsky, M. J., *J. Solid State Chem.* **2000,** *152*, 261-270.
135. Ko, J. W.; Min, K. S.; Suh, M. P., *Inorg. Chem.* **2002,** *41*, 2151-2157.
136. Wang, Z.; Kravtsov, V. C.; Zaworotko, M. J., *Angewandte Chemie, International Edition* **2005,** *44*, 2877-2880.
137. Wu, Q.; Hook, A.; Wang, S., *Angewandte Chemie, International Edition* **2000,** *39*, 3933-3935.

138. Lin, X.-M.; Fang, H.-C.; Zhou, Z.-Y.; Chen, L.; Zhao, J.-W.; Zhu, S.-Z.; Cai, Y.-P., *CrystEngComm* **2009,** *11*, 847-854.
139. He, J.; Zhang, Y.; Pan, Q.; Yu, J.; Ding, H.; Xu, R., *Microporous Mesoporous Mater.* **2006,** *90*, 145-152.
140. Rebilly, J.-N.; Bacsa, J.; Rosseinsky, M. J., *Chem.--Asian J.* **2009,** *4*, 892-903.

Chapter 4

Solvothermal Synthesis and Structural Studies of Crystalline Coordination Networks with Cobalt (II) and Neutral Rigid Bis(imidazole) Ligands with Different Spacer Size and Solvent

Name of author and affiliation: Hirofumi Motegi, Carla Slebodnick, Brian E. Hanson* (tel.:001-540-231-7206, hanson@vt.edu) Department of Chemistry, Virginia Polytechnic Institute and State University, Blacksburg, VA 24061, USA

Abstract:

Six new cobalt (II) coordination networks, [Co(**L1**)(BDC^{2-})(H_2O)] •(H_2O) (**4.1**), [$Co_{0.5}$(**L2**)$_{0.5}$(BDC^{2-})$_{0.5}$] (**4.2**), [Co(**L3**)$_2$(BDC^{2-}), Co(**L3**)(BDC^{2-})(H_2O)$_2$] •2H_2O (**4.3**), [Co_3(**L3**)$_3$(BTC^{3-})$_2$(H_2O)$_2$]·10H_2O (**4.4**), [Co_4(BTC^{3-})$_2$(**L3**)$_5Cl_2$]•1.094(C_2H_3N)•7.088(H_2O) (**4.5**), and [Co_6(BTC^{3-})$_2$($HCOO^-$)$_6$(**L3**)$_3$]•x(C_3H_7NO)•y(H_2O) (**4.6**), where 1,4-bis(imidazol-1-yl)benzene (**L1**), 1,4-bis(imidazol-1-yl)naphthalene (**L2**), and 9,10-bis(imidazol-1-yl)anthracene (**L3**), 1,4-benzenedicarboxylic acid (H_2BDC), and 1,3,5-benzenetricarboxylic acid (H_3BTC), were synthesized under solvothermal conditions and characterized by single crystal X-ray diffraction analysis and thermogravimetric analysis (TGA). In **4.1**-**4.3**, the size of **L1**-**L3** determines the degree of interpenetration in the network constructed with H_2BDC ligand. In **4.4**-**4.6**, **L3** serves as a pillar building block to construct networks by applying with H_3BTC ligand.

Compound **4.1** has a five-fold interpenetrating three-dimensional (3D) network, which consists of diamond like connectivity. Compound **4.2** has a four-fold interpenetrating 3D

network, which consists of slightly stretched adamantine(similar to the structure of adamantane) cages. Compound **4.3** has a 3D network that of pores are filled with 2D layers. Compound **4.4** forms a non-interpenetrating 3D network structure with ten lattice water molecules. Compound **4.5** forms a non-interpenetrating 3D network structure with smaller pores that are filled with disordered solvent molecules. Compound **4.6** forms a non-interpenetrating 3D network structure. Solvent molecules on void space in **4.6** were not able to precisely identify. The solvent exchange experiment for **4.4** is further discussed.

Keywords:
Metal-organic framework, Solvothermal synthesis, imidazole, solvent exchange, spacer ligand

4.1 Introduction

The construction of functional crystalline inorganic and organic hybrid materials, metal-organic frameworks(MOFs) or porous coordination polymers(PCPs), is an active research topic due to the potential for the creation of solids with permanent void spaces of molecular dimension. The great variety of molecular building blocks(metal cations, anionic and neutral ligands) contributes to endless possibilities for three-dimensional (3D) structures. Potential applications of MOFs/PCPs include small molecule storage and separation based on the size and functionality of the pores within the framework architecture.[21, 22, 49, 91-95]

Although the molecular building block approach is often used to construct functional porous materials,[1, 7, 30, 32, 33, 96-100] the synthesis of crystalline coordination networks is still a challenge and relies to a great extent on trial and error to generate new

structures. Crystalline samples of MOFs/PCPs are typically formed in a one step reaction from a mixture of building blocks under solvothermal conditions. The ability to predict the final self-assembled structure becomes more difficult as the complexity and flexibility of the building blocks are increased.

The development of new crystalline MOF materials remains important in the exploration of new structural motifs. It is often the case that potential void space is consumed by the formation of interpenetrating structures.[101-103] Interpenetrating structures tend to have no void space or less accessible pore spaces. There are few systematic studies of how the degrees of interpenetrations are influenced by the size of spacer ligands, such as the different size of terminal groups and the length of core aromatic rings.[104, 105] The results in the literature show that the larger the size of terminal group results in a lower degree of interpenetration and longer the length of the spacer ligand produces a higher degree of interpenetration.

In this context we examine how the aromatic group of spacer ligands affects the formation of crystalline networks in terms of degree of interpenetration. We have chosen three bidentate imidazole containing neutral ligands, 1,4-bis(imidazol-1-yl)benzene(**L1**), 1,4-bis(imidazol-1-yl)naphthalene(**L2**), and 9,10-bis(imidazol-1-yl)anthracene(**L3**). The ligands **L2** and **L3** are new. The difference in the size of the aromatic core may influence the degree of interpenetration in the final self-assembled structure. These three neutral ligands have terminal imidazole groups linked directly to the aromatic ring system and are thus relatively rigid.

These rigid imidazole ligands have not been widely utilized in the construction of MOFs/PCPs compared to flexible imidazole ligands.[106-110] The simplest of these ligands,

L1, has previously been used to construct crystalline coordination networks.[104, 111-116] Di- or tri- carboxylate anionic ligands in combination with **L1** lead to interpenetrating 3D frameworks with first row divalent transition metals, such as Ni and Mn.[113]

Bulky aromatic ligands are difficult to work with for MOF synthesis due to their low solubility in typical hydro- or solvo- thermal synthesis. There are several reported frameworks with anthracene bridging ligands, such as 9,10-bis(N-benzimidazolyl)anthracene[117], 9,10-ditetrazolateanthracene[118], 9,10-bis(4-pyridyl)anthracene[119], 9,10-anthracenedicarboxylate[120], 9,10-bis(3,5-dicyano-1-phenyl)anthracene[121], and 5,5'-(9,10-anthracenediyl)di-isophthalate[122]. These showed interesting topologies in the resulting MOFs.

The combination of neutral ligands with di-, tri-, or tetra- carboxylate anionic ligands in the synthesis of crystalline coordination networks is a promising synthetic method in this field.[77, 79, 84, 123-131] We have chosen di- and tri- benzenetricarboxylic acids, such as 1,4-benzenedicarboxylic acid(H_2BDC) and 1,3,5-benzenetricarboxylic acid (H_3BTC), to balance the total charge of a network. These have been shown to construct excellent rigid frameworks.[132-136] H_3BTC has a triangular shape that is capable of three network connections while H_2BDC produces a linear topology with metal ions. Thus, the combination of rigid neutral and anionic ligands, **L1**-**L3** and H_2BDC or H_3BTC, in construction of MOFs/PCPs has the potential for generating framework structures. We have synthesized three interpenetrating 3D frameworks with different degrees of interpenetration and three unique non-interpenetrated covalently bonded 3D crystalline coordination frameworks with these ligands.

All of the compounds were characterized by a single crystal X-ray diffraction study and TGA. Solvent exchange was examined in compound **4.4**.

4.2 Experimental Section

4.2.1 Materials and physical measurements

All commercially available starting materials are of reagent grade and used as received without further purification. The rigid ligands were prepared by slightly modified previously reported procedure. FT-IR spectra were recorded from KBr pellets in the range 4000−400 cm^{-1} on a Perkin Elmer FT-IR Spectrum One spectrometer. Thermogravimetric analysis (TGA) measurements were performed on a TGA Q500 thermal analyzer under flowing N_2 stream with the heating rate of 10 °C•min^{-1}.

4.2.2 Synthesis of ligands

The naphthalene and anthracene based rigid neutral ligands (**L2** and **L3**) were synthesized according to a modified literature procedure.[137]

4.2.3 1,4-bis(1-imidazolyl)naphthalene (**L2)**

1,4-Dibromoanthracene(5.00 g, 17.5 mmol), imidazole(9.10 g, 134 mmol), K_2CO_3(6.20 g, 45.0 mmol), anhydrous $CuSO_4$(0.100 g, 0.600 mmol) were mixed and then placed in 250 mL Schlenk flask under N_2(g). The mixture was heated at 180 °C for 48 hours. Upon completion, the reaction mixture was light blue green. After the reaction mixture was cooled to ambient temperature, distilled water (300 mL) was added. The mixture was filtered then washed with distilled water (50.0 mL × 3) to extract unreacted imidazole, $CuSO_4$, and K_2CO_3. The filtered light tanned solids were dried and the product

was extracted with CH_2Cl_2. The organic extracts were dried over anhydrous sodium sulfate and further purified by a silica gel column with hexanes/ethyl acetate to obtain a colorless solution. Removal of the solvent yielded a white powder of **L2**. It was recrystallized from CH_3CN and H_2O to obtain white needle crystals. Yield 2.00 g, 60 %. Melting point: 175 °C. ^{1}H NMR (400 MHz, $CDCl_3$): d = 7.91 (s, 2H), 7.68(m, 2Hs), 7.65 (m, 2Hs), 7.56 (s, 2Hs), 7.39 (m, 2Hs), 7.33(m, 2Hs). ESI-MS ($C_{16}H_{12}N_4$): m/z = 261.26$[L-H]^+$.

4.2.4 9,10-bis(1-imidazolyl)anthracene (**L3**)

9,10-Dibromoanthracene(5.00 g, 14.9 mmol), imidazole(9.10 g, 134 mmol), K_2CO_3(6.20 g, 45.0 mmol), anhydrous $CuSO_4$(0.100 g, 0.600 mmol) were treated as same procedure as **L2**. The mixture was heated at 180 °C for 48 hours. Upon completion, the reaction mixture was deep brown. After the reaction mixture was cooled to ambient temperature, distilled water (300 mL) was added. The mixture was filtered then washed with distilled water (50.0 mL × 3) to extract unreacted imidazole, $CuSO_4$, and K_2CO_3. The filtered brown solids were dried and the product was extracted with CH_2Cl_2. The organic extracts were dried over anhydrous sodium sulfate and further purified by a silica gel column with hexanes/ethyl acetate to obtain a light yellow solution. Removal of the solvent yielded a light yellow powder of **L3**. Yield 2.00 g, 40 %. Melting point: 315 °C. ^{1}H NMR (400 MHz, DMSO-d^6): d = 8.10 (s, 2H), 7.67(m, 6Hs), 7.38 (m, 6Hs). ESI-MS($C_{20}H_{14}N_4$): m/z = 311.13$[L-H]^+$.

4.2.5 Synthesis of Complexes

Our synthetic protocol for the preparation of hybrid materials is to charge a heavy-walled glass tube (0.15 × 15 cm) with the solid precursors for the desired inorganic

metal ions and organic bridging ligands and 6-8 mL of water/acetonitrile(CH_3CN) or water/dimethylformamide (DMF) mixture. The glass tube is then frozen, evacuated, and sealed with a flame. The sealed tube is placed in an oven at 130 °C for up to six days. Upon cooling, the glass tube is examined and crystalline products, if any, are collected by filtration. The products are then washed with distilled water several times and dried at room temperature.

4.2.5.1 Synthesis of $[Co(C_{12}H_{10}N_4)(C_8H_4O_4)(H_2O)] \bullet(H_2O)$ (**4.1**)

Solvothermal treatment of cobalt(II) chloride hexahydrate (24.0 mg, 0.100 mmol), **L1** (21.0 mg, 0.100 mmol), benzenedicarboxylate(H_2BDC) (17.0 mg, 0.100 mmol), CH_3CN (3.0 mL), and distilled water (5.0 mL) for 3 days at 130 °C yielded purple crystalline products. The crystals were collected by filtration and washed with distilled water. Yield 30 mg. FT-IR (cm^{-1}): 3436 (m), 3131 (m), 3079 (m), 1552 (s), 1533 (s), 1399 (s), 1306 (m), 1246 (m), 1119 (m), 1066 (s), 959 (w), 834 (m), 770 (m), 728 (m), 653 (m), 546 (w), 506 (m).

4.2.5.2 Synthesis of $[Co(C_{16}H_{12}N_4)(C_8H_4O_4)]$ (**4.2**)

Solvothermal treatment of cobalt(II) chloride hexahydrate (24.0 mg, 0.100 mmol), **L2** (26.0 mg, 0.100 mmol), benzenedicarboxylate(H_2BDC) (17.0 mg, 0.100 mmol), CH_3CN (3.0 mL), and distilled water (5.0 mL) for 3 days at 130 °C yielded purple crystalline products. The crystals were collected by filtration and washed with distilled water. Yield 40 mg. FT-IR (cm^{-1}): 3435 (m), 3119 (m), 1598 (s), 1504 (m), 1353 (s), 1237 (m), 1146 (w), 1085 (m), 1037 (w), 946 (m), 828 (m), 750 (s), 656 (m), 569 (m), 508 (m).

4.2.5.3 Synthesis of $[Co(C_{20}H_{14}N_4)_2(BDC^{2-}), Co(C_{20}H_{14}N_4)(BDC^{2-})(H_2O)_2]\bullet 2H_2O$ (**4.3**)

Solvothermal treatment of cobalt(II) nitrate hexahydrate (29.0 mg, 0.100 mmol), **L3** (31.0 mg, 0.100 mmol), benzenedicarboxylate(H_2BDC) (17.0 mg, 0.100 mmol), DMF (3.0 mL), and distilled water (5.0 mL) for 3 days at 130 °C yielded a pink crystalline product. The crystals were collected by filtration and washed with distilled water. Yield 60 mg. FT-IR (cm^{-1}): 3131 (m), 3069 (m), 1567 (s), 1500 (s), 1438 (m), 1420 (s), 1390 (s), 1368 (s), 1328 (m), 1247 (w), 1220 (w), 1104 (m), 1077 (m), 1028 (m), 929 (m), 913 (m), 803 (m), 774 (s), 763 (s), 754 (s), 735 (m), 663 (m), 656 (m), 522 (w).

4.2.5.4 Synthesis of $[Co_3(C_{20}H_{14}N_4)_3(C_9H_3O_6)_2(H_2O)_2]\cdot 10H_2O$ (**4.4**)

Solvothermal treatment of cobalt(II) chloride hexahydrate (48 mg, 0.200 mmol), **L3** (31.0 mg, 0.100 mmol), benzenetricarboxylate(H_3BTC) (21.0 mg, 0.100 mmol), CH_3CN (2.0 mL), and distilled water (5.0 mL) for 3 days at 130 °C yielded a orange crystalline product. The crystals were collected by filtration and washed with distilled water. Yield 50 mg. FT-IR (cm^{-1}): 3337 (m), 3132 (m), 1618 (s), 1549 (s), 1499 (s), 1440 (s), 1364 (s), 1109 (m), 1080 (m), 1030 (m), 935 (m), 825 (w), 772 (s), 728 (m), 661 (m).

4.2.5.5 Synthesis of $[Co_2(C_9H_3O_6)(C_{20}H_{14}N_4)_{2.5}Cl]\bullet 0.547(C_2H_3N)\bullet 3.544H_2O$ (**4.5**)

Solvothermal treatment of cobalt(II) chloride hexahydrate (96.0 mg, 0.400 mmol), **L3** (93.0 mg, 0.300 mmol), benzenetricarboxylate(H_3BTC) (42.0 mg, 0.200 mmol), acetonitrile (4.0 mL), and distilled water (4.0 mL) for 7 days at 130 °C yielded a dark purple crystalline product. The crystals were collected by filtration and washed with distilled water. Yield 50 mg. FT-IR (cm^{-1}): 3401 (m), 3104 (m), 1620 (s), 1567 (m), 1519

(w), 1493 (m), 1439 (m), 1413 (m), 1363 (s), 1214 (w), 1111 (m), 1077 (m), 1028 (m), 932 (w), 911 (w), 768 (s), 723 (m), 711 (m), 660 (s), 604 (w), 568 (w).

4.2.5.6 Synthesis of $[Co_6(C_9H_3O_6)_2(HCOO^-)_6(C_{20}H_{14}N_4)_3]\bullet x(C_3H_7NO)\bullet y(H_2O)$ (**4.6**)

Solvothermal treatment of cobalt(II) chloride hexahydrate (96.0 mg, 0.400 mmol), **L3** (93.0 mg, 0.300 mmol), benzenetricarboxylate(H_3BTC) (42.0 mg, 0.200 mmol), DMF (4.0 mL), and distilled water (4.0 mL) and 7 days at 130 °C yielded a red hexagonal shape crystalline product. The crystalline product was collected by filtration and washed with distilled water. Yield 50 mg. FT-IR (cm^{-1}): 3125 (w), 2875 (w), 1635 (s), 1562 (m), 1524 (w), 1497 (m), 1416 (m), 1377 (s), 1345 (m), 1087 (m), 1026 (w), 938 (w), 786 (m), 770 (m), 713 (m), 658 (m), 559 (w).

4.3 X-ray Crystallography

A single crystal of **L3** (pale yellow plate, 0.010 × 0.050 × 0.20 mm^3) was centered on the goniometer of an Oxford Diffraction SuperNova E diffractometer operating with CuKα radiation and at 100 K. Single crystals of **L2** (colorless rod, 0.08 x 0.09 x 0.56 mm^3), compound **4.1** (purple rectangle, 0.010 × 0.052 × 0.035 mm^3), compound **4.2** (purple rod, 0.32 × 0.090 × 0.085 mm^3), compound **4.3** (A pink rod, 0.050 × 0.090 × 0.33 mm^3), compound **4.4** (orange plate, 0.090 × 0.10 × 0.35 mm^3), compound **4.5** (purple prism, 0.27 × 0.38 × 0.41 mm^3), and compound **4.6** (pink plate, 0.153 × 0.103 × 0.027 mm^3), and A pink hexagonal plate (0.03 × 0.10 × 0.15 mm^3) were centered on the goniometer of an Oxford Diffraction Gemini A Ultra diffractometer operating with MoKα radiation and at 100 K except compound **4.1** was taken at 298 K and **4.2** was taken at 150 K. The data collection routine, unit cell refinement, and data processing were carried out with the program CrysAlisPro.[87] The Laue symmetry and systematic

absences were consistent with the monoclinic space group $P2_1/c$ for **L2**, the orthorhombic space group *Pnna* for compound **4.2**, and the trigonal space group P-3 for compound **4.6**. The Laue symmetry was consistent with the triclinic space groups P1 and P-1 for **L3**, **1, 3**, **4.4**, **4.5**, and **4.4'**. The centric space group P-1 was chosen based on the E-statistics.

Structure solution and refinement were performed with the graphical user interface WinGX.[88] The structure was solved by direct methods and refined using SHELXTL NT.[90] Anisotropic displacement parameters were refined for all non-hydrogen atoms.

A riding model was used for all hydrogen atoms except the hydrogen atoms of water molecules. For **L2** and **L3**, the final refinement model involved anisotropic displacement parameters for non-hydrogen atoms and a riding model for all hydrogen atoms.

For compound **4.1**, after locating the framework structure, one strong residual electron density peak was assigned as the oxygen of a water molecule. The hydrogen atom positions on this water molecule could not be located in the residual electron density map and were not included in the refinement.

For compound **4.2**, after locating the framework structure, the neutral ligand **L2** appeared to be an anthracene structure. This is caused by tetragonal symmetry of following carbon atom positions, C2, C3, C4, and C5 on **L2** ligand. These carbon atoms showed high thermal ellipsoid. Those four carbon atoms were treated as a half occupied and refined. The hydrogen atom positions were not included in the refinement.

For compound **4.3**, the hydrogen atom positions of the O5 water were located in the residual electron density map and refined independently. The hydrogen atoms of the

O6 water could not be located in the residual electron density map and therefore were not included in the refinement.

In compound **4.4**, after locating the network structure, five strong residual electron density peaks were assigned as the oxygen atoms of water molecules. The hydrogen atom positions on O8 oxygen atom were located in the residual electron density map and refined with restraints. The hydrogen atoms on the other water molecules, O9, O10, O11, and O12, could not be located in the residual electron density map and were not included in the refinement.

For compound **4.5**, after locating the framework structure, strong residual electron density peaks were modeled as a combination of water and acetonitrile. Two water molecules (O7 and O8) were refined as fully occupied. Another region within the framework was modeled as having either one CH_3CN molecule or three water molecules (O9, O10, O11), with relative occupancies that refined to 0.547(3) and 0.473(3), respectively. A final residual electron density peak of 2.2 $e^-/Å^3$ was modeled as a partially occupied water molecule with a refined occupancy of 0.183(3). The final refinement model involved anisotropic displacement parameters for non-hydrogen atoms and a riding model for all aromatic hydrogen atoms. The hydrogen atom positions on O7, O8, and O9 were located from the residual electron density map and refined with soft distance restraints. The hydrogen atom positions on O10, O11, and O12 could not be determined from the residual electron density map. These hydrogen atoms were not included in the refinement.

In compound **4.6**, the framework structure has solvent cavities centered at $^1/_3$, $^2/_3$, –0.122 and 0, 0, 0. A 3-fold disordered DMF molecule was modeled as occupying the

cavity $^1/_3$, $^2/_3$, –0.122, with occupancies constrained to $^1/_3$. The solvent disorder in the 0, 0, 0 cavity could not be modeled; therefore the SQUEEZE subroutine of the PLATON program package was used. A total of $16e^-$ was subtracted from the 132 $Å^3$ voids and assumed to correspond to two disordered H_2O molecules.

In compound **4.4'**, the exchanged solvent molecules of network structure are partially identified and modeled although structure contains 54.0 $Å^3$ voids, which corresponds to disordered water or chloroform molecules.

The crystal parameters, data collection, and refinement results for compounds **4.1**, **4.2**, **4.3**, **4.4**, **4.5**, **4.6**, and **4.4'** are summarized in Table 4.1.

Table 4.1 Crystallographic data and structure refinement details for **L2**, **L3**, **4.1**, **4.2**, **4.3**, **4.4**, **4.5** and **4.6**.

	L2	**L3**	**4.1**	**4.2**
Empirical formula	$C_{16}H_{12}N_4$	$C_{20}H_{14}N_4$	$C_{40}H_{32}Co_2N_8O_{12}$	$C_{24}H_{14}CoN_4O_4$
Formula weight	260.3	310.35	934.6	481.32
Temperature (K)	150(2)	100(2)	293(2)	100(2)
Space group	$P2_1/c$	P -1	P -1	P n n a
a (Å)	11.4592(3)	5.6625(5)	8.7410(11)	14.821(4)
b (Å)	11.2063(3)	8.1374(8)	9.6468(10)	17.485(4)
c (Å)	9.9427(3)	8.5717(8)	12.5605(14)	8.1548(16)
α (°)	90°	93.279(8)	71.272(10)	90
β (°)	96.501(2	104.125(8)	89.284(9)	90
γ (°)	90	94.306(8)	79.910(9)	90
Volume ($Å^3$)	1268.58(6)	380.78(6)	986.46(19)	2113.3(9)
Z	4	1	1	4
Density (mg/m^3)	1.363	1.353	1.573	1.513
Absorption coefficient (mm^{-1})	0.085	0.656	0.917	0.852
F(000)	544	162	478	980
Reflections collected	23794	5474	11392	22102
Independent reflections	4306	1485	4596	2443
R_{int}	0.0429	0.0355	0.1394	0.0974
GOF	0.888	1.246	0.834	1.185
R_1/wR_2 [I>2sigma(I)]	0.0424/0.0992	0.0586/0.1988	0.0699/0.1341	0.0729/0.1515

4.3	**4.4**	**4.5**	**4.6**	**4.4'**
$C_{76}H_{58}Co_2N_{12}O_{12}$	$C_{78}H_{60}Co_3N_{12}O_{24}$	$C_{59}H_{38}ClCo_2N_{10}O_6 \bullet 0.547CH_3CN \bullet 3.544H_2O$	$C_{45}H_{36}Co_3N_7O_{14}$	$C_{80}H_{62}C_{16}Co_3N_{12}O_{18}$
1449.2	1726.17	1222.54	1075.6	1868.91
100(2)	100(2)	100(2)	100(2)	100(2)
P -1	P -1	P -1	P -3	P -1
11.2622(4)	9.9626(11)	9.5744(2)	14.0808(3)	9.9913(8)
13.2533(5)	13.2797(17)	13.9026(3)	14.0808(3)	13.3514(10)
13.5985(4)	15.916(2)	20.6532(4)	12.9837(5)	16.5009(2)
62.024(4)	109.309(13)	90.146(2)	90	71.287(8)
71.933(3)	95.241(11)	90.201(2)	90	81.802(8)
75.375(3)	91.213(10)	91.074(2)	120	89.910(6)
1690.26(10)	1976.0(4)	2748.62(10)	2229.38(11)	2061.2(2)
1	1	2	2	1
1.424	1.451	1.477	1.602	1.506
0.565	0.707	0.723	1.181	0.867
748	885	1257	1096	953
57756	21599	63740	30329	22904
9905	9111	16086	4367	9481
0.0640	0.0463	0.033	0.0924	0.0259
0.999	1.111	1.062	0.882	1.005
0.0465/0.1178	0.0618/ 0.1593	0.0338/ 0.0920	0.0380/0.0697	0.0703/ 0.2085

Rint: internal-R value from averaging the reflections in point group -1. GOF: goodness of fit value should converge to 1.0 for a very good structure at the end of refinement. R_1/wR_2: These values are all standard algorithms for presenting the quality of the agreement for observed data.

4.4 Results and Discussion

4.4.1 Structural description of the ligand, 1, 4-Bis(1-imidazolyl)naphthalene (**L2**)

The structure of **L2** with atom numbering scheme is shown in Figure 4.1. The ligand crystallized with $P2_1/c$. The dihedral angle between nitrogen atoms of imidazole group and naphthalene group is 160.76°. The imidazole groups are positioned nearly perpendicular to naphthalene group and each nitrogen atom with lone-paired electron on imidazole groups, which will form a coordination bond to a metal ion, are pointing above and below the naphthalene plane.

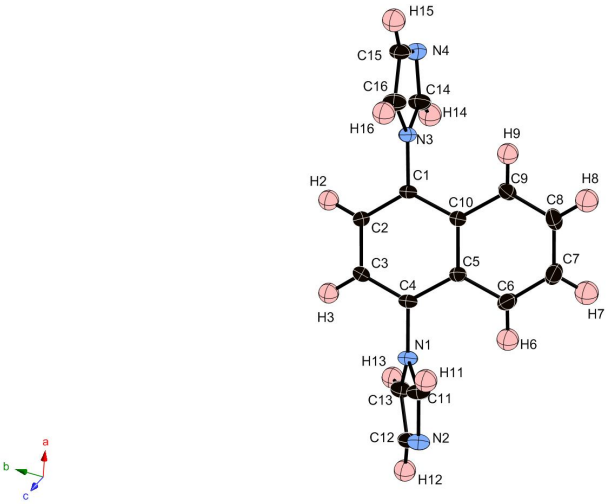

Figure 4.1 L2 with atom numbering scheme with the ellipsoids drawn at the 50 %probability level.

4.4.2 Structural description of the ligand, 9, 10-Bis(1-imidazolyl)anthracene (**L3**)

The structure of **L3** with atom numbering scheme is shown in Figure 4.2. The ligand crystallized with centrosymmetric, P-1. The dihedral angle between nitrogen atoms of imidazole group and anthracene group is 160.84°. The imidazole groups are positioned nearly perpendicular to anthracene group and each nitrogen atom with lone-

paired electron on imidazole groups, which will form a coordination bond to a metal ion, are pointing above and below the anthracene plane.

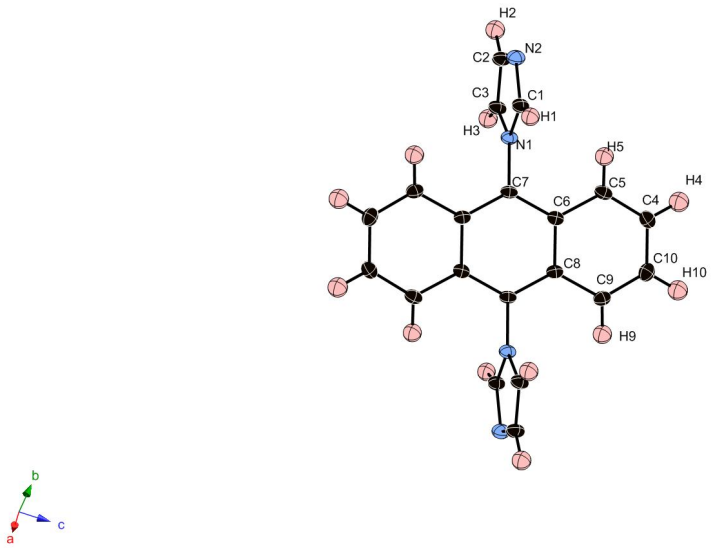

Figure 4.2 L3 with atom numbering scheme with the ellipsoids drawn at the 50 %probability level.

4.4.3 Structural description of $[Co(C_{12}H_{10}N_4)(C_8H_4O_4)(H_2O)] \cdot (H_2O)$ (**4.1**)

The structure of **4.1** with atom numbering scheme is shown in Figure 4.3. The isostructural nickel (II) compound has been reported.[113] Selected bond lengths and angles are summarized in Table 4.2. Crystallographic analysis shows that compound **4.1** forms a covalently bonded three-dimensional (3D) framework with one lattice water molecule that is five-fold interpenetrated. The asymmetric unit of **4.1** contains one octahedral cobalt(II) ion, one fully deprotonated BDC^{2-} ligand, one **L1** ligand, one coordinated water molecule, and one lattice water molecule. The octahedral cobalt (II) metal cation is coordinated to two carboxylate groups of the BDC^{2-} ligand (one in a chelating, η^2-fashion,

and one using a single oxygen atom), two nitrogen atoms from one **L1** ligand, and the oxygen atom of coordinated water molecule.

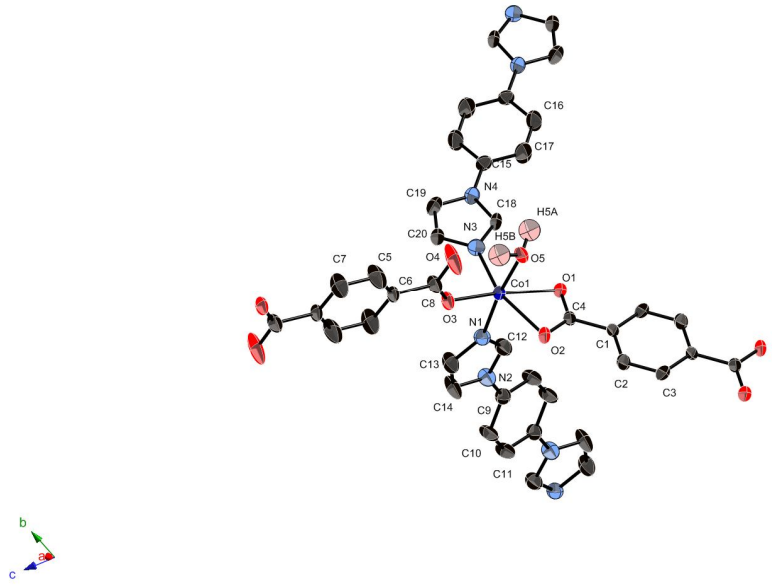

Figure 4.3 Coordination environment of cobalt(II) ion in **4.1** with the ellipsoids drawn at the 50 %probability level. Hydrogen atoms are omitted for clarity.

Table 4.2 Bond lengths (Å) and angles (°) for compound **4.1**.

Bond lengths	(Å)
C(4)-O(2)	1.246(6)
C(4)-O(1)	1.281(6)
C(8)-O(3)	1.251(6)
C(8)-O(4)	1.249(6)
N(1)-Co(1)	2.110(4)
N(3)-Co(1)	2.085(4)
O(1)-Co(1)	2.185(3)

O(2)-Co(1)	2.207(3)
O(3)-Co(1)	2.038(3)
O(5)-Co(1)	2.145(4)
C(4)-O(2)	1.246(6)
Bond angles	(°)
O(3)-Co(1)-N(3)	93.98(16)
O(3)-Co(1)-N(1)	90.60(15)
N(3)-Co(1)-N(1)	93.74(16)
O(3)-Co(1)-O(5)	90.61(14)
N(3)-Co(1)-O(5)	94.08(15)
N(1)-Co(1)-O(5)	171.98(15)
O(3)-Co(1)-O(1)	168.30(15)
N(3)-Co(1)-O(1)	96.79(16)
N(1)-Co(1)-O(1)	93.22(15)
O(5)-Co(1)-O(1)	84.11(13)
O(3)-Co(1)-O(2)	109.22(14)
N(3)-Co(1)-O(2)	156.79(16)
N(1)-Co(1)-O(2)	86.82(14)
O(5)-Co(1)-O(2)	85.30(13)

The network architecture of compound **4.1** is best described as diamond-like (Figure 4.4a). Although the cobalt is octahedrally coordinated, it is only four-connected in the network. Two coordination sites are occupied by water molecules and two sites are occupied by a chelating carboxylate group. There are four distinct types of connections between cobalt ions in the diamond network, two bis-imidazole linkages and two BDC^{2-} linkages. The network can be generated from hexagonal layers of cobalt ions linked by two BDC^{2-} and one bis-imidazole group, $[Co(BDC^{2-})(\mathbf{L1})]_n$ (Figure 4.4b).

(a)

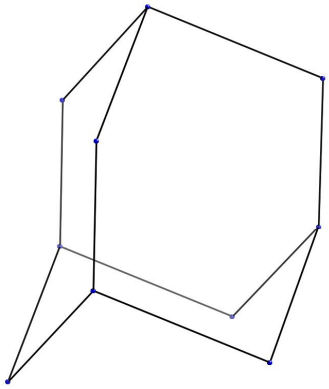

(b)

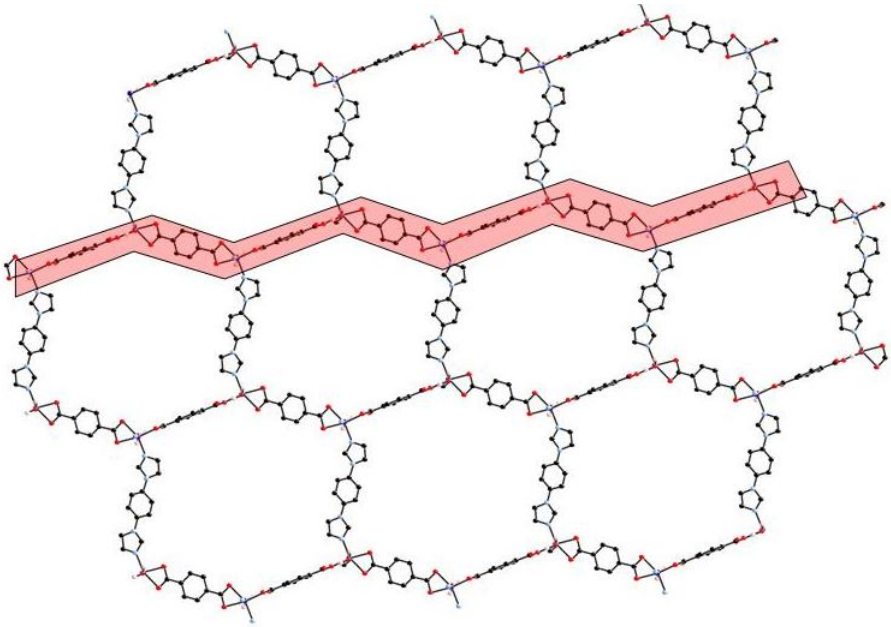

Figure 4.4 (a) An adamantine cage, which is represented by ten cobalt ions, of **4.1**. (b) A 2D hexagonal layer, $[Co(BDC^{2-})(\mathbf{L2})]_n$, of compound **4.1**. The zigzag ribbon represents a neutral 1D chain, which is constructed from cobalt(II) metal ions and BDC^{2-} anions, $[Co(BDC^{2-})]$.

These layers are connected by the remaining bis-imidazole group (Figure 4.5a). The adamantine cages generated by ten cobalt atoms have a dimensions of 16.8 × 18.2 × 18.5 × 20.6 Å. These very large spaces are filled with atoms from four identical frameworks, leaving a room for only one water molecule per cobalt ion, which is hydrogen bonded to the coordinated water molecule (Figure 4.5b).

(a)

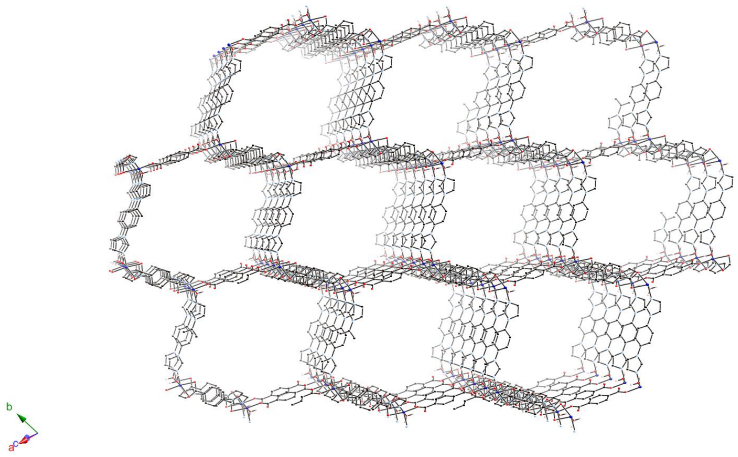

(b)

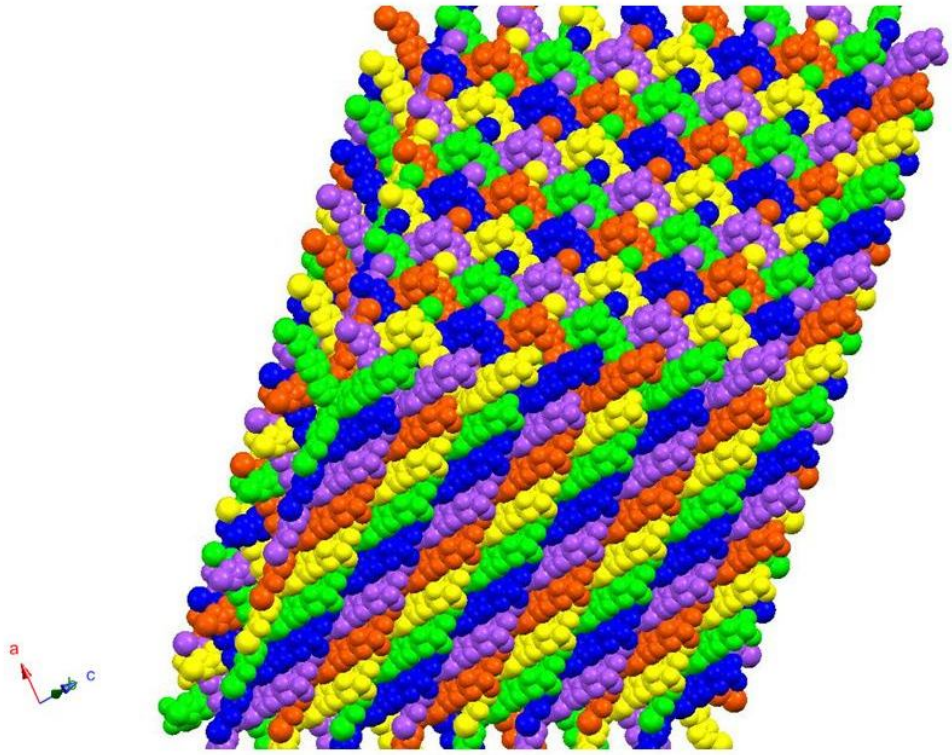

Figure 4.5 (a) A single 3D framework of **4.1** (b) Five fold interpenetrating 3D frameworks of **4.1**.

4.4.4 Structural description of $[Co_{0.5}(C_{16}H_{12}N_4)_{0.5}(C_8H_4O_4)_{0.5}]$ (**4.2**)

Compound **4.2** forms a four-fold interpenetrating 3D framework. The structure of **4.2** with atom numbering scheme is shown in figure 4.6. Selected bond lengths and angles are summarized in Table 4.3. The asymmetric unit of the 3D framework consists of a half of a tetrahedral cobalt(II) ion is coordinated by half of a BDC^{2-} ligand and half an **L2** ligand. The tetrahedral cobalt(II) ion is coordinated to an oxygen atom from each of two monodentate carboxylate groups of the BDC^{2-} ligand and two imidazole groups from two **L2** ligands.

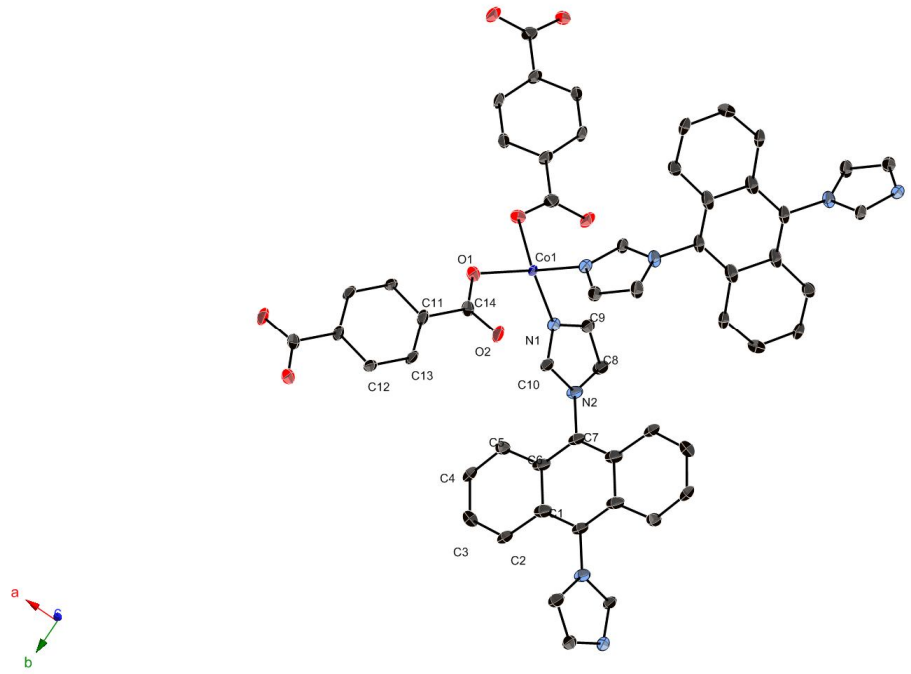

Figure 4.6 Coordination environment of cobalt(II) ion in **4.2** with the ellipsoids drawn at the 50 % probability level. Hydrogen atoms are omitted for clarity. Anthracene motif, instead of naphthalene, is appeared due to the tetragonal symmetry on aromatic group.

Table 4.3 Bond lengths (Å) and angles (°) for compound **4.2**.

Bond lengths	(Å)
N(1)-Co(1)	2.047(4)
O(1)-Co(1)	1.969(3)
Co(1)-O(1)#	1.969(3)
Co(1)-N(1)#	2.047(4)
Bond angles	(°)
O(1)-Co(1)-O(1)	90.8(2)
O(1)-Co(1)-N(1)#	120.42(16)
O(1)#-Co(1)-N(1)#	115.65(15)
O(1)-Co(1)-N(1)	115.65(15)
O(1)#-Co(1)-N(1)	120.42(16)
N(1)#-Co(1)-N(1)	96.0(2)

Symmetry transformations used to generate equivalent atoms: #; x,-y+1/2,-z+1/2

The network architecture of compound **4.2** is best described as slightly distorted diamond-like as similar to **4.1** (Figure 4.7).

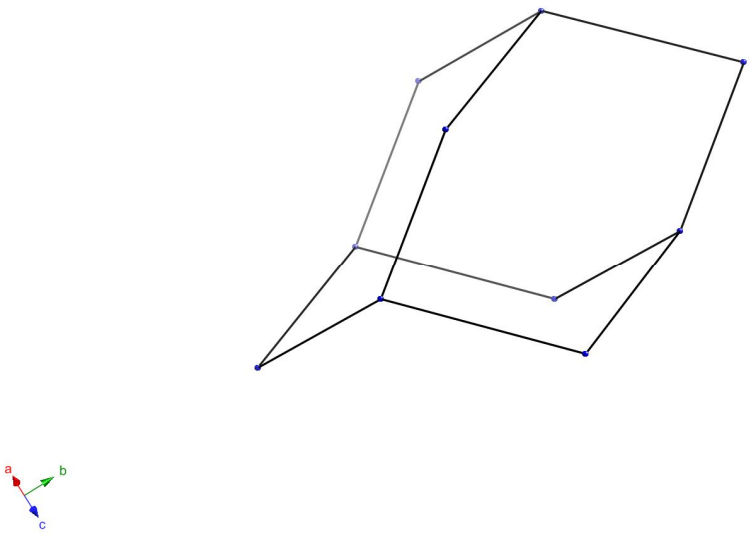

Figure 4.7 A distorted adamantine cage of **4.2**.

The network can be generated from hexagonal layers of cobalt ions linked by two BDC^{2-} and one bis-imidazole groups of **L2**, $[Co(BDC^{2-})(\mathbf{L2})]_n$ (Figure 4.8a). These layers are connected by the remaining bis-imidazole group of **L2** to complete the 3D network (Figure 4.8b).

(a)

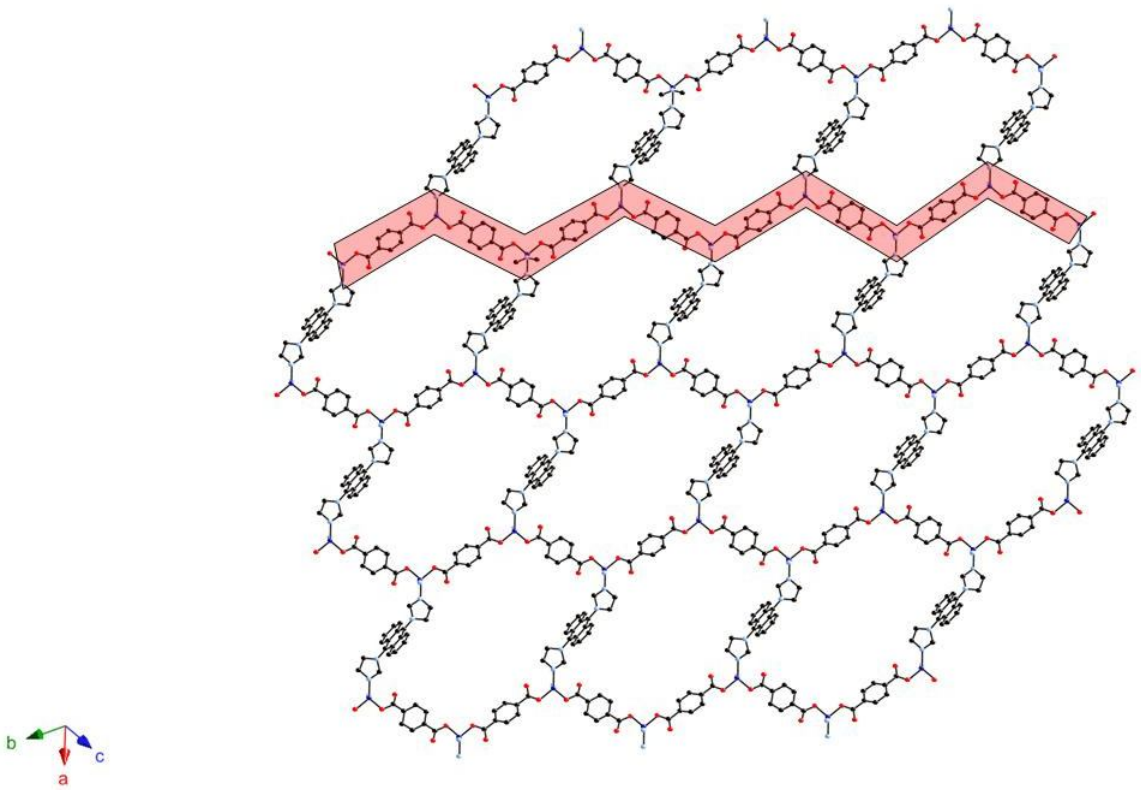

Figure 4.8 (a) A hexagonal 2D layers of **4.2**, $[Co(BDC^{2-})(\mathbf{L2})]$. The zigzag ribbon represents a neutral 1D chain, which is constructed from cobalt(II) ions and BDC^{2-} anions, $[Co(BDC^{2-})]_n$.

(b)

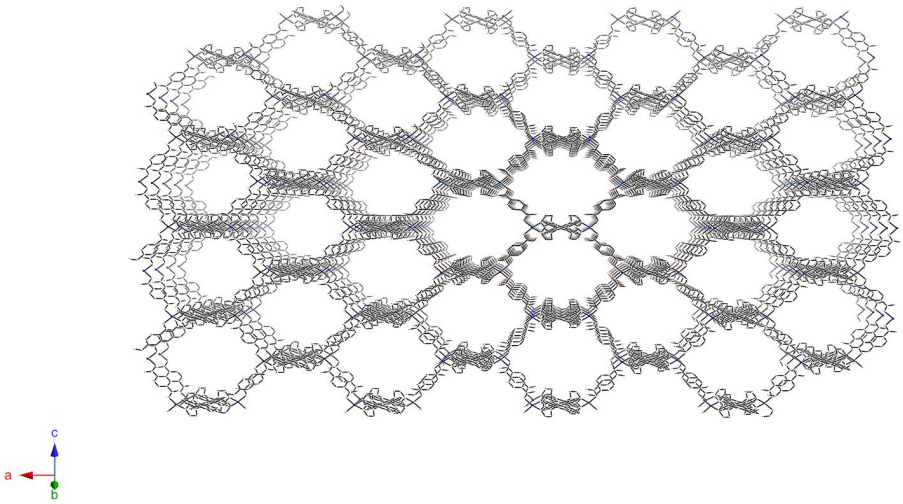

(c)

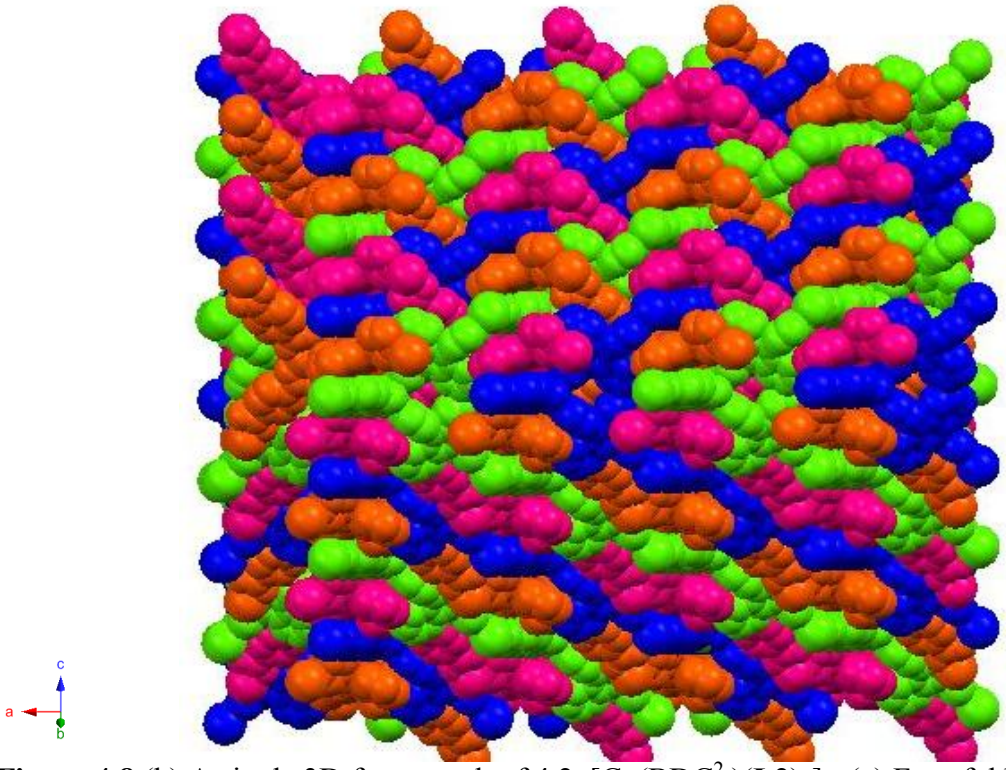

Figure 4.8 (b) A single 3D framework of **4.2,** $[Co(BDC^{2-})(\mathbf{L2})_2]_n$. (c) Four fold interpenetrating 3D networks of compound **4.2**.

The adamantine like cages of **4.2** have dimensions of 15.6 × 18.3 × 19.4 × 19.7 Å. As in **4.1**, these cavities are all filled by identical networks to complete the

interpenetrating 3D networks of **4.2** (Figure 8c). Crystallographic analysis shows that there is only small void space in **4.2** precluding its use as a potential porous material.

The neutral naphthalene ligand **L2** is disordered in **4.2** because of the tetragonal symmetry. The disordered naphthalene rings give the appearance of anthracene in the structure.

4.4.5 Structural description of $[Co(C_{20}H_{14}N_4)_2(C_8H_4O_4), Co(C_{20}H_{14}N_4)(C_8H_4O_4)(H_2O)_2] \bullet 2H_2O$ (**4.3**)

Compound **4.3** consists of two independent and different coordination networks that fill space completely. The structure of **4.3** with atom numbering scheme is shown in Figure 4.9. Selected bond lengths and angles are summarized in Table 4.4. The portion of the composition in the asymmetric unit that is a 3D network consists of a half octahedral cobalt(II) ion, a half BDC^{2-} ligand, and one **L3** ligand. The portion that is a 2D layer consists of a half octahedral cobalt(II) ion, a half BDC^{2-} ligand, a half **L3** ligand, and one coordinated water molecule.

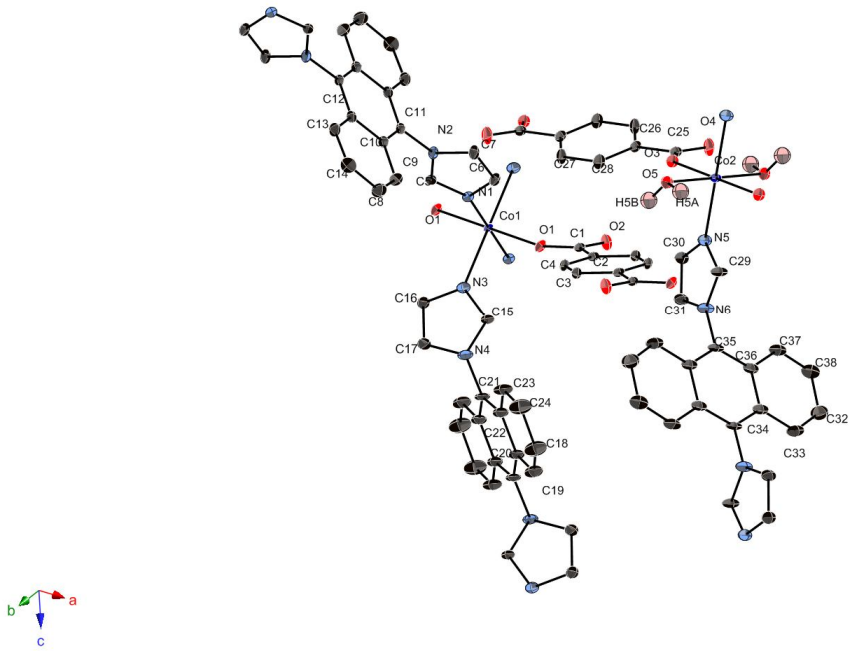

Figure 4.9 Coordination environment of cobalt(II) ion in **4.3** with the ellipsoids drawn at the 50 % probability level.

Table 4.4 Bond lengths (Å) and angles (°) for compound **4.3**.

Bond lengths	(Å)
Co(1)-O(1)#1	2.0763(12)
Co(1)-O(1)	2.0763(12)
Co(1)-N(1)	2.1317(16)
Co(1)-N(3)	2.1597(16)
Co(2)-O(3)	2.0327(13)
Co(2)-N(5)	2.1045(17)
Co(2)-O(5)	2.1542(16)
Bond angles	(°)
O(1)#1-Co(1)-O(1)	180.000(18)
O(1)#1-Co(1)-N(1)	87.25(6)

O(1)-Co(1)-N(1)	92.75(6)
N(1)-Co(1)-N(1)#1	180.00(14)
O(1)#1-Co(1)-N(3)	94.70(6)
O(1)-Co(1)-N(3)	85.30(6)
N(1)-Co(1)-N(3)	84.54(6)
N(1)#1-Co(1)-N(3)	95.46(6)
N(3)-Co(1)-N(3)#1	180.00(6)
O(3)#2-Co(2)-O(3)	180
O(3)#2-Co(2)-N(5)	88.35(6)
O(3)-Co(2)-N(5)	91.65(6)
N(5)-Co(2)-N(5)#2	180.00(11)
O(3)#2-Co(2)-O(5)#2	88.93(6)
O(3)-Co(2)-O(5)#2	91.07(6)
N(5)-Co(2)-O(5)#2	89.27(6)
N(5)#2-Co(2)-O(5)#2	90.73(6)

Symmetry transformations used to generate equivalent atoms: #1; -x+1,-y+1,-z, #2; -x,-y+2,-z

The octahedral cobalt ion (Co1) of the 3D network sits on inversion center; it is coordinated to oxygen (O1) of two BDC^{2-} anions and four nitrogen atoms (N1 and N3) from two **L3** ligands. The 3D framework is described by three structural motifs. First, neutral 1D chains are formed by cobalt(II) ions and fully deprotonated BDC^{2-} ligands, $[Co(BDC^{2-})]_n$. Layers are formed by **L3** links between $[(Co(BDC^{2-})]_n$ chains (Figure 4.10a). Additional **L3** ligands form pillars to hold these 2D layers of cobalt(II) ions to complete the 3D network structure (Figure 10b).

(a)

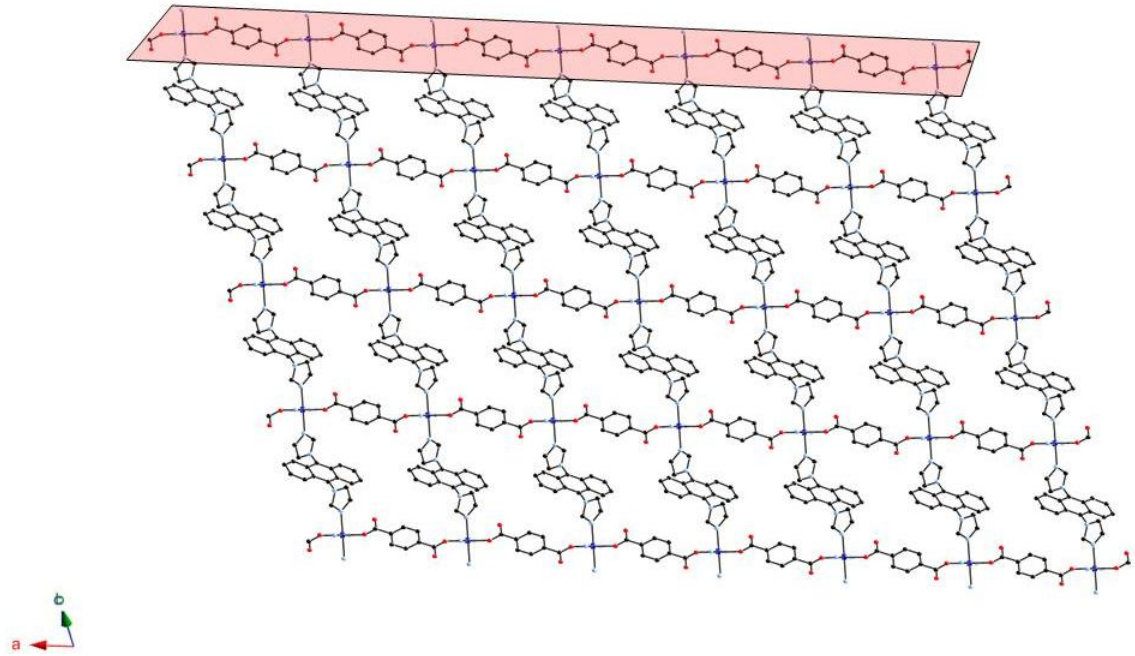

(b)

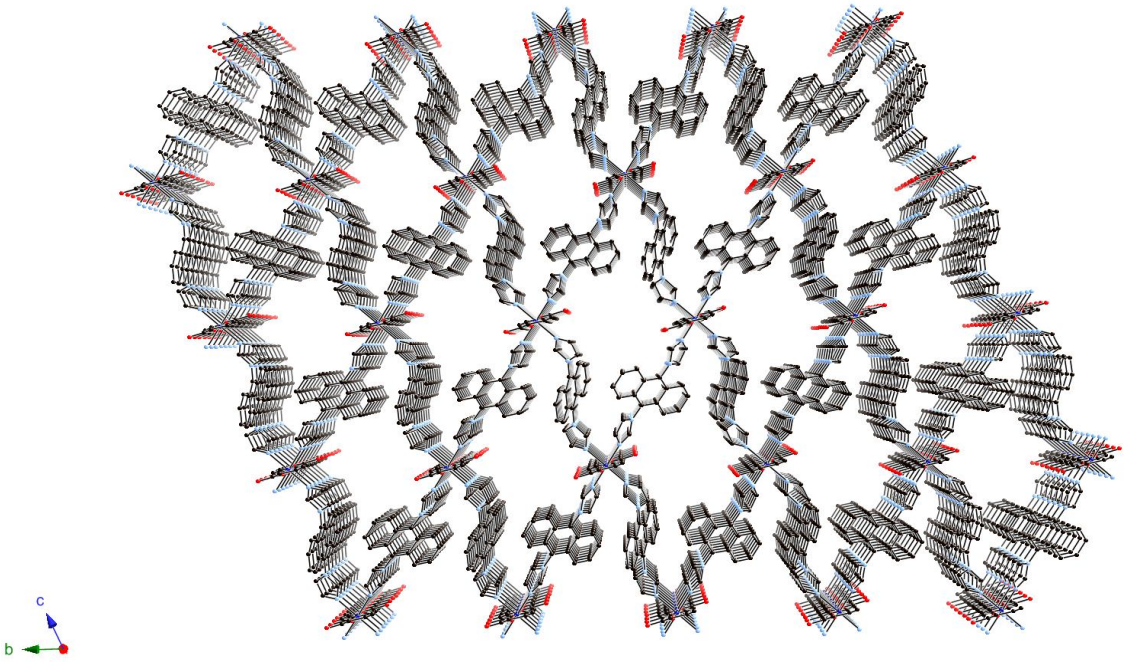

Figure 4.10 (a) A 2D layer network of 3D framework in compound **4.3**, where red ribbon represents a neutral 1D chain. (b) A 3D framework of compound **4.3** without 2D layers and lattice water molecules.

The 2D layer networks that fill the cavities of the 3D network are formed by **L3** links between neutral 1D chains of $[Co(BDC^{2-})(H_2O)_2]_n$ to form sheets (Figure 4.11a). The sheet is similar to the layer motif in the 3D network however there is no space to complete another 3D network, rather the remaining coordination sites on cobalt ions are occupied by water (Figure 4.11b).

(a)

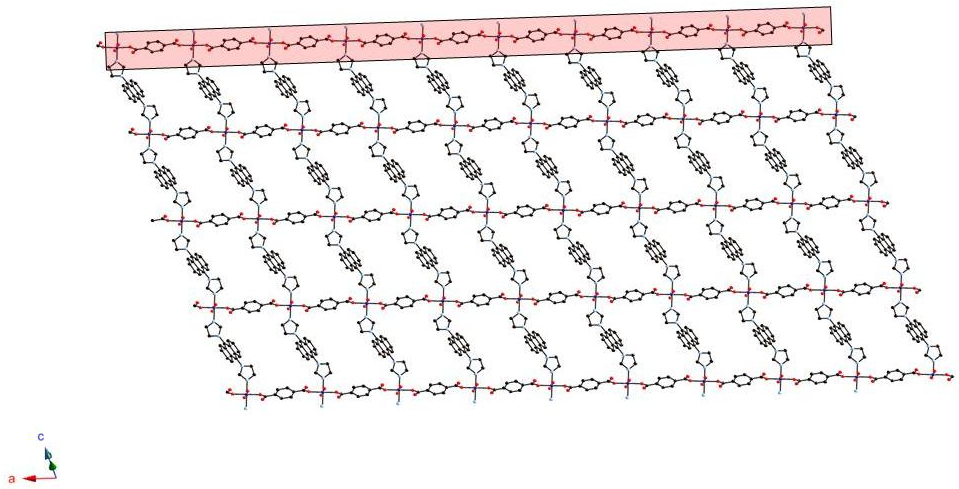

(b)

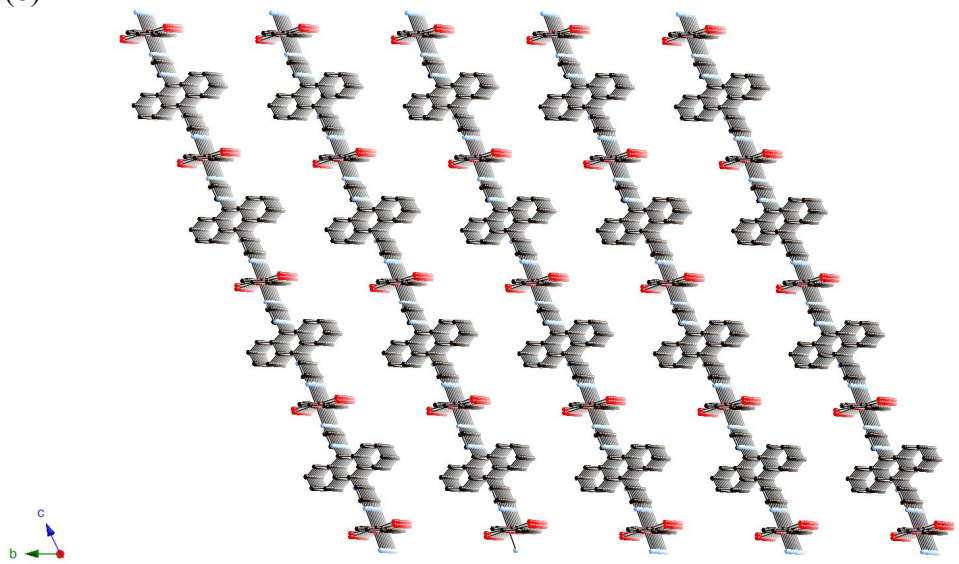

Figure 4.11 (a) A 2D network in compound **4.3**, where neutral 1D chain is indicated as red ribbon. (b) 2D networks of compound **4.3** on [100]**.**

The nitrogen to nitrogen distance in **L3** ligand is 9.9 Å in the 3D network and the distance between Co2 ions in adjacent layers of the 2D network is 13.0 Å. The miss match in distances and presence of bulky anthracene ligands prevents the formation of a second interpenetrating 3D network. Thus, the 2D sheets can be viewed as an intermediate building block of the 3D network. If there were enough space to accommodate additional **L3** ligands instead of simply coordinated water molecules on cobalt(II) ion, the compound **4.3** would be a two-fold interpenetrating network. Although there is one lattice water molecule in the cavity in this structure, there is no accessible void space to accommodate another **L3** ligand in order to form the second 3D network within this structure (Figure 4.12).

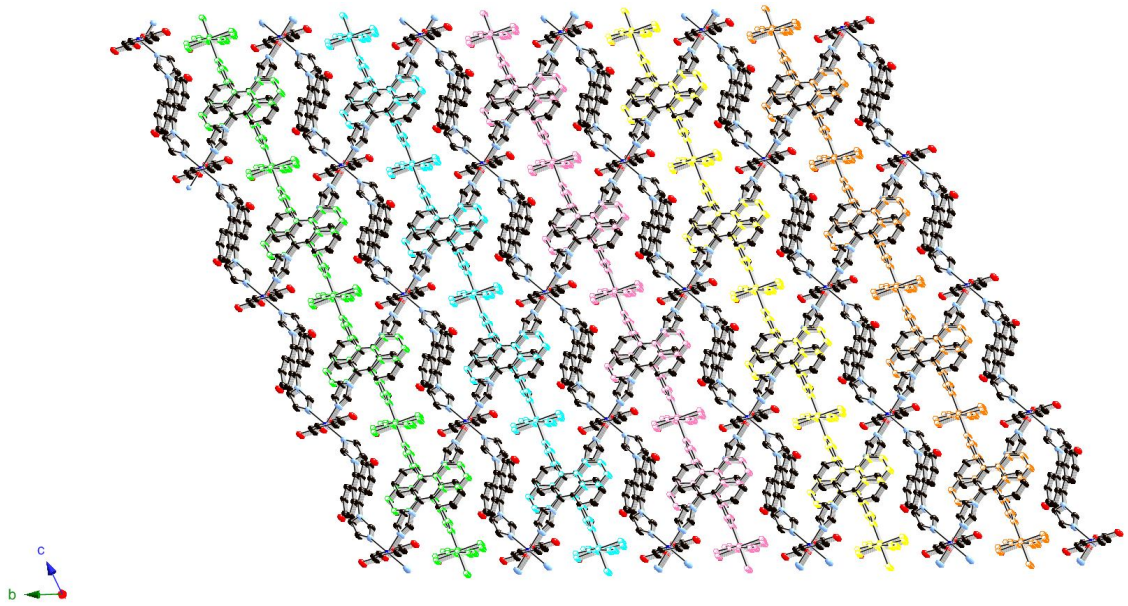

Figure 4.12 2D layers are woven into 3D network of **4.3**. Each 2D network is colored differently.

4.4.6 Effect of size of ligand, L1, L2, and L3, in network formation

Frameworks **4.1**, **4.2**, and **4.3** are each formed with two different linear ligands, BDC^{2-} and a bis imidazole ligand. The bis imidazole ligands, **L1**, **L2**, and **L3** differ in

size with trans imidazole groups grafted onto benzene, naphthalene, and anthracene, respectively. Each has equivalent N···N distances across the aromatic ring. The narrowest ligand, **L1**, forms the most open framework. Cobalt-Cobalt distances of 16.8 Å to 20.6 Å are observed. The large voids are filled completely with five identical interpenetrating frameworks. With **L2** as the neutral ligand, the pores are nearly as large in diamond-like network. However, the disordered naphthalene ring occupies a larger volume and only a four-fold interpenetration is possible. The anthracene based ligand, **L3**, blocks additional space so that interpenetration of identical networks is not possible. However, rather than leaving vacant space, a second 2D network forms to fill the voids in the 3D network.

4.4.7 Structural description of $[Co_3(C_{20}H_{14}N_4)_3(C_9H_3O_6)_2(H_2O)_2]\cdot 10H_2O$ (**4.4**)

The cobalt metal coordination environment of **4.4** with atom numbering scheme is shown in Figure 4.13. Selected bond length and angles are summarized in Table 4.5. The asymmetric unit of **4.4** contains one and a half octahedral cobalt(II) ions, one BTC^{3-} ligand, one and a half **L3** ligands, one coordinated water molecule, and five free lattice water molecules. Compound **4.4** forms a neutral non-interpenetrating covalently bonded three-dimensional (3D) network with ten water molecules per formula unit in void spaces.

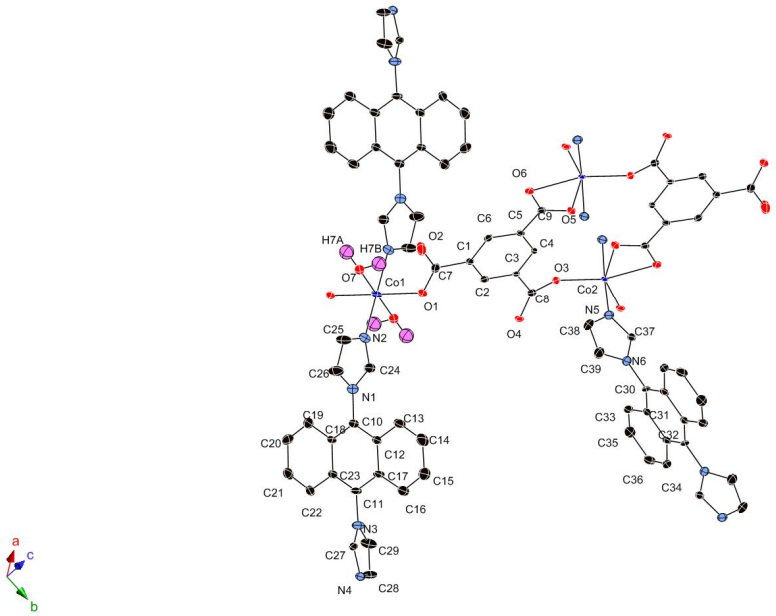

Figure 4.13 Coordination environment of cobalt(II) ion in **4.4** with the ellipsoids drawn at the 50 % probability level.

Table 4.5 Bond lengths (Å) and angles (°) for compound **4.4**.

Bond lengths	(Å)
Co(1)-O(1)#4	2.077(2)
Co(1)-N(2)#4	2.133(3)
Co(1)-O(7)#4	2.135(3)
Co(2)-O(3)	2.016(2)
Co(2)-O(4)#2	2.031(2)
Co(2)-O(5)#3	2.106(2)
Co(2)-N(4)#1	2.119(3)
Co(2)-N(5)	2.118(3)
Co(2)-O(6)#3	2.296(2)
Bond angles	(°)
O(1)#4-Co(1)-O(1)	180
O(1)#4-Co(1)-N(2)#4	86.69(11)
O(1)-Co(1)-N(2)#4	93.31(11)
O(1)-Co(1)-N(2)	86.69(11)
N(2)#4-Co(1)-N(2)	180.00(14)
O(1)#4-Co(1)-O(7)	88.57(10)
O(1)-Co(1)-O(7)	91.43(10)
N(2)#4-Co(1)-O(7)	91.42(12)
N(2)-Co(1)-O(7)	88.58(12)

O(7)-Co(1)-O(7)#4	180
O(3)-Co(2)-O(4)#2	109.83(9)
O(3)-Co(2)-O(5)#3	101.09(9)
O(4)#2-Co(2)-O(5)#3	149.06(9)
O(3)-Co(2)-N(5)	92.11(11)
O(4)#2-Co(2)-N(5)	91.87(11)
O(5)#3-Co(2)-N(5)	88.07(11)
O(3)-Co(2)-N(4)#1	90.10(11)
O(4)#2-Co(2)-N(4)#1	91.43(11)
O(5)#3-Co(2)-N(4)#1	87.27(11)
N(5)-Co(2)-N(4)#1	175.15(11)
O(3)-Co(2)-O(6)#3	160.54(9)
O(4)#2-Co(2)-O(6)#3	89.59(9)
O(5)#3-Co(2)-O(6)#3	59.48(9)
N(5)-Co(2)-O(6)#3	88.52(10)
N(4)#1-Co(2)-O(6)#3	87.96(10)

Symmetry transformations used to generate equivalent atoms: #1; -x,-y+1,-z-1, #2; -x+1,-y,-z-1, #3; -x,-y,-z-1, #4; -x+1,-y+1,-z

The 3D framework consists of two different octahedral geometries for three cobalt(II) cations. These are coordinated to two BTC^{3-} anions and three **L3** ligands. One of the three octahedral cobalt ion(Co1) sits on inversion center and is coordinated to two symmetry related oxygen atoms of a monodentate carboxylate group from the BTC^{3-} anion, two nitrogen atoms from one **L3** ligand, and two water molecules. The two additional octahedral cobalt ions(Co2) are coordinated to two symmetry related oxygen atoms of a chelating carboxylate group(O5 and O6) from BTC^{3-} anion, two symmetry related oxygen atoms of a monodentate carboxylate group, and two nitrogen atoms from one **L3** ligand.

The cobalt(II) cations and BTC^{3-} anions link to form 2D layers (Figure 4.14a). The 2D layer contains two distinct rings and is shown schematically in Figure 4.14b. The BTC^{3-} groups are fully connected within the layers. Each cobalt ion is connected to the adjacent layers via **L3,** which forms pillars. The pillaring leaves interlayer voids that are filled with water. Eight of ten lattice waters per formula unit occupy the interlayer voids. The two additional water molecules are hydrogen bonded to water molecules coordinated to Co1 and are thus strongly associated with the $[Co_3BTC^{3-})_2]_n$ layers.

(a)

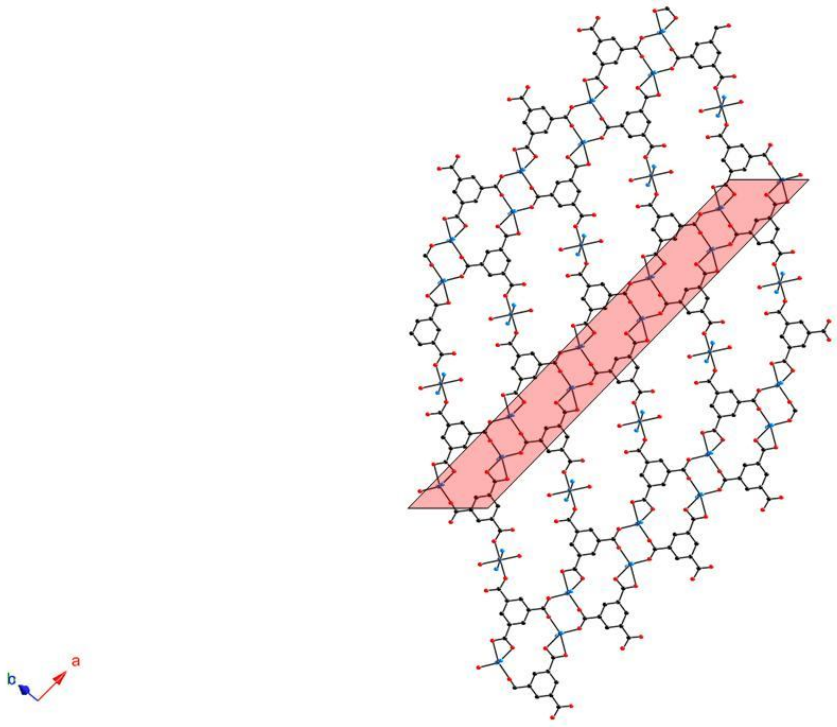

Figure 4.14 (a) A neutral 2D layer of **4.4**, $[Co_3(BTC^{3-})_2]$. An anionic 1D double chain, $[Co_2(BTC^{3-})_2]^{2-}$, is indicated as a rectangle.

(b)

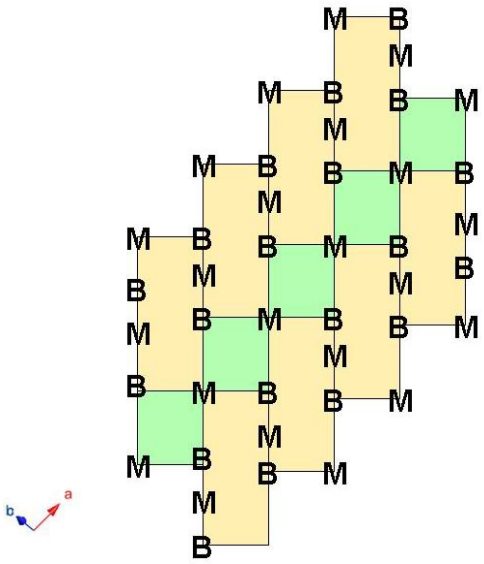

Figure 4.14 (b) A schematic representation of 2D sheet, (8, 4) rings. (**M**: cobalt ion and **B**: BTC^{3-} anion)

The pillaring is depicted in Figure 4.15. The channels created by pillaring have dimensions of 7.3 Å × 12.0 Å in the *b*-*c* plane. The distances between coordinated water molecules of the octahedral Co1 ions and the lattice waters are in the range of 2.60 to 2.74 Å consistent with hydrogen bonds. The hydrogen atoms of the water molecules within the more hydrophobic channels could not be modeled. Further analysis of lattice water molecules, TGA, and solvent exchange experiments will be discussed in a following section.

(a)

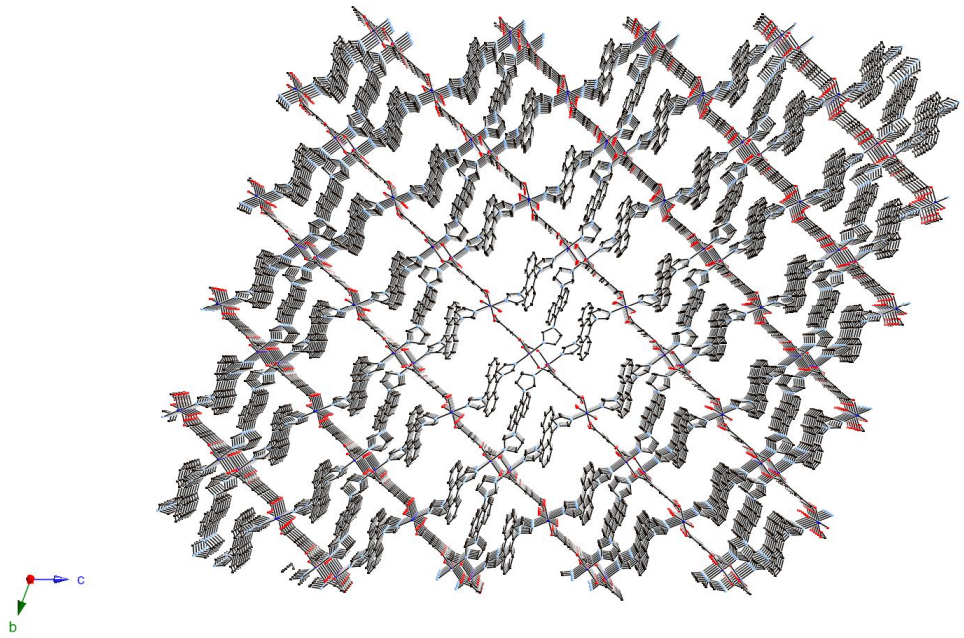

(b)

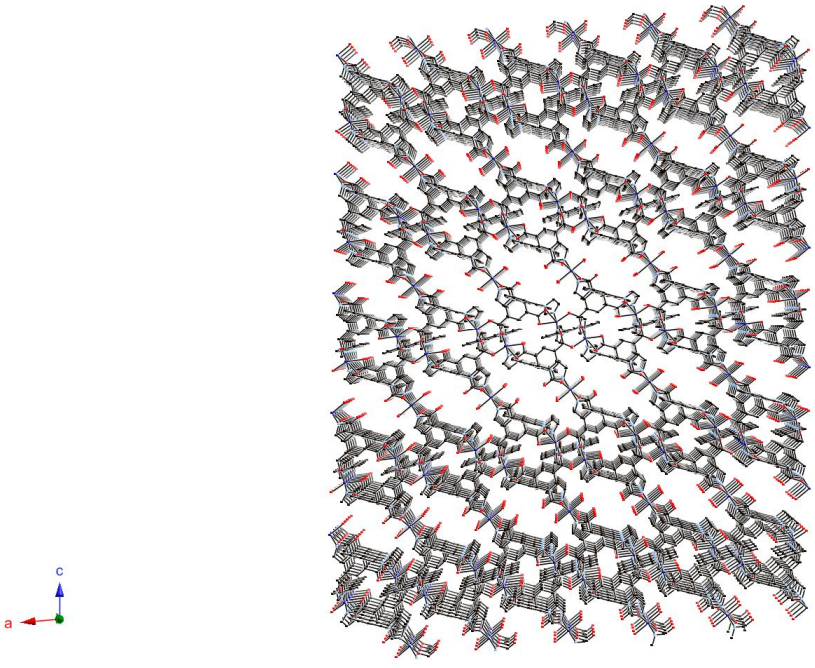

Figure 4.15 (a) Larger 1D channels on [100] without free lattice water molecules. (b) Narrower 1D channels on [010] without free lattice water molecules.

4.4.8 Structural description of $[Co_4(C_9H_3O_6)_2(C_{20}H_{14}N_4)_5Cl_2]\bullet 1.094(C_2H_3N)\bullet 7.088(H_2O)$ (**4.5**)

The compound **4.5** is prepared similarly to **4.4** but at a higher ratio of acetonitrile 50/50 by volume and double the concentration of metal ion and **L3**. The cobalt coordination environment of **4.5** with atom numbering scheme is shown in Figure 4.16. Selected bond length and angles are summarized in Table 4.6. The asymmetric unit of **4.5** consists of two octahedral cobalt(II) ions, one BTC^{3-} ligand, one chloride anion, two and a half **L3** ligands, and partially occupied acetonitrile molecule and water molecules.

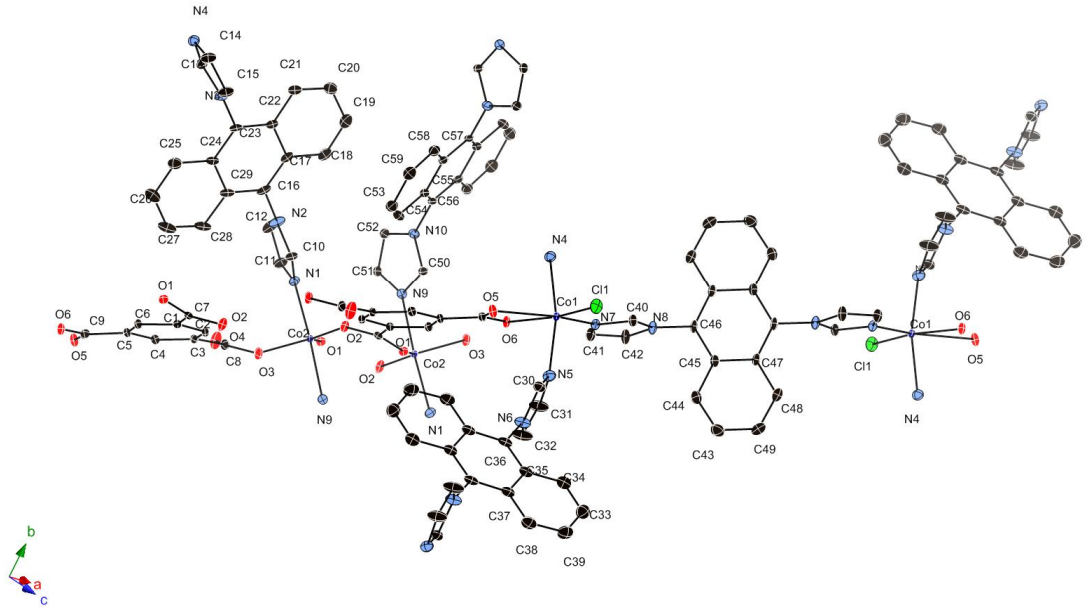

Figure 4.16 Coordination environment of cobalt(II) ion in **4.5** with the ellipsoids drawn at the 50 % probability level.

Table 4.6 Bond lengths (Å) and angles (°) for compound **4.5**.

Bond lengths	(Å)
Co(1)-N(7)	2.0942(12)
Co(1)-O(6)#1	2.1010(10)
Co(1)-N(5)	2.1121(12)
Co(1)-N(4)	2.1279(12)
Co(1)-Cl(1)	2.3429(4)
Co(1)-O(5)#1	2.4028(10)
Co(2)-O(2)#2	1.9886(10)
Co(2)-O(1)	1.9913(9)
Co(2)-O(3)#3	1.9980(10)
Co(2)-N(1)	2.0925(11)
Co(2)-N(9)	2.1285(11)
Co(1)-N(7)	2.0942(12)
Bond angles	(°)
N(7)-Co(1)-O(6)#1	95.63(4)
N(7)-Co(1)-N(5)	97.25(5)
O(6)#1-Co(1)-N(5)	87.25(5)
N(7)-Co(1)-N(4)	96.31(5)
O(6)#1-Co(1)-N(4)	86.53(4)
N(5)-Co(1)-N(4)	165.57(5)
N(7)-Co(1)-Cl(1)	103.86(3)
O(6)#1-Co(1)-Cl(1)	160.44(3)
N(5)-Co(1)-Cl(1)	91.77(4)
N(4)-Co(1)-Cl(1)	89.75(4)
N(7)-Co(1)-O(5)#1	154.08(4)
O(6)#1-Co(1)-O(5)#1	58.45(3)
N(5)-Co(1)-O(5)#1	83.04(4)
N(4)-Co(1)-O(5)#1	82.60(4)
Cl(1)-Co(1)-O(5)#1	102.03(3)
O(2)#2-Co(2)-O(1)	130.72(4)
O(2)#2-Co(2)-O(3)#3	107.75(4)
O(1)-Co(2)-O(3)#3	121.41(4)
O(2)#2-Co(2)-N(1)	90.18(4)
O(1)-Co(2)-N(1)	91.45(4)
O(3)#3-Co(2)-N(1)	91.74(5)
O(2)#2-Co(2)-N(9)	92.80(4)
O(1)-Co(2)-N(9)	88.12(4)
O(3)#3-Co(2)-N(9)	85.45(4)

Symmetry transformations used to generate equivalent atoms: #1; x-1,y+1,z, #2; -x+2,-y+1,-z+1 #3 x-1,y,z

As in **4.4** the cobalt(II) cations and BTC^{3-} anions are confined to layers. The BTC^{3-} groups are fully connected within the layers. However, in **4.5** one **L3** ligand is also completely incorporated within the layers. This can be visualized as the insertion of an additional octahedral cobalt(Co1) site plus one **L3** to the layered structure of **4.4**. All of the Co1 ions carry an additional chloride to balance the charge (Figure 4.17a). The 2D layer contains from two distinct rings, as shown in Figure 4.17b.

(a)

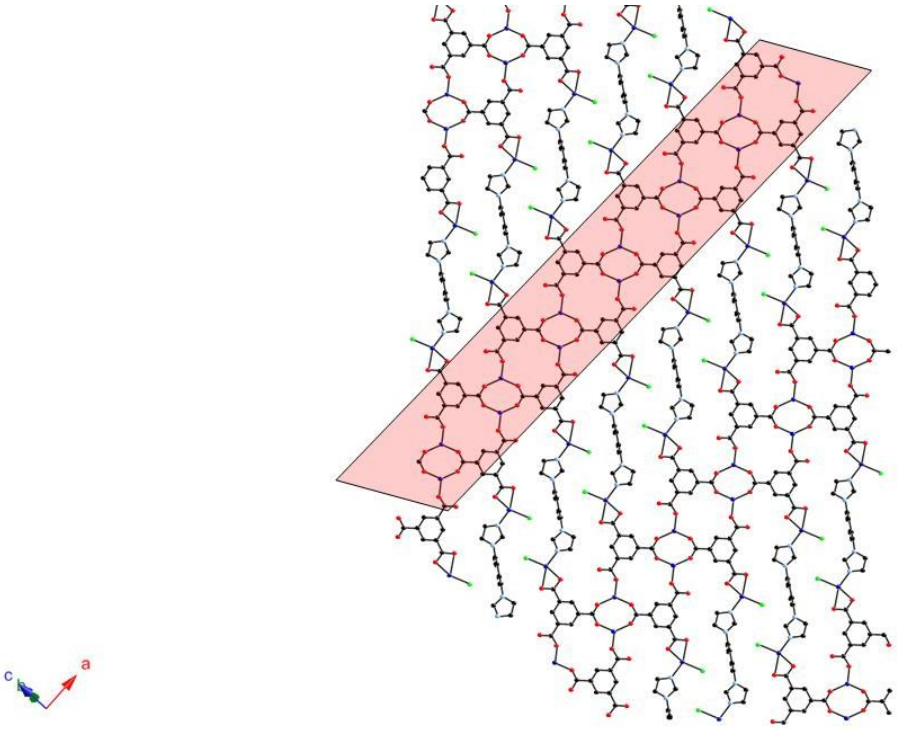

Figure 4.17 (a) 2D sheet of **4.5**, $[Co_2(BTC^{3-})_2Co_2Cl_2(\mathbf{L3})]$. An anionic 1D double chain, $[Co_2(BTC^{3-})_2]^{-2}$, is indicated as a rectangle.

(b)

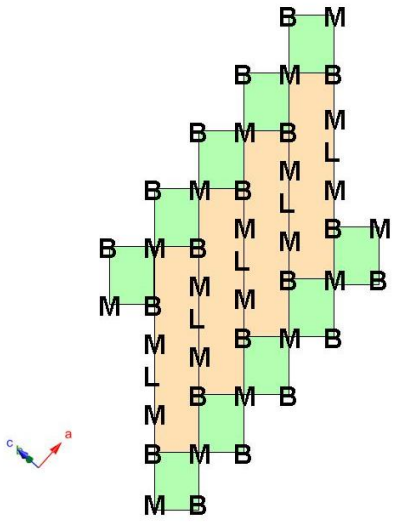

Figure 4.17 (b) Schematic representation of 2D sheet, (12, 4) rings. (M: cobalt ion, B: BTC^{3-} anion, L:**L3** ligand.)

The layers are connected by **L3,** which forms pillars, to complete 3D network of **4.5** (Figure 4.18). Solvent molecules again fill the channels however these are much smaller than in **4.4**.

(a)

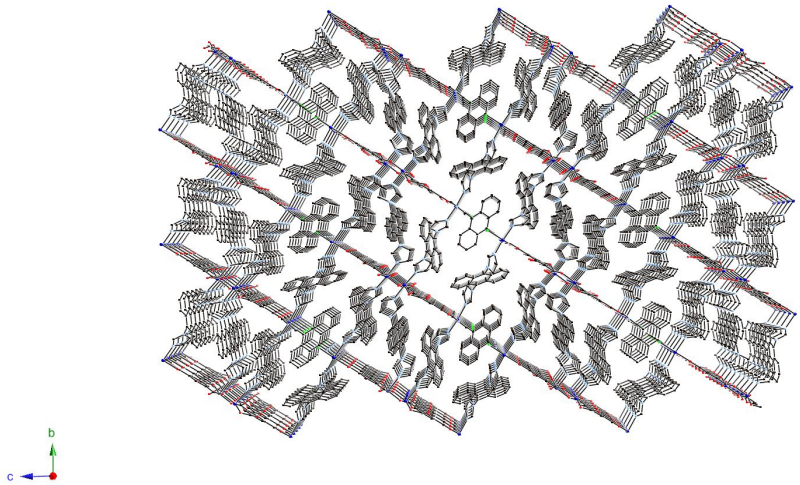

Figure 4.18 (a) A view down on [100] of **4.5** without free solvent molecules**.**

(b)

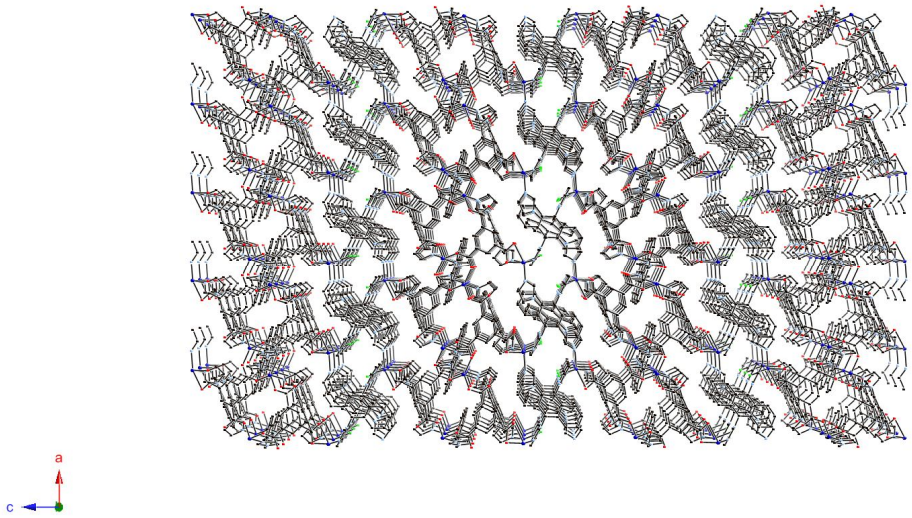

Figure 4.18 (b) A view down on [010] of **4.5** without free solvent molecules.

4.4.9 Structural description of $[Co_6(C_9H_3O_6)_2(HCOO^-)_6(C_{20}H_{14}N_4)_3]\bullet x(C_3H_7NO)\bullet y(H_2O)$ (**4.6**)

The structure of **4.6** with atom numbering scheme is shown in Figure 4.19. Selected bond lengths and angles are summarized in Table 4.7. The asymmetric unit of **4.6** contains one octahedral cobalt(II) ions, one deprotonated formate anion($HCOO^-$), one third of a BTC^{3-} ligand, half an **L3** ligand, and disordered DMF and water solvent molecules.

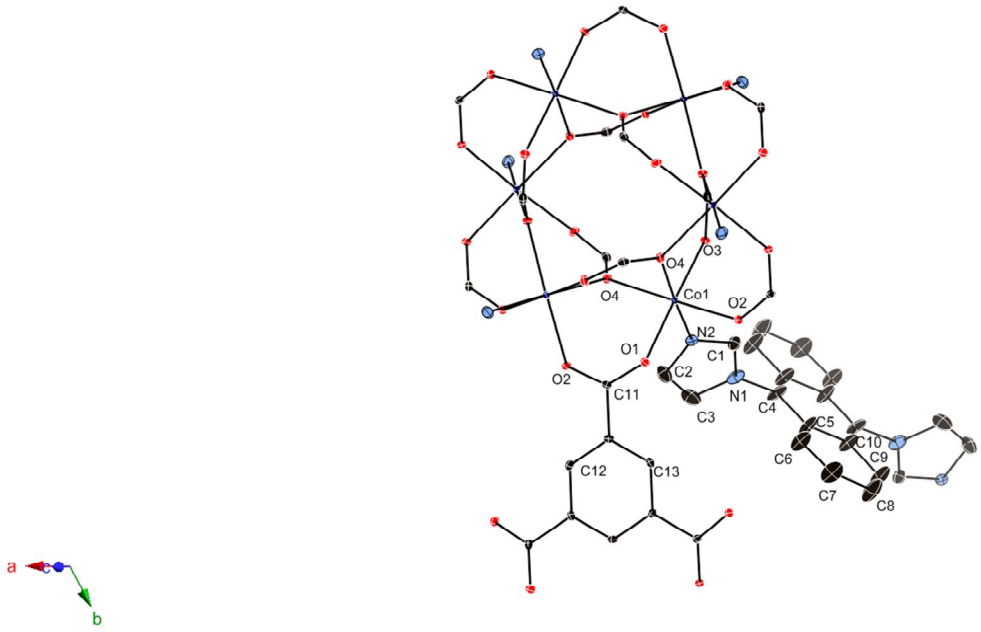

Figure 4.19 Coordination environment of cobalt(II) ion in **4.6** with the ellipsoids drawn at the 50 % probability level.

Table 4.7 Bond lengths (Å) and angles (°) for compound **4.6**.

Bond lengths	(Å)
Co(1)-O(2)	2.0541(14)
Co(1)-O(1)	2.0712(13)
Co(1)-O(4)#1	2.1032(14)
Co(1)-N(2)	2.1165(17)
Co(1)-O(3)	2.1415(14)
Co(1)-O(4)#2	2.1503(13)
O(4)-Co(1)#3	2.1503(13)
Bond angles	(°)
O(2)-Co(1)-O(1)	88.52(5)
O(2)-Co(1)-O(4)#1	89.32(5)
O(1)-Co(1)-O(4)#1	95.06(5)
O(2)-Co(1)-N(2)	89.94(6)
O(1)-Co(1)-N(2)	88.01(6)
O(4)#1-Co(1)-N(2)	176.82(6)

O(2)-Co(1)-O(3)	92.84(5)
O(1)-Co(1)-O(3)	173.93(5)
O(4)#1-Co(1)-O(3)	90.88(5)
N(2)-Co(1)-O(3)	86.07(6)
O(2)-Co(1)-O(4)#2	178.09(6)
O(1)-Co(1)-O(4)#2	92.13(5)
O(4)#1-Co(1)-O(4)#2	88.84(6)
N(2)-Co(1)-O(4)#2	91.87(6)
O(3)-Co(1)-O(4)#2	86.70(5)

Symmetry transformations used to generate equivalent atoms: #1; y, -x+y, -z+1, #2; -x+y,-x, z, #3; -y, x-y, z

Like the previous compounds in this study compound **4.6** is formed under solvothermal conditions. Decomposition (hydrolysis) of DMF leads the formation of formate anion, HCO^-, [138-140] and the presence of formate anion allows the construction of $[Co_6(HCO_2^-)_6]^{6+}$ clusters (Figure 4.20a). These clusters are linked by BTC^{3-} groups to form compact neutral layers of $\{[Co_6(HCO_2^-)_6](BTC^{3-})_2\}_n$ (Figure 4.20b).

(a)

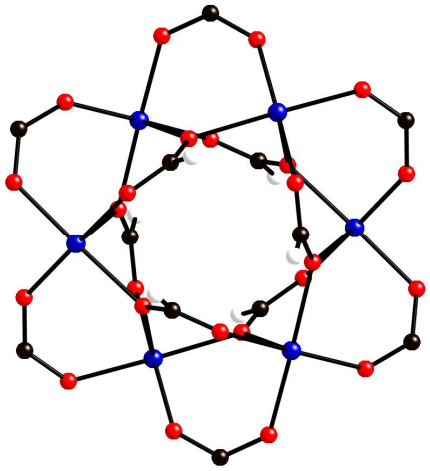

Figure 4.20 (a) A neutral cobalt metal cluster of **4.6**, $[Co_6(HCOO)_6(RCOO)_6]$: Blue:cobalt, red:oxygen, black:carbon and white:hydrogen.

(b)

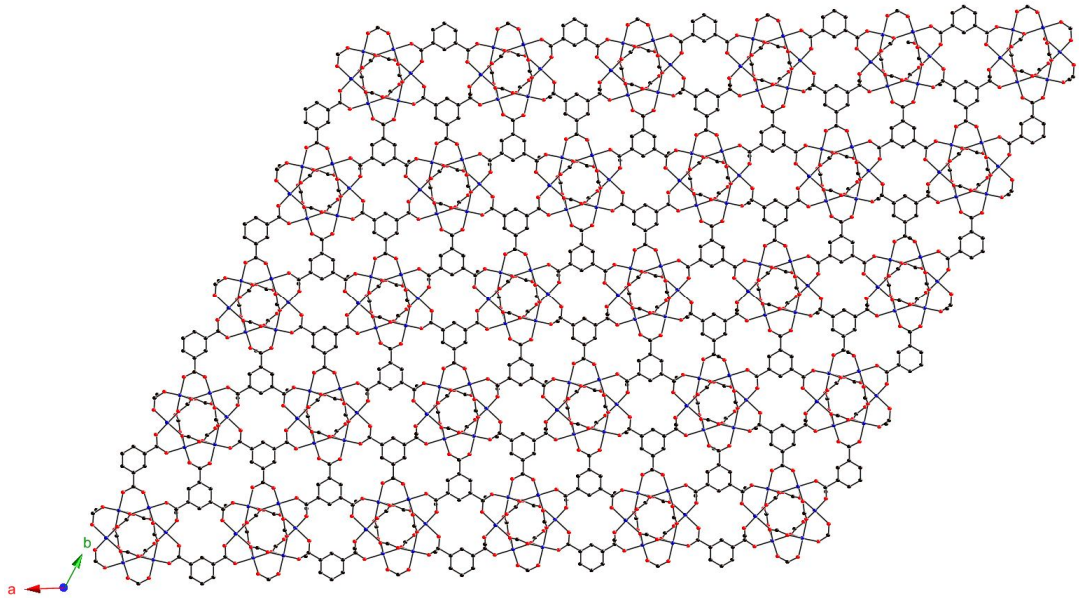

(c)

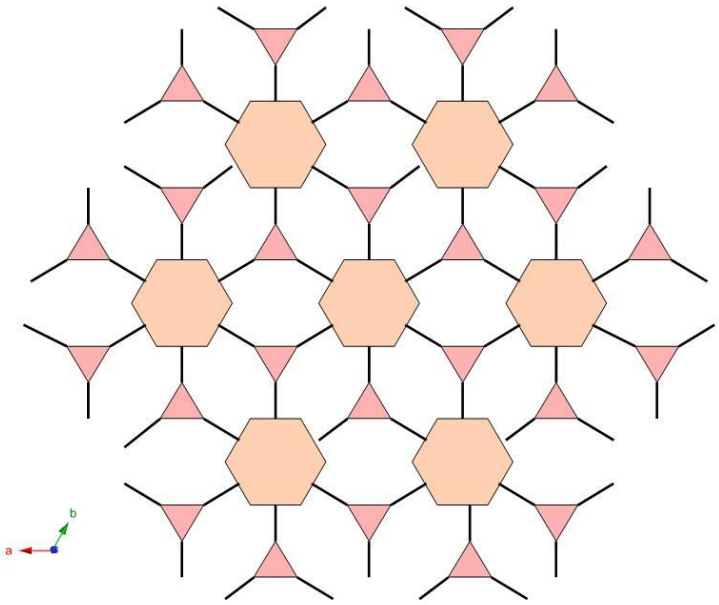

Figure 4.20 (b) A neutral 2D layer network of **4.6**, $[Co_6(HCOO^-)_6(BTC^{3-})_2]$. (c) A schematic representation of 2D layer of **4.6**. ($[Co_6(HCOO^-)_6(BTC^{3-})_2]$: hexagon: Cobalt formate cluster, $[Co_6(HCOO^-)_6(COO^-)_6]$, triangle: BTC^{3-})

These layers are connected by pillars of **L3** to complete the 3D network (Figure 4.21). The number of solvent molecules, DMF and water, that occupy interstitial spaces could not be definitively determined by X-ray crystallography.

(a) [100]

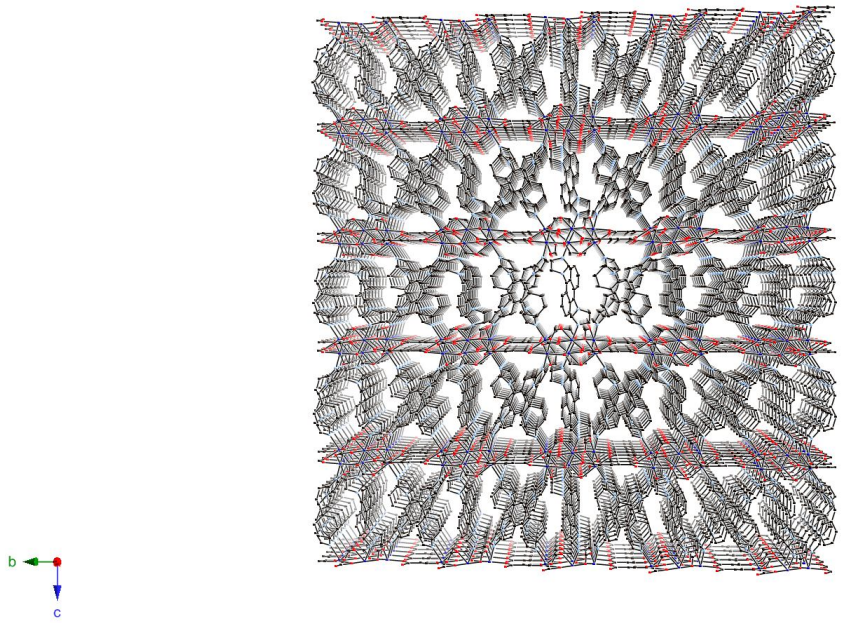

(b) [001]

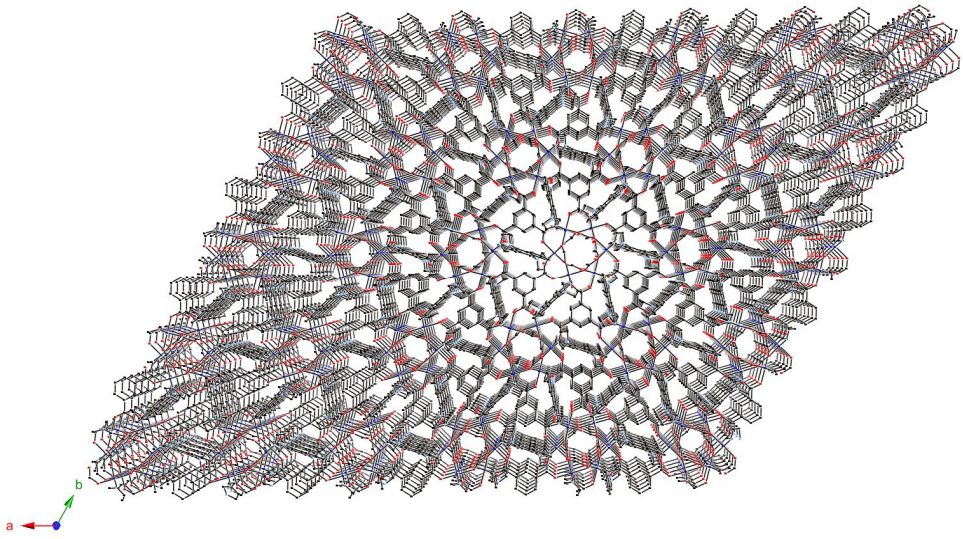

Figure 4.21 Two views of non-interpenetrating 3D framework of **4.6**.

4.4.10 Synthesis of Frameworks of BTC^{3-} and L3

Compounds **4.4**, **4.5**, and **4.6** are each formed from cobalt, **L3**, and BTC^{3-}. Compound **4.4**, with Co:**L3**:BTC ratio of 3:3:2, is formed in a solvent system 4/1, H_2O/CH_3CN, vol./vol. The anthracene ligand, **L3**, has poor solubility yet at high temperature sufficient ligand dissolves to allow the framework to form. In an attempt to improve the yield of **4.4**, the ratio of acetonitrile was increased to 50/50 by volume with water. Under these reaction condition, **4.5** is formed with a Co:**L3**:BTC ratio of 4:5:2. The increase in **L3** content may be directly related to an increase in **L3** concentration due to the change in solvent. When acetonitrile is replaced by DMF completely different chemistry is observed. The DMF appears to be the source of formate anion which leads to the formation of $[Co_6(HCOO^-)]_6^{6+}$ clusters. It is these clusters that serve as the basic building block for the metal organic framework, **4.6**.

4.5 Thermogravimetric analysis (TGA)

To investigate the thermal stability of the crystalline coordination networks, thermogravimetric analysis (TGA) was performed under a flow of nitrogen stream with the heating rate of 10 °Cmin^{-1} on bulk crystalline samples of compound **4.1-4.6** (Figure 4.22a-f).

The TGA curve of **4.1** up to 250 °C shows a total weight loss of 3.7 %, which corresponds to loss of one coordinated and one lattice water molecule (calculated, 3.8%). Decomposition of **4.1** begins about 400 °C.

(a)

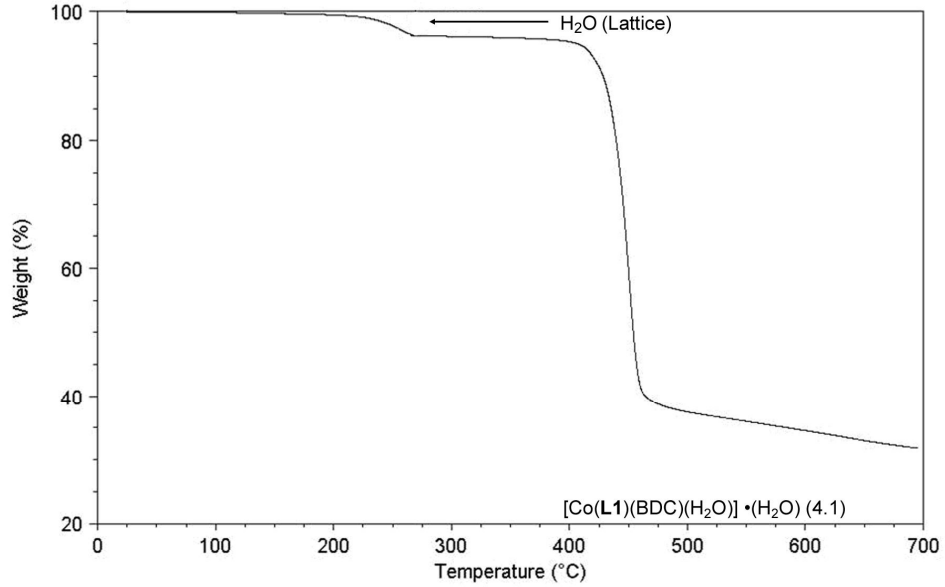

Figure 4.22 (a) The TGA curve of compound **4.1**.

The TGA curve of **4.2** shows a minimal weight loss up to 380 °C when decomposition begins above 380 °C. The

(b)

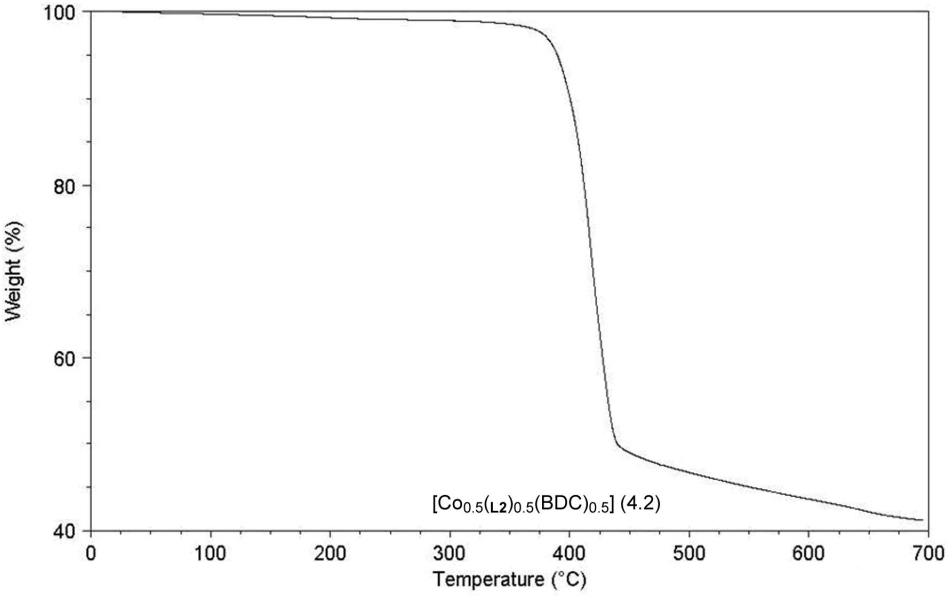

Figure 4.22 (b) The TGA curve of compound **4.2**.

TGA curve of **4.3** displays a weight loss of 5.1 % by 150 °C. This corresponds to loss of two coordinated water molecules and two lattice water molecules (calculated, 5.0 %). Decomposition of **4.3** begins above 310 °C.

(c)

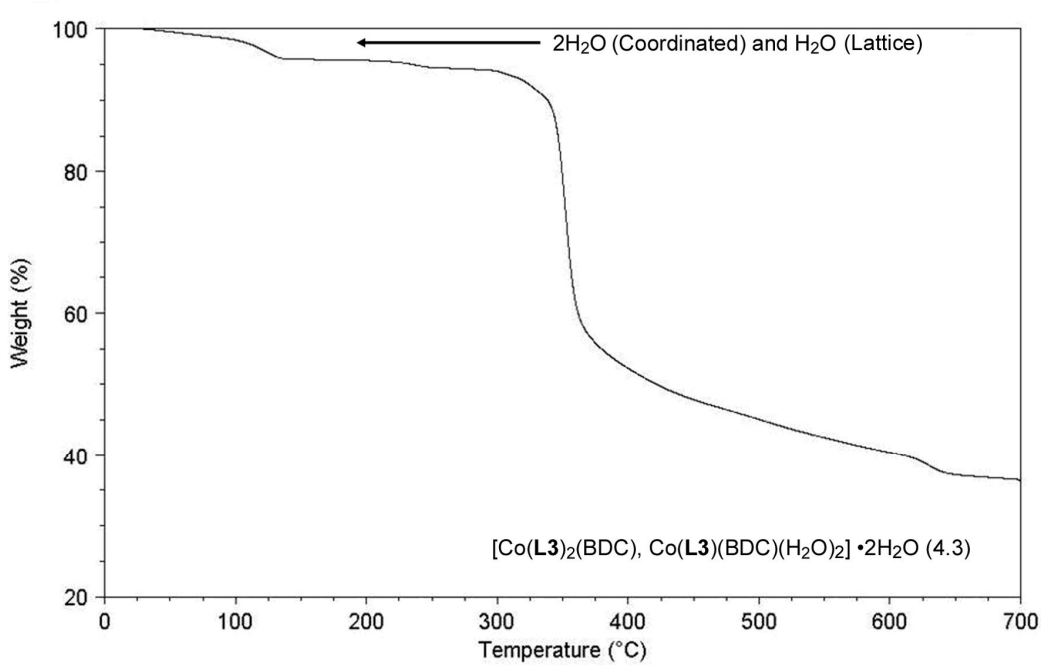

Figure 4.22 (c) The TGA curve of compound **4.3**.

The TGA curve of **4.4** displays a weight loss of 9.9 % by 90 °C, which corresponds to ten lattice water molecules (calculated, 10.4 %). This result indicates that those lattice water molecules are loosely occupied within the pore of 3D frameworks. Crystallographic analysis reveals that eight water molecules have large thermal ellipsoid, which indicates those water molecules do not have well defined positions at 100 K. An additional weight loss was observed between 90 °C and 155 °C to give a total weight loss

of 12.1 %, consistent with the loss of ten lattice water molecules plus the two coordinated water molecules (calculated, 12.5 %). Compound **4.4** starts to decompose around 350 °C.

(d)

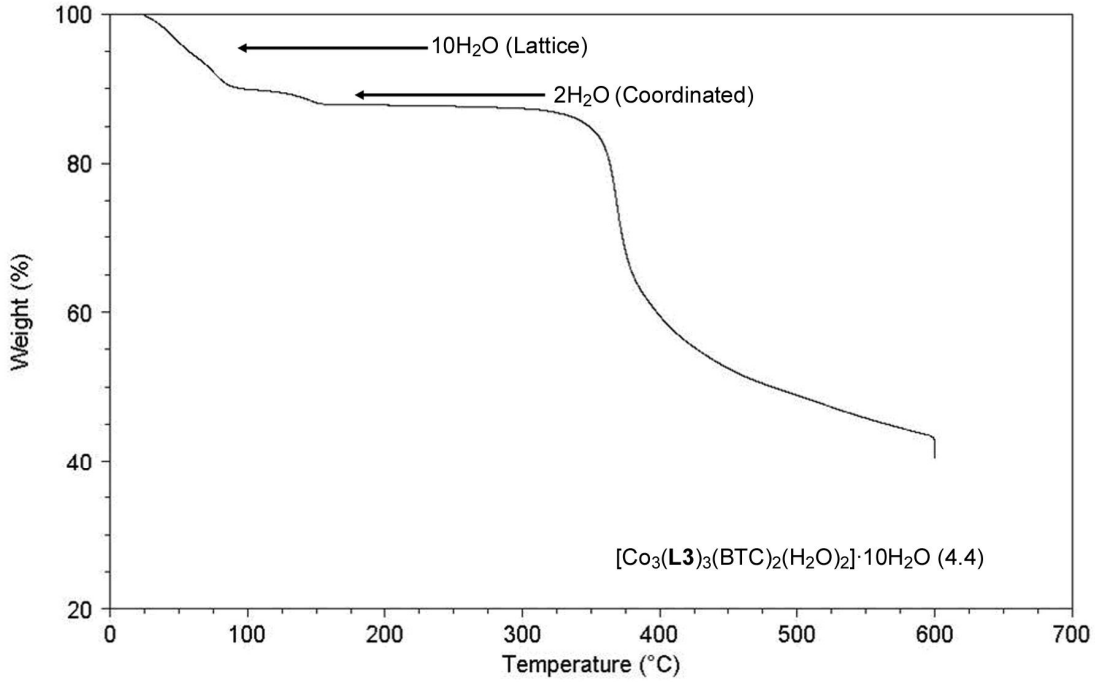

Figure 4.22 (d) The TGA curve of compound **4.4**.

The TGA curve of **4.5** displays a weight loss of 4.9 % by 120 °C. This corresponds to the loss of free lattice water molecules (calculated, 5.2%). Subsequent weight loss of about 2.0 % takes place by 310 °C when decomposition begins.

(e)

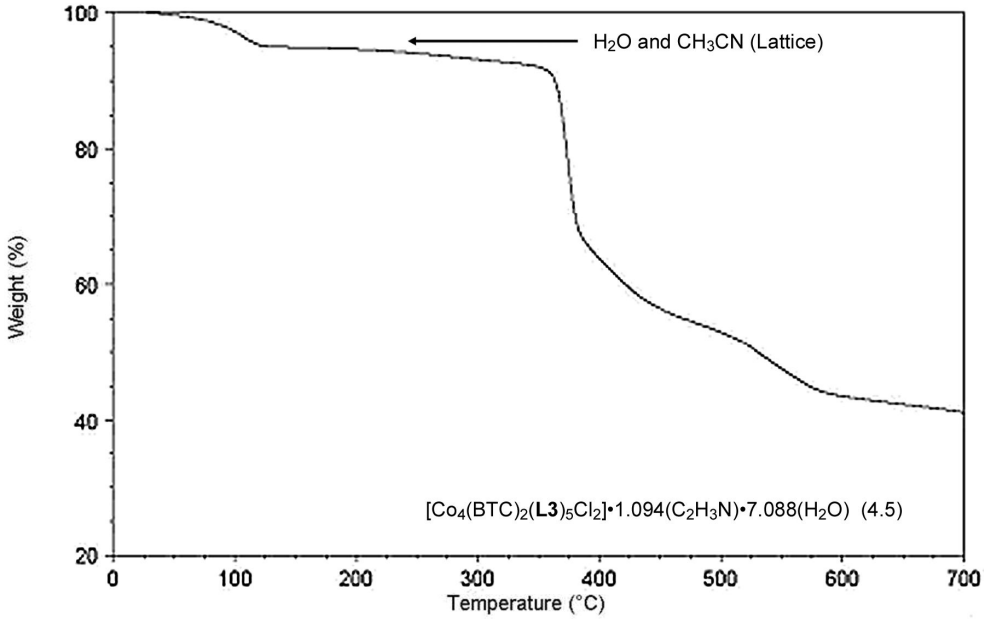

Figure 4.22 (e) The TGA curve of compound **4.5**.

In compound **4.6**, in determinant quantities of DMF and water solvent molecules are found to be disordered by X-ray diffraction. The TGA curve of bulk sample of compound **4.6** shows a weight loss of 1.5 % up to 200 °C.

(f)

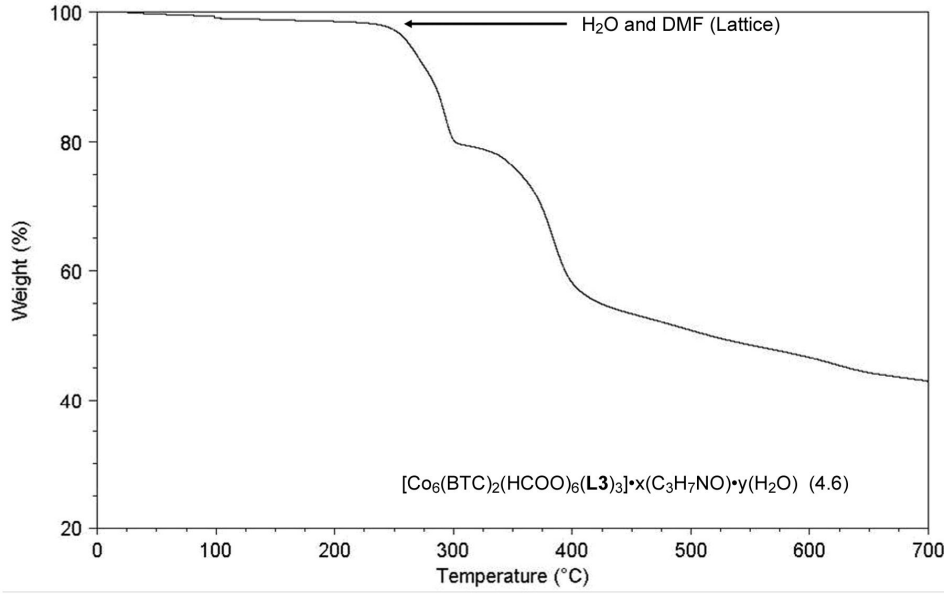

Figure 4.22 (f) The TGA curve of compound **4.6**.

4.6 Dehydration experiment and solvent exchange experiment of compound **4.4**

In an attempt to determine whether compound **4.4** remains crystalline after dehydration; single crystals of **4.4** were subjected to heating under N_2 or vacuum at temperatures of 35, 55, 85, and 100 °C. At 35 and 55 °C, crystallinity was retained and was confirmed by unit cell determination. A few crystals heated at 85 °C retained crystallinity. Data collection on sample heated to 55 and 85 °C showed water molecules are partially occupied in the pores of 3D framework. The water positions are poorly defined in these crystalline samples. Upon heating to temperatures greater than 85 °C, the samples become opaque and X-ray data could not be determined. Although TGA shows that compound **4.4** is thermally stable up to 350 °C, it is apparent that the crystallinity, and very likely the framework architecture, is lost upon complete dehydration.

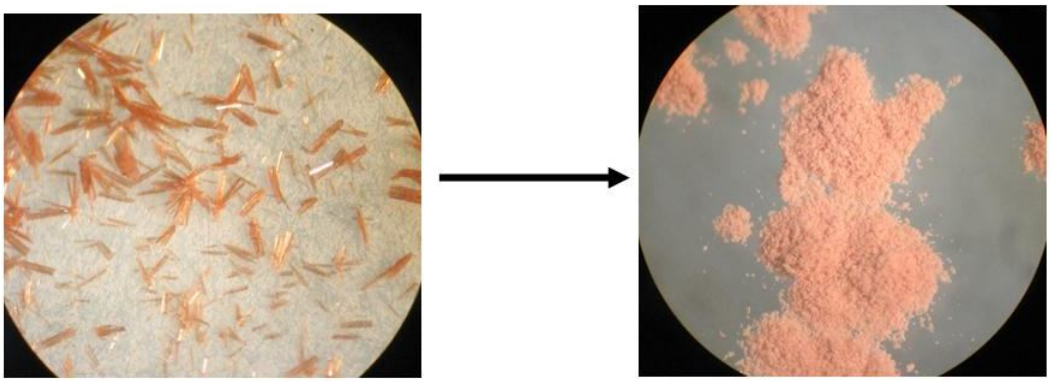

Figure 4.23 Microscopic pictures of original crystals and dehydrated crystals.

4.7 Solvent exchange experiment of compound **4.4**

It was noted earlier that water occupies relatively hydrophobic channels in **4.4**.We attempted several solvent exchange experiments with **4.4** and examined the resulting crystals.

Single crystals of compound **4.4** were carefully selected and immersed into chloroform for seven days. A single crystal X-ray diffraction study on the chloroform exchanged crystals, **4.4'**. The XRD study revealed that six of the lattice water molecules of **4.4** are exchanged by two chloroform molecules (Figure 4.23). Review of the structure reveals that the 3D framework architecture is retained with slight sliding the $[Co_3(BTC)_2]_n$ layers compared to the original structure. This appears to be due to the loss of hydrogen bonds from those free water molecules around the coordinated water molecules on cobalt(II) ions. Thus, this study shows that this framework retains crystallinity after exchanging six water molecules to two chloroform molecules at room temperature.

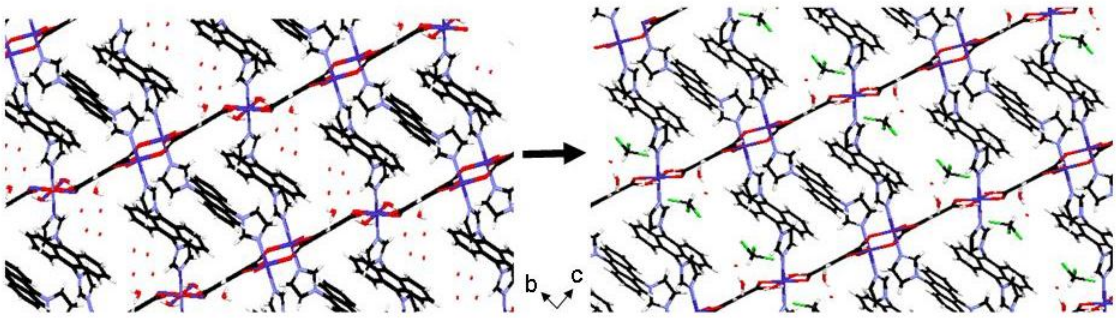

Figure 4.24 Solvent exchange experiment of **4.4**.1D channels on [100] for original structure to $CHCl_3$ exchanged crystal structure of **4.4'**.

4.9 Conclusions

In this paper, we report the synthesis and structural analyses of six different structures of crystalline coordination networks that were prepared using rigid building ligands. Using smaller rigid linkers can create large void spaces by using rigid anionic ligand (BDC) although the void spaces are filled with mutual frameworks to form interpenetrating frameworks. The rigid anthracene ligand (**L3**) may be form 3D networks

with cavities by using other rigid anionic ligands that have potential to form 2D layers. We also found that a choice of solvent governs the final network structure in this study. Solubility and concentration of **L3** completely changed the structures although void spaces in these 3D frameworks became much smaller in compounds **4.5** and **4.6**. This work contributes to the development for construction of crystalline coordination networks with a mixed ligand system by using co-solvent system.

4.10 References

1. Li, J.-R.; Kuppler, R. J.; Zhou, H.-C., Selective gas adsorption and separation in metal-organic frameworks. *Chem. Soc. Rev.* **2009,** *38* (5), 1477-1504.
2. Czaja, A. U.; Trukhan, N.; Muller, U., Industrial applications of metal-organic frameworks. *Chem. Soc. Rev.* **2009,** *38* (5), 1284-1293.
3. Dinca, M.; Long, J. R., Hydrogen storage in microporous metal-organic frameworks with exposed metal sites. *Angewandte Chemie, International Edition* **2008,** *47* (36), 6766-6779.
4. Mueller, U.; Schubert, M.; Teich, F.; Puetter, H.; Schierle-Arndt, K.; Pastre, J., Metal-organic frameworks-prospective industrial applications. *J. Mater. Chem.* **2006,** *16* (7), 626-636.
5. Murray, L. J.; Dinca, M.; Long, J. R., Hydrogen storage in metal-organic frameworks. *Chem. Soc. Rev.* **2009,** *38* (5), 1294-1314.
6. Rowsell, J. L. C.; Yaghi, O. M., Strategies for hydrogen storage in metal-organic frameworks. *Angewandte Chemie, International Edition* **2005,** *44* (30), 4670-4679.
7. Thomas, K. M., Adsorption and desorption of hydrogen on metal-organic framework materials for storage applications: comparison with other nanoporous materials. *Dalton Trans.* **2009,** (9), 1487-1505.
8. Shimomura, S.; Bureekaew, S.; Kitagawa, S., Porous coordination polymers towards gas technology. *Struct. Bonding (Berlin, Ger.)* **2009,** *132* (Molecular Networks), 51-86.
9. Tranchemontagne, D. J.; Ni, Z.; O'Keeffe, M.; Yaghi, O. M., Reticular chemistry of metal-organic polyhedra. *Angewandte Chemie, International Edition* **2008,** *47* (28), 5136-5147.
10. Eddaoudi, M.; Moler, D. B.; Li, H.; Chen, B.; Reineke, T. M.; O'Keeffe, M.; Yaghi, O. M., Modular Chemistry: Secondary Building Units as a Basis for the Design of Highly Porous and Robust Metal-Organic Carboxylate Frameworks. *Acc. Chem. Res.* **2001,** *34* (4), 319-330.
11. Rowsell, J. L. C.; Yaghi, O. M., Metal-organic frameworks: a new class of porous materials. *Microporous Mesoporous Mater.* **2004,** *73* (1-2), 3-14.

12. Yaghi, O. M.; O'Keeffe, M.; Ockwig, N. W.; Chae, H. K.; Eddaoudi, M.; Kim, J., Reticular synthesis and the design of new materials. *Nature (London, U. K.)* **2003,** *423* (6941), 705-714.
13. Perry, J. J. I. V.; Perman, J. A.; Zaworotko, M. J., Design and synthesis of metal-organic frameworks using metal-organic polyhedra as supermolecular building blocks. *Chem. Soc. Rev.* **2009,** *38* (5), 1400-1417.
14. Zaworotko, M. J., Nanoporous structures by design. *Angewandte Chemie, International Edition* **2000,** *39* (17), 3052-3054.
15. Ockwig, N. W.; Delgado-Friedrichs, O.; O'Keeffe, M.; Yaghi, O. M., Reticular Chemistry: Occurrence and Taxonomy of Nets and Grammar for the Design of Frameworks. *Acc. Chem. Res.* **2005,** *38* (3), 176-182.
16. Ferey, G., Some suggested perspectives for multifunctional hybrid porous solids. *Dalton Trans.* **2009,** (23), 4400-4415.
17. Ferey, G., Hybrid porous solids: past, present, future. *Chem. Soc. Rev.* **2008,** *37* (1), 191-214.
18. Kitagawa, S.; Kitaura, R.; Noro, S.-i., Functional porous coordination polymers. *Angewandte Chemie, International Edition* **2004,** *43* (18), 2334-2375.
19. Batten, S. R., Glorious uncertainty-challenges for network design. *J. Solid State Chem.* **2005,** *178* (8), 2475-2479.
20. Carlucci, L.; Ciani, G.; Proserpio, D. M., Polycatenation, polythreading and polyknotting in coordination network chemistry. *Coord. Chem. Rev.* **2003,** *246* (1-2), 247-289.
21. Batten, S. R.; Robson, R., Interpenetrating nets: ordered, periodic entanglement. *Angewandte Chemie, International Edition* **1998,** *37* (11), 1461-1494.
22. Li, Z.-X.; Xu, Y.; Zuo, Y.; Li, L.; Pan, Q.; Hu, T.-L.; Bu, X.-H., Varying Ligand Backbones for Modulating the Interpenetration of Coordination Polymers Based on Homoleptic Cobalt(II) Nodes. *Crystal Growth & Design* **2009,** *9* (9), 3904-3909.
23. Li, Z.-X.; Hu, T.-L.; Ma, H.; Zeng, Y.-F.; Li, C.-J.; Tong, M.-L.; Bu, X.-H., Adjusting the Porosity and Interpenetration of Cadmium(II) Coordination Polymers by Ligand Modification: Syntheses, Structures, and Adsorption Properties. *Crystal Growth & Design 10* (3), 1138-1144.
24. Yang, J.; Ma, J.-F.; Liu, Y.-Y.; Ma, J.-C.; Batten, S. R., A Series of Cu(II) Complexes Based on Different Bis(imidazole) Ligands and Organic Acids: Formation of Water Clusters and Fixation of Atmospheric Carbon Dioxide. *Crystal Growth & Design* **2008,** *8* (12), 4383-4393.
25. Carlucci, L.; Ciani, G.; Proserpio, D. M.; Spadacini, L., Supramolecular isomers in the same crystal: a new case involving two different types of layers polycatenated in the 3D architecture of [Cu(bix)2(SO4)].7.5H2O [bix = 1,4-bis(imidazol-1-ylmethyl)benzene]. **2004,** *6*, 96-101.
26. Willans, C. E.; French, S.; Barbour, L. J.; Gertenbach, J.-A.; Junk, P. C.; Lloyd, G. O.; Steed, J. W., A catenated imidazole-based coordination polymer exhibiting significant CO2 sorption at low pressure. *Dalton Trans.* **2009,** (33), 6480-6482.
27. Xu, G.-C.; Ding, Y.-J.; Okamura, T.-a.; Huang, Y.-Q.; Bai, Z.-S.; Hua, Q.; Liu, G.-X.; Sun, W.-Y.; Ueyama, N., Coordination Polymers with Varied Metal Centers and Flexible Tripodal Ligand 1,3,5-Tris(imidazol-1-ylmethyl)benzene: Synthesis, Structure, and Reversible Anion Exchange Property. *Crystal Growth & Design* **2009,** *9* (1), 395-403.

28. Zhang, Z.-H.; Song, Y.; Okamura, T.; Hasegawa, Y.; Sun, W.-Y.; Ueyama, N., Syntheses, Structures, Near-Infrared and Visible Luminescence, and Magnetic Properties of Lanthanide-Organic Frameworks with an Imidazole-Containing Flexible Ligand. *Inorg. Chem.* **2006,** *45* (7), 2896-2902.
29. Liu, Y.; Qi, Y.; Lv, Y.-Y.; Che, Y.-X.; Zheng, J.-M., Polyrotaxane-like and Interpenetrating Metal-Organic Frameworks (MOFs) Constructed from Biphenyl-4,4'-Dicarboxylate and Bis(imidazole) Ligand. *Crystal Growth & Design* **2009,** *9* (11), 4797-4801.
30. Yang, G.-S.; Lan, Y.-Q.; Zang, H.-Y.; Shao, K.-Z.; Wang, X.-L.; Su, Z.-M.; Jiang, C.-J., Two eight-connected self-penetrating porous metal-organic frameworks: configurational isomers caused by different linking modes between terephthalate and binuclear nickel building units. *CrystEngComm* **2009,** *11* (2), 274-277.
31. Qi, Y.; Che, Y.-X.; Zheng, J.-M., Self-Penetrating and Interpenetrating 3D Metal-Organic Frameworks Constructed from the Rigid 1,4-Bis(1-imidazolyl)-benzene Ligand and Aromatic Carboxylate. *Crystal Growth & Design* **2008,** *8* (10), 3602-3608.
32. Chu, Q.; Liu, G.-X.; Huang, Y.-Q.; Wang, X.-F.; Sun, W.-Y., Syntheses, structures, and optical properties of novel zinc(II) complexes with multicarboxylate and N-donor ligands. *Dalton Trans.* **2007,** (38), 4302-4311.
33. Fan, J.; Yee, G. T.; Wang, G.; Hanson, B. E., Syntheses, Structures, and Magnetic Properties of Inorganic-Organic Hybrid Cobalt(II) Phosphites Containing Bifunctional Ligands. *Inorg. Chem.* **2006,** *45* (2), 599-608.
34. Fan, J.; Hanson, B. E., Novel Zinc Phosphate Topologies Defined by Organic Ligands. *Inorg. Chem.* **2005,** *44* (20), 6998-7008.
35. Li, L.; Hu, T.-L.; Li, J.-R.; Wang, D.-Z.; Zeng, Y.-F.; Bu, X.-H., Metal-organic coordination architectures of 9,10-bis(N-benzimidazolyl)anthracene: syntheses, structures and emission properties. *CrystEngComm* **2007,** *9* (5), 412-420.
36. Li, J.-R.; Tao, Y.; Yu, Q.; Bu, X.-H., A pcu-type metal-organic framework with spindle [Zn7(OH)8]6+ cluster as secondary building units. *Chemical Communications (Cambridge, United Kingdom)* **2007,** (15), 1527-1529.
37. Marin, G.; Andruh, M.; Madalan, A. M.; Blake, A. J.; Wilson, C.; Champness, N. R.; Schroeder, M., Structural Diversity in Metal-Organic Frameworks Derived from Binuclear Alkoxo-Bridged Copper(II) Nodes and Pyridyl Linkers. *Crystal Growth & Design* **2008,** *8* (3), 964-975.
38. Tanaka, D.; Horike, S.; Kitagawa, S.; Ohba, M.; Hasegawa, M.; Ozawa, Y.; Toriumi, K., Anthracene array-type porous coordination polymer with host-guest charge transfer interactions in excited states. *Chemical Communications (Cambridge, United Kingdom)* **2007,** (30), 3142-3144.
39. Akimoto, K.; Kondo, Y.; Endo, K.; Yamada, M.; Aoyama, Y.; Hamada, F., A porous coordination architecture assembled by silver triflate and 9,10-bis(3,5-dicyano-1-phenyl)anthracene and its gas adsorption profile. *Tetrahedron Letters* **2008,** *49* (52), 7361-7363.
40. Ma, S.; Sun, D.; Simmons, J. M.; Collier, C. D.; Yuan, D.; Zhou, H.-C., Metal-Organic Framework from an Anthracene Derivative Containing Nanoscopic Cages Exhibiting High Methane Uptake. *Journal of the American Chemical Society* **2008,** *130* (3), 1012-1016.

41. Nelson, A. P.; Parrish, D. A.; Cambrea, L. R.; Baldwin, L. C.; Trivedi, N. J.; Mulfort, K. L.; Farha, O. K.; Hupp, J. T., Crystal to Crystal Guest Exchange in a Mixed Ligand Metal-Organic Framework. *Crystal Growth & Design* **2009,** *9* (11), 4588-4591.
42. Xu, L.; Choi, E.-Y.; Kwon, Y.-U., A new 3D nickel(II) framework composed of large rings: Ionothermal synthesis and crystal structure. *J. Solid State Chem.* **2008,** *181* (11), 3185-3188.
43. Wen, L.-L.; Dang, D.-B.; Duan, C.-Y.; Li, Y.-Z.; Tian, Z.-F.; Meng, Q.-J., 1D Helix, 2D Brick-Wall and Herringbone, and 3D Interpenetration d10 Metal-Organic Framework Structures Assembled from Pyridine-2,6-dicarboxylic Acid N-Oxide. *Inorg. Chem.* **2005,** *44* (20), 7161-7170.
44. Liu, M.; Li, X.; Li, J.; Sun, W.; Yang, Z.; Gong, F.; Chen, J.; Ma, J.; Yang, G., Synthesis and structures of two cobalt(II) coordination networks formed from aromatic polycarboxylates and 1,4-bis(imidazole-1-ylmethyl)benzene. *Transition Met. Chem. (Dordrecht, Neth.)* **2009,** *34* (2), 185-190.
45. Zhu, S.; Zhang, H.; Zhao, Y.; Shao, M.; Wang, Z.; Li, M., Synthesis, structures and luminescence of three coordination polymers constructed from rigid 1,3,5-benzenetricarboxylic acid and flexible bis(imidazol-1-ylmethyl)benzene. *J. Mol. Struct.* **2008,** *892* (1-3), 420-426.
46. Ma, B.-Q.; Mulfort, K. L.; Hupp, J. T., Microporous Pillared Paddle-Wheel Frameworks Based on Mixed-Ligand Coordination of Zinc Ions. *Inorg. Chem.* **2005,** *44* (14), 4912-4914.
47. Hu, Y.; Li, G.; Liu, X.; Hu, B.; Bi, M.; Gao, L.; Shi, Z.; Feng, S., Hydrothermal synthesis and characterization of metal-organic networks with helical units in a mixed ligand system. *CrystEngComm* **2008,** *10* (7), 888-893.
48. Ai, W.; He, H.; Liu, L.; Liu, Q.; Lv, X.; Li, J.; Sun, D., Synthesis, crystal structures and properties of three metal-organic supramolecular architectures based on mixed organic ligands. *CrystEngComm* **2008,** *10* (10), 1480-1486.
49. Hao, N.; Shen, E.; Li, Y.; Wang, E.; Hu, C.; Xu, L., A novel three-dimensional metal-organic interpenetrating framework constructed from mixed adipate and 4,4'-bipy ligands: [Co(OOC(CH2)4COO)(4,4'-bipy)] (H2-adipate = HOOC(CH2)4COOH, 4,4'-bipy = 4,4'-bipyridine). *Inorg. Chem. Commun.* **2004,** *7* (4), 510-512.
50. Bai, H.-Y.; Ma, J.-F.; Yang, J.; Zhang, L.-P.; Ma, J.-C.; Liu, Y.-Y., Eight Two-Dimensional and Three-Dimensional Metal-Organic Frameworks Based on a Flexible Tetrakis(imidazole) Ligand: Synthesis, Topological Structures, and Photoluminescent Properties. *Crystal Growth & Design 10* (4), 1946-1959.
51. Wen, L.-L.; Wang, F.; Feng, J.; Lv, K.-L.; Wang, C.-G.; Li, D.-F., Structures, Photoluminescence, and Photocatalytic Properties of Six New Metal-Organic Frameworks Based on Aromatic Polycarboxylate Acids and Rigid Imidazole-Based Synthons. *Crystal Growth & Design* **2009,** *9* (8), 3581-3589.
52. Yao, J.; Lu, Z.-D.; Li, Y.-Z.; Lin, J.-G.; Duan, X.-Y.; Gao, S.; Meng, Q.-J.; Lu, C.-S., Three-dimensional metal-organic frameworks constructed from bix and 1,2,4-benzenetricarboxylate. *CrystEngComm* **2008,** *10* (10), 1379-1383.
53. Eddaoudi, M.; Li, H.; Yaghi, O. M., Highly porous and stable metal-organic frameworks. Structure design and sorption properties. *Journal of the American Chemical Society* **2000,** *122* (7), 1391-1397.

54. Loiseau, T.; Lecroq, L.; Volkringer, C.; Marrot, J.; Ferey, G.; Haouas, M.; Taulelle, F.; Bourrelly, S.; Llewellyn, P. L.; Latroche, M., MIL-96, a Porous Aluminum Trimesate 3D Structure Constructed from a Hexagonal Network of 18-Membered Rings and micro 3-Oxo-Centered Trinuclear Units. *Journal of the American Chemical Society* **2006,** *128* (31), 10223-10230.
55. Kepert, C. J.; Prior, T. J.; Rosseinsky, M. J., Hydrogen bond-directed hexagonal frameworks based on coordinated 1,3,5-benzenetricarboxylate. *J. Solid State Chem.* **2000,** *152* (1), 261-270.
56. Ko, J. W.; Min, K. S.; Suh, M. P., A Hybrid Consisting of Coordination Polymer and Noncovalent Organic Networks: A Highly Ordered 2-D Phenol Network Assembled by Edge-to-Face pi-pi Interactions. *Inorg. Chem.* **2002,** *41* (8), 2151-2157.
57. Wang, Z.; Kravtsov, V. C.; Zaworotko, M. J., Ternary nets formed by self-assembly of triangles, squares, and tetrahedra. *Angewandte Chemie, International Edition* **2005,** *44* (19), 2877-2880.
58. Wu, Q.; Hook, A.; Wang, S., A blue luminescent starburst molecule and its orange luminescent trinuclear PdII complex: 1,3,5-tris(7-azaindol-1-yl)benzene (tabH) and [PdII3(tab)2Cl4]. *Angewandte Chemie, International Edition* **2000,** *39* (21), 3933-3935.
59. *CrysAlisPro 171*, Oxford Diffraction: Wroclaw, Poland, 2004.
60. Farrugia, L. J., WinGX suite for small-molecule single-crystal crystallography. *J. Appl. Crystallogr.* **1999,** *32* (4), 837-838.
61. Sheldrick, G. M., A short history of SHELX. *Acta Crystallogr., Sect. A: Found. Crystallogr.* **2008,** *A64* (1), 112-122.
62. Lin, X.-M.; Fang, H.-C.; Zhou, Z.-Y.; Chen, L.; Zhao, J.-W.; Zhu, S.-Z.; Cai, Y.-P., Temperature- and solvent-controlled dimensionality in a zinc 6-(1H-benzimidazol-2-yl)pyridinecarboxylate system. *CrystEngComm* **2009,** *11* (5), 847-854.
63. He, J.; Zhang, Y.; Pan, Q.; Yu, J.; Ding, H.; Xu, R., Three metal-organic frameworks prepared from mixed solvents of DMF and HAc. *Microporous Mesoporous Mater.* **2006,** *90* (1-3), 145-152.
64. Rebilly, J.-N.; Bacsa, J.; Rosseinsky, M. J., 1D tubular and 2D metal-organic frameworks based on a flexible amino acid derived organic spacer. *Chem.--Asian J.* **2009,** *4* (6), 892-903.

Chapter 5

5.1 Summary and Conclusions

The goal of this research was to investigate the synthesis of potentially porous materials by combining a transition metal ion with neutral and anionic bridging organic ligands in a crystalline network. Also, this research attempted to determine how the mixed ligand system influences coordination network structure. The size and flexibility of the ligands dictated the final network structure.

The ability to incorporate anthracene into network structure is a significant advance. Anthracene groups in porous materials are of great interest as molecular sensors due to the fluorescence of anthracene.[11] Anthracene based MOFs have not been explored much due to its poor solubility under typical MOF synthetic conditions. We believe that a use of anthracene as a building block with anionic bridging ligand offers the opportunity to prepare porous networks for molecular sensor applications. **Further, anthracene bridging groups bonded directly to imidazole ligands are relatively rigid and, as proposed, the incorporation of these rigid bridging ligands leads to permanent void space in one of the successfully prepared compound, namely, compound 4.4**.

We constructed 1D, 2D, and 3D networks with the neutral bis- or tetra- dentate flexible ligands, 9,10-bis(imidazol-1-ylmethyl)anthracene (Chapter 2) and 1, 2, 4, 5-tetrakis(imidazol-1ylmethyl)benzene (Chapter 3).

Flexible bis imidazole ligand in combination with cobalt(II) or zinc(II) ion and H_3BTC form 1D chain networks. Two metal coordination sites are occupied by imidazole groups to form 1D chain networks in this case. The presence of anthracene groups influence the networks by forming $\pi\cdots\pi$ stacks. Hydrogen bonding between carboxylate

groups and lattice water further connect the networks. These weak interactions and flexibility of the ligand may adopt the 1D network in this case.

Flexible tetradentate ligand, 1, 2, 4, 5-tetrakis(imidazol-1ylmethyl)benzene, has many potential conformations. The construction of coordination networks with this ligand reveals three different conformations. All of the imidazole coordination sites are used in the structures of **3.2** and **3.3**. A comparison of compound **3.2** and **3.3** in Chapter 3 illustrates how this ligand can lead to 2D and 3D structures. In **3.2**, the tetradentate ligand is a linear rod with a chair conformation. In **3.3**, the tetradentate ligand adopts a pinwheel fashion to act as 2D building block with intersecting directionality. The key for constructing 3D networks with flexible tetradentate ligands is to form the pinwheel conformation although from this study we are not able to control the conformations by design and synthesis. **These ligands, also with aromatic spacers but with an intervening methylene group, are more flexible, 9,10-bis(imidazol-1-ylmethyl)anthracene and 1, 2, 4, 5-tetrakis(imidazol-1ylmethyl)benzene. As proposed, MOFs generated with flexible bridging ligands pack efficiently and form compact crystals with no permanent void space.**

The aromatic spacer group has a profound effect on the degree of interpenetration in the final network structure. The linear rigid ligands, **L1**, **L2**, or **L3**, form 3D networks with large cavities (Chapter 4). The 3D networks with **L1** or **L2** and BDC^{2-}, which has also a linear shape, form diamond-like networks. The large cavities are filled with interpenetrating 3D networks. The least bulky ligand, **L1**, forms five fold interpenetrated

3D networks and **L2** forms four fold interpenetrated 3D networks. The bulkiest spacer ligand, **L3**, is interpenetrated 3D networks by an independent 2D networks. Thus, the length of linker and bulkiness of aromatic ring influences the degree of interpenetration with a rigid rod anionic ligand (BDC) in this study. **Specifically, the degree of interpenetration in a network structure is diminished as the bridging ligand increases in size.**

The rigid aromatic carboxylate ligands coordinate in this study to form neutral 1D chains or 2D sheets with metal ions (Chapter 3 and 4). A typical example is compound **4.4**, in which a 2D sheets is formed from cobalt(II) ions and BTC^{3-}. Bidentate imidazole anthracene ligand, **L3**, acts as a pillar to form a 3D network with 1D channels. Thus, the rigid linkers acted as pillars by connecting 2D layers of Co(II) ions and BTC anionic ligand. As a result in this study, the rigid linkers have less flexibility to fill the spaces and form networks with potential void spaces.

The rational design of coordination networks still remains a challenge. Simple changes in synthetic conditions can lead to completely different structures (Chapter 4). For example, the different non-interpenetrating 3D networks **4.5** and **4.6** are formed by changing solvent and stoichiometry with the same building blocks. The concentration of **L3** appears to be the key factor in favoring one structure over the other.

Construction of crystalline coordination networks does not work by simple molecular design and prediction of the final structure. This is due to the difficulty in the synthesis and many the variables required finding the best synthetic condition. From this

work, we found that co-solvent system works for anthracene type bridging ligands, which have very poor solubility in hydrothermal synthesis. The choice of organic solvent needs to be miscible in water and must have some solubility for the selected bridging ligand. Other variables in the synthesis, such as temperature, concentration, ratio of starting materials, order of mixing the starting materials, synthetic container, and pH also play a role. The process of crystal growth in this field is complicated and difficult to understand how these crystalline coordination networks are formed. This study is one of the examples for the synthesis and incorporation of anthracene ligands. Finding synthetic conditions remains a challenge in this field because small changes, such as concentration or volume of solvent ratio, can adopt the completely different final structures as we have seen in this study.

5.2 Reference

1. Doty, F.P.; Baucer, C. A.; Skulan, A. J.; Grant, P. G.; Allendorf, M. D., *Adv. Mater.* (*Weinheim, Ger.*) **2009**, 21, 95-101
2. Tanaka, D.; Horike, S.; Kitagawa, S.; Ohba, M.; Hasegawa, M.; Ozawa, Y.; Toriumi, K., *Chem. Commun. (Cambridge, U. K.)* **2007**, 3142-3144.

Appendix A: NMR spectra

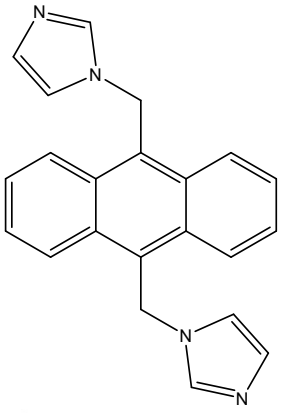

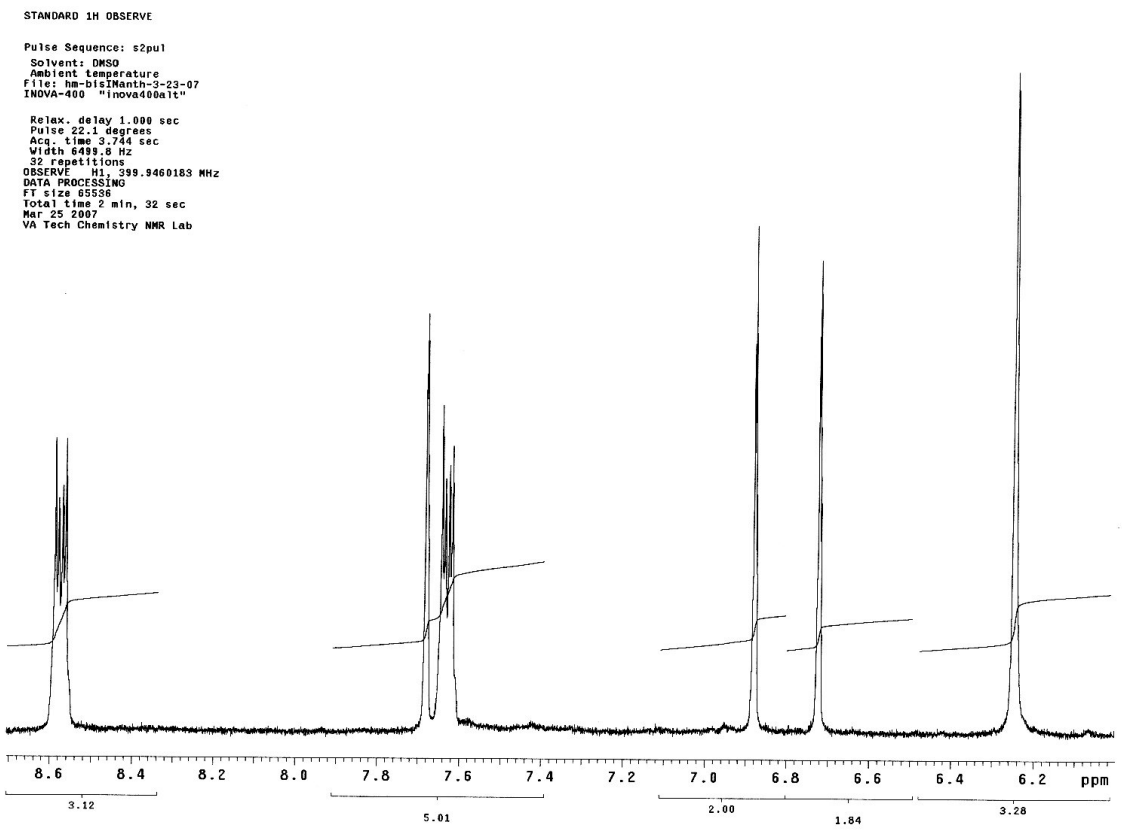

1. ^{1}H-NMR spectrum of **L** (Chapter 2) in DMSO at room temperature.

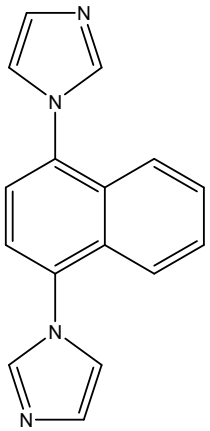

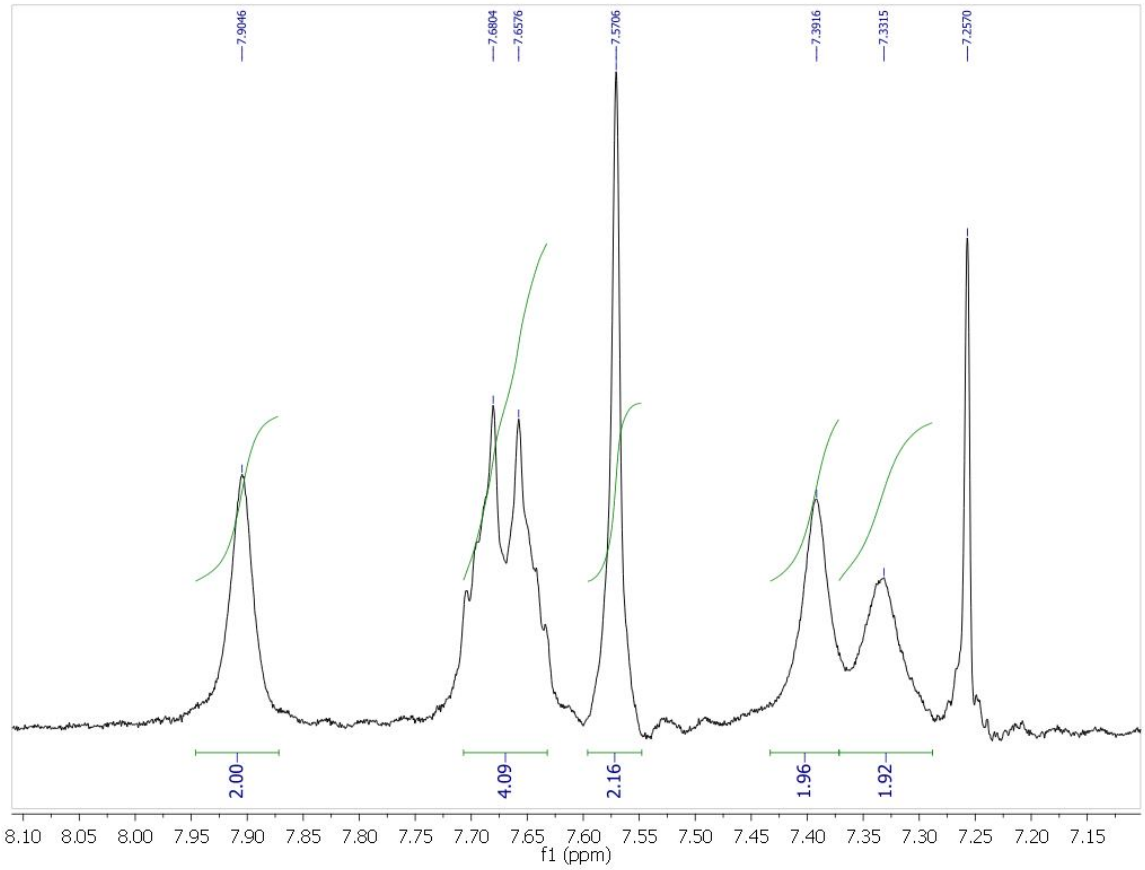

2. ^{1}H-NMR spectrum of **L2** (Chapter 4) in chloroform at room temperature.

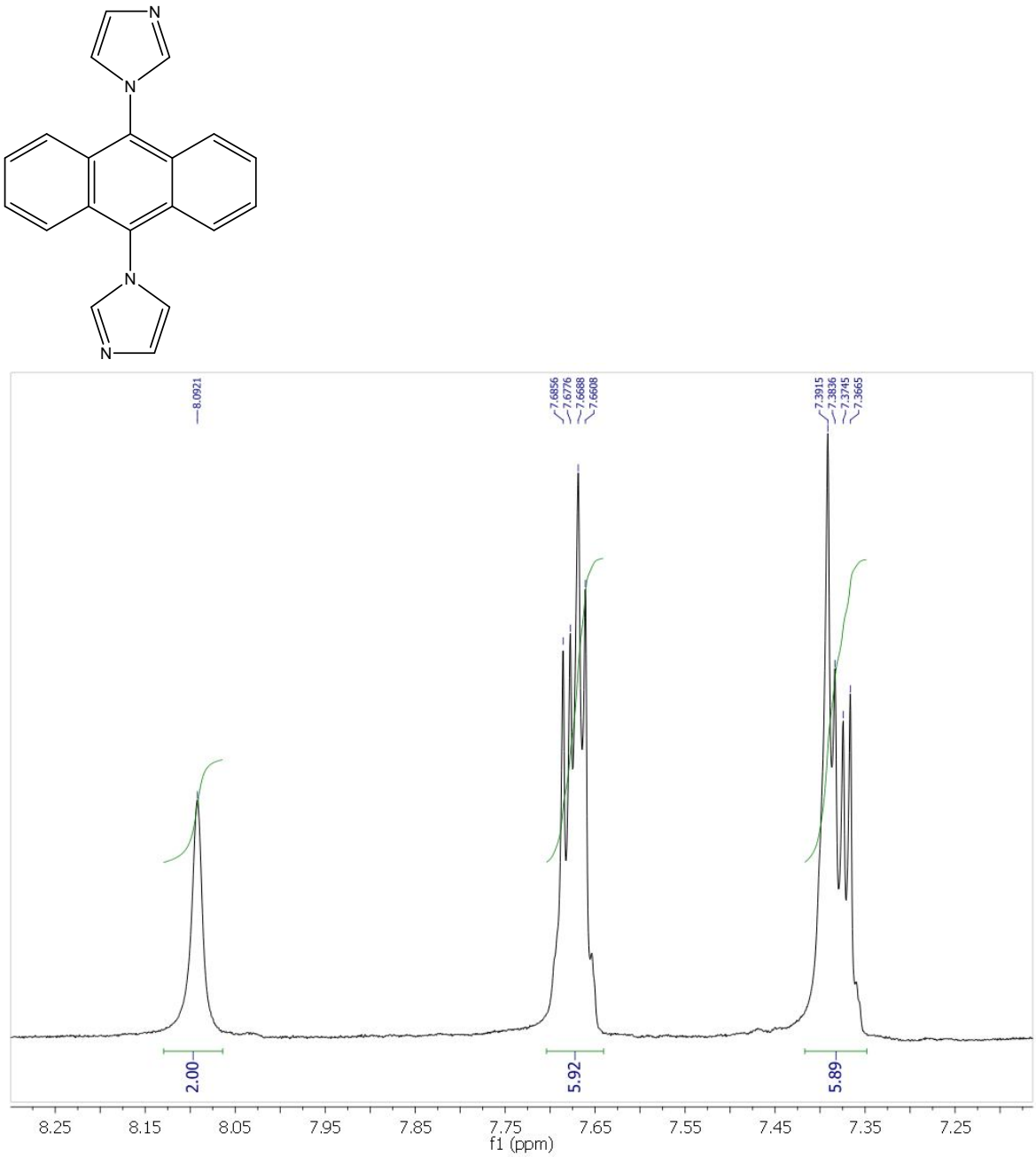

3. ^{1}H-NMR spectrum of **L3** (Chapter 4) in DMSO at room temperature.

Appendix B: Mass Spectroscopy

1. A mass spectroscopy data for 9,10-bis(imidazol-1-ylmethyl)anthracene (**L**) (Chapter 2)

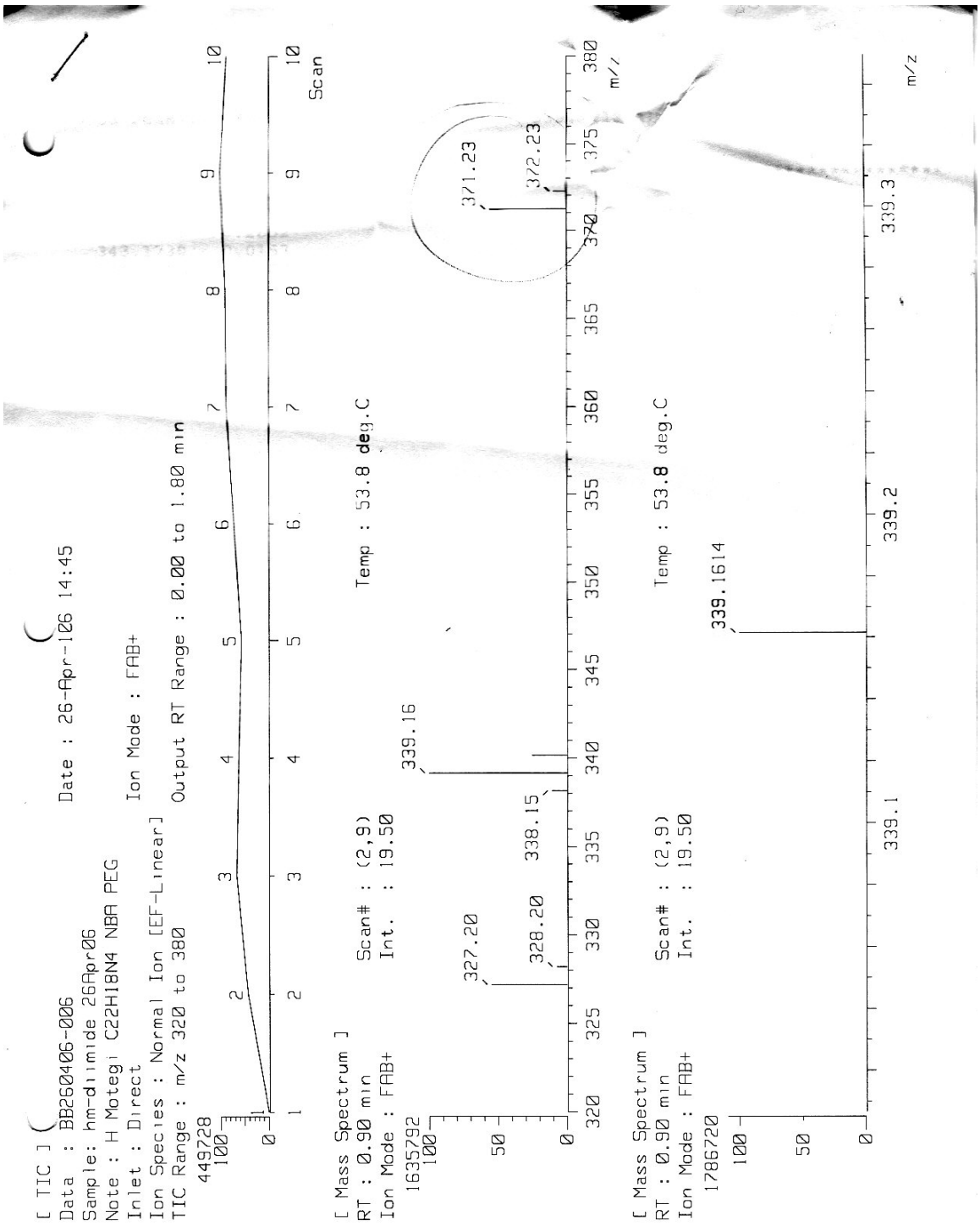

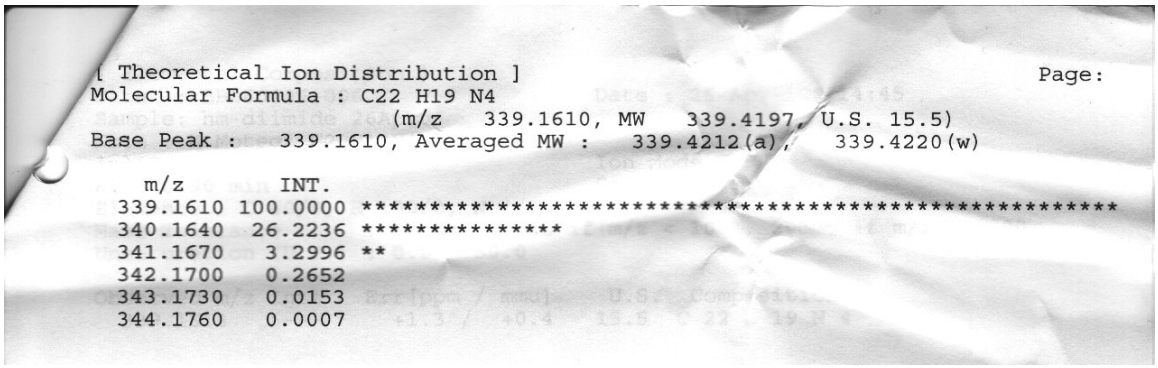

```
[ Theoretical Ion Distribution ]                                    Page:
Molecular Formula : C22 H19 N4
                          (m/z   339.1610, MW   339.4197, U.S. 15.5)
Base Peak :   339.1610, Averaged MW :   339.4212(a),   339.4220(w)

    m/z       INT.
  339.1610 100.0000 ********************************************************
  340.1640  26.2236 **************
  341.1670   3.2996 **
  342.1700   0.2652
  343.1730   0.0153
  344.1760   0.0007
```

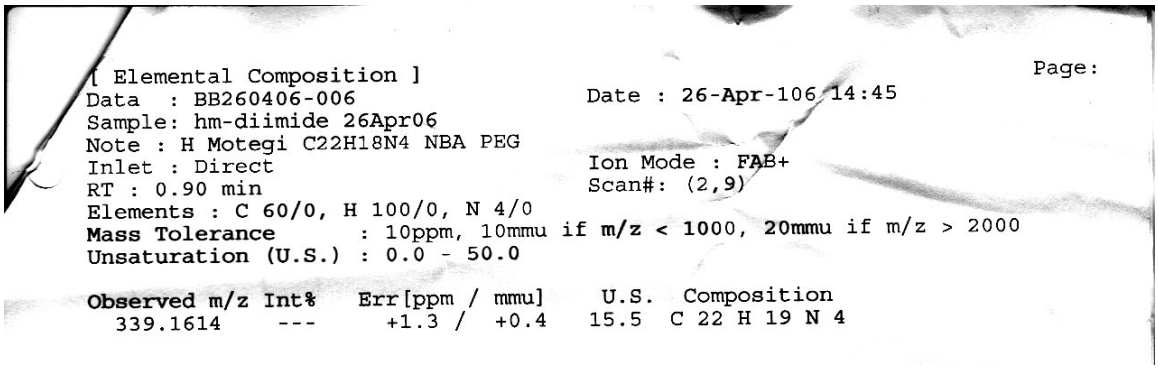

```
[ Elemental Composition ]                                           Page:
Data  : BB260406-006                    Date : 26-Apr-106 14:45
Sample: hm-diimide 26Apr06
Note : H Motegi C22H18N4 NBA PEG
Inlet : Direct                          Ion Mode : FAB+
RT : 0.90 min                           Scan#: (2,9)
Elements : C 60/0, H 100/0, N 4/0
Mass Tolerance       : 10ppm, 10mmu if m/z < 1000, 20mmu if m/z > 2000
Unsaturation (U.S.) : 0.0 - 50.0

Observed m/z Int%   Err[ppm / mmu]    U.S.  Composition
  339.1614    ---     +1.3 /  +0.4   15.5  C 22 H 19 N 4
```

2. A mass spectroscopy data for 1,4-Bis-(1-imidazolyl)naphthalene (**L2**) (Chapter 4)

Qualitative Compound Report

Data File	hm_019_ls_esi_u.d	**Sample Name**	hm_019_l2
Sample Type	Sample	**Position**	P1-E4
Instrument Name	Instrument 1	**User Name**	
Acq Method	MMI_esi_union.m	**IRM Calibration Status**	All Ions Missed
DA Method	msautoproc.m	**Comment**	438473

Compound Table

Compound Label	RT	Mass	Abund	Formula	Tgt Mass	Diff (ppm)
Cpd 1: C16 H12 N4	0.299	260.1075	4039592	C16 H12 N4	260.1062	4.97

Compound Label	RT	Algorithm	Mass
Cpd 1: C16 H12 N4	0.299	Find By Formula	260.1075

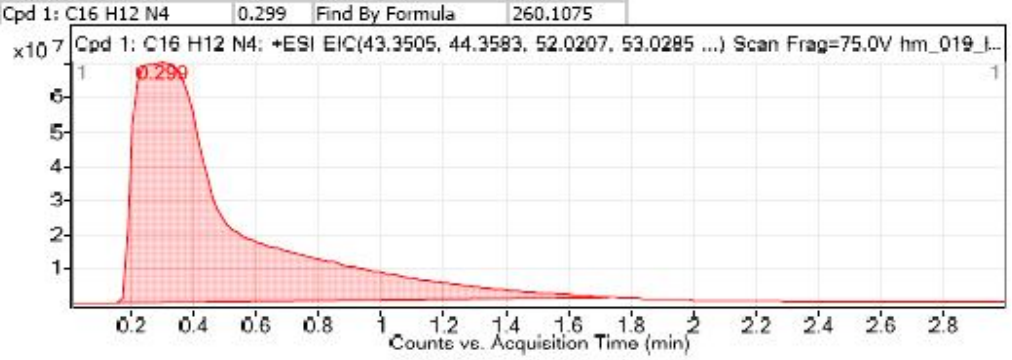

MS Spectrum

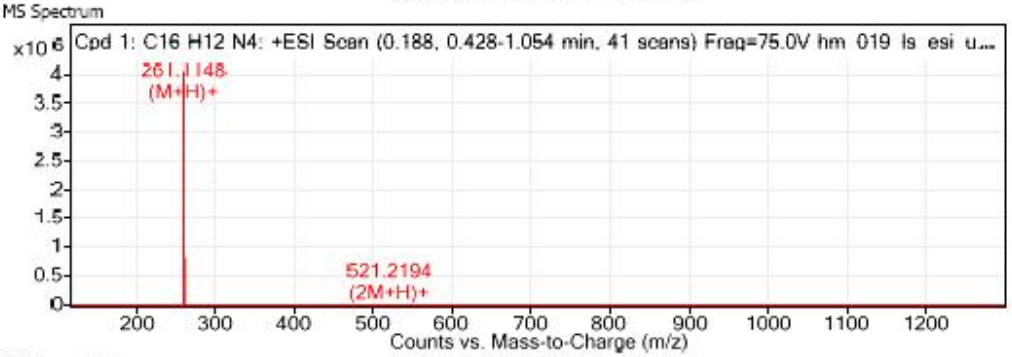

MS Zoomed Spectrum

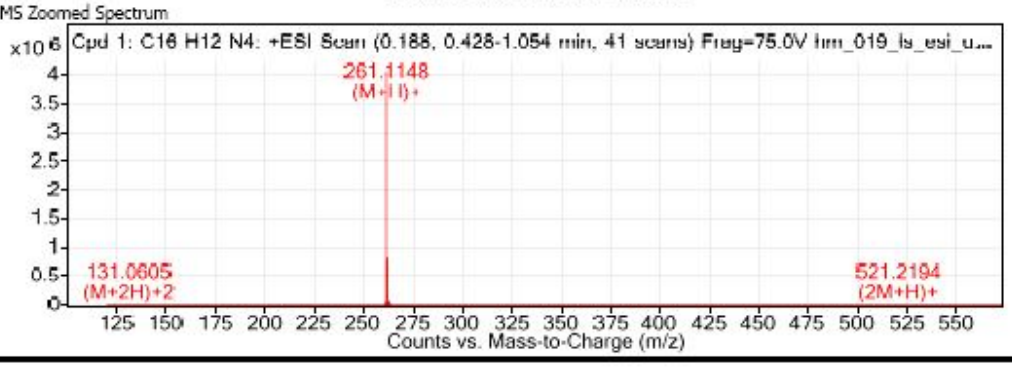

Qualitative Compound Report

MS Spectrum Peak List

m/z	*Calc m/z*	Diff(ppm)	z	Abund	Formula	Ion
131.0605	131.0604	0.87	2	10098	C16 H14 N4	(M+2H)+2
261.1148	261.1135	4.96		4081658	C16 H13 N4	(M+H)+
261.2611				235189		
261.3202				80707		
261.4589				42066		
262.1173	262.1164	3.65		810219	C16 H13 N4	(M+H)+
263.1199	263.1192	2.6		69681	C16 H13 N4	(M+H)+
283.0953	283.0954	-0.35	1	519	C16 H12 N4 Na	(M+Na)+
521.2194	521.2197	-0.44	1	499	C32 H25 N8	(2M+H)+
543.1966	543.2016	-9.26	1	391	C32 H24 N8 Na	(2M+Na)+

--- End Of Report ---

3. A mass spectroscopy data for 9,10-Bis(1-imidazolyl)anthracene (**L3**) (Chapter 4)

Qualitative Compound Report

Data File	liq_4_esi.d	**Sample Name**	liq_4
Sample Type	Sample	**Position**	P1-D4
Instrument Name	Instrument 1	**User Name**	
Acq Method	MMI_esi_col.m	**IRM Calibration Status**	Some Ions Missed
DA Method	msautoproc2.m	**Comment**	456199

Fragmentor Voltage 70 **Collision Energy** 0 **Ionization Mode** Esi

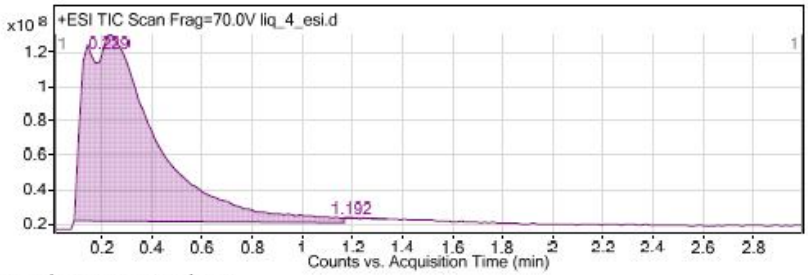

User Chromatogram Peak List

Peak #	RT	Height	Height %	Area	Area %	Area Sum %	Base Peak m/z	Symmetry	Width
1	0.229	107801231	100	2149755709	100	100.07	311.1352	0.58	0.279
2	1.192	-131718	-0.12	-1527653	-0.07	-0.07	311.1338	0.59	

Compound Table

Compound Label	RT	Mass	Abund	Formula	Tgt Mass	Diff (ppm)
Cpd 1: C20 H14 N4	1.094	310.1232	2428453	C20 H14 N4	310.1218	4.41

Compound Label	RT	Algorithm	Mass
Cpd 1: C20 H14 N4	1.094	Find By Formula	310.1232

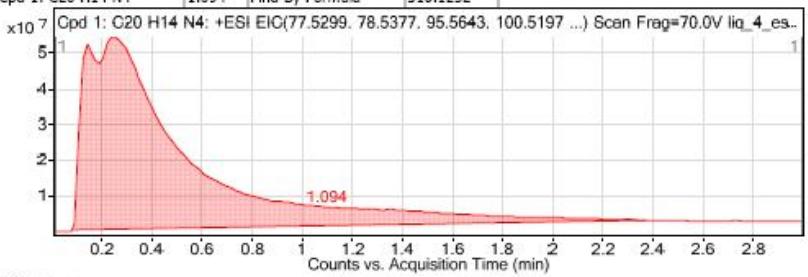

MS Spectrum

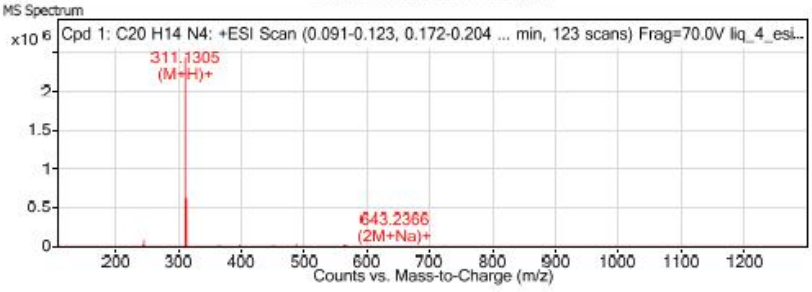

MS Zoomed Spectrum

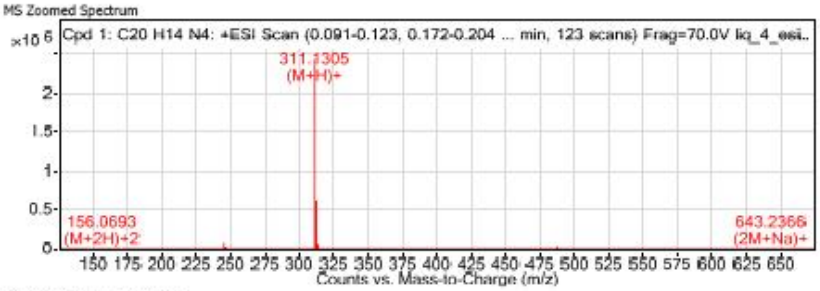

MS Spectrum Peak List

m/z	*Calc m/z*	Diff(ppm)	z	Abund	Formula	Ion
156.0693	156.0682	7.17	2	1191	C20 H16 N4	(M+2H)+2
311.1305	311.1291	4.39		2525750	C20 H15 N4	(M+H)+
311.2918				132679		
311.3638				40174		
312.1336	312.1321	4.83		629284	C20 H15 N4	(M+H)+
312.295				30223		
313.1367	313.1351	5.39		69608	C20 H15 N4	(M+H)+
333.1123	333.1111	3.69	1	3747	C20 H14 N4 Na	(M+Na)+
621.2501	621.251	-1.39	1	821	C40 H29 N8	(2M+H)+
643.2366	643.2329	5.74	1	1677	C40 H28 N8 Na	(2M+Na)+

--- End Of Report ---

Appendix C: A Powder X-ray Diffraction Data for compound **4.4**.

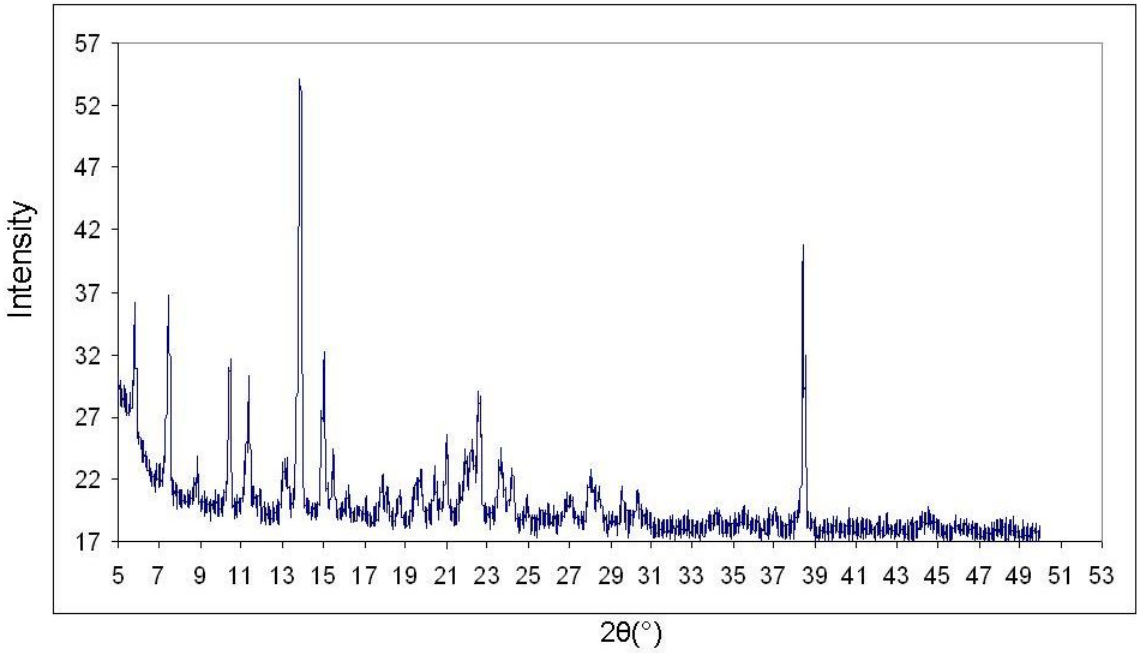

1. Powder X-ray diffraction data of dehydrated crystalline materials of **4.4**.

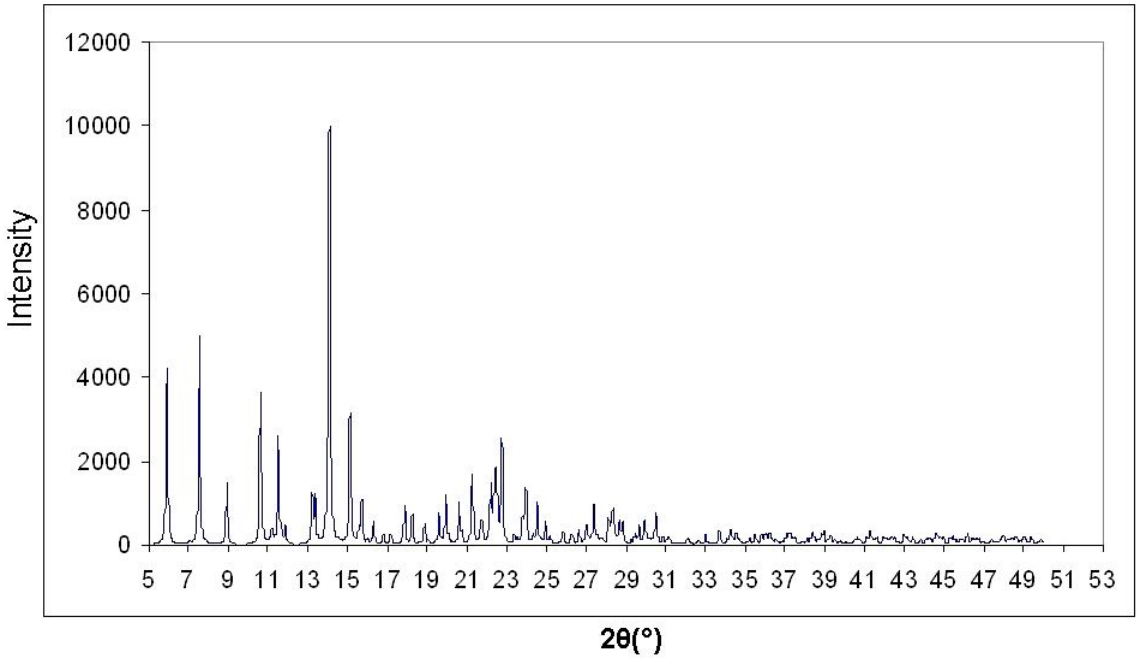

2. Calculated powder X-ray diffraction pattern from single XRD data of compound **4.4**.

Appendix D: TGA experiments of solvent exchanged compound **4.4**.

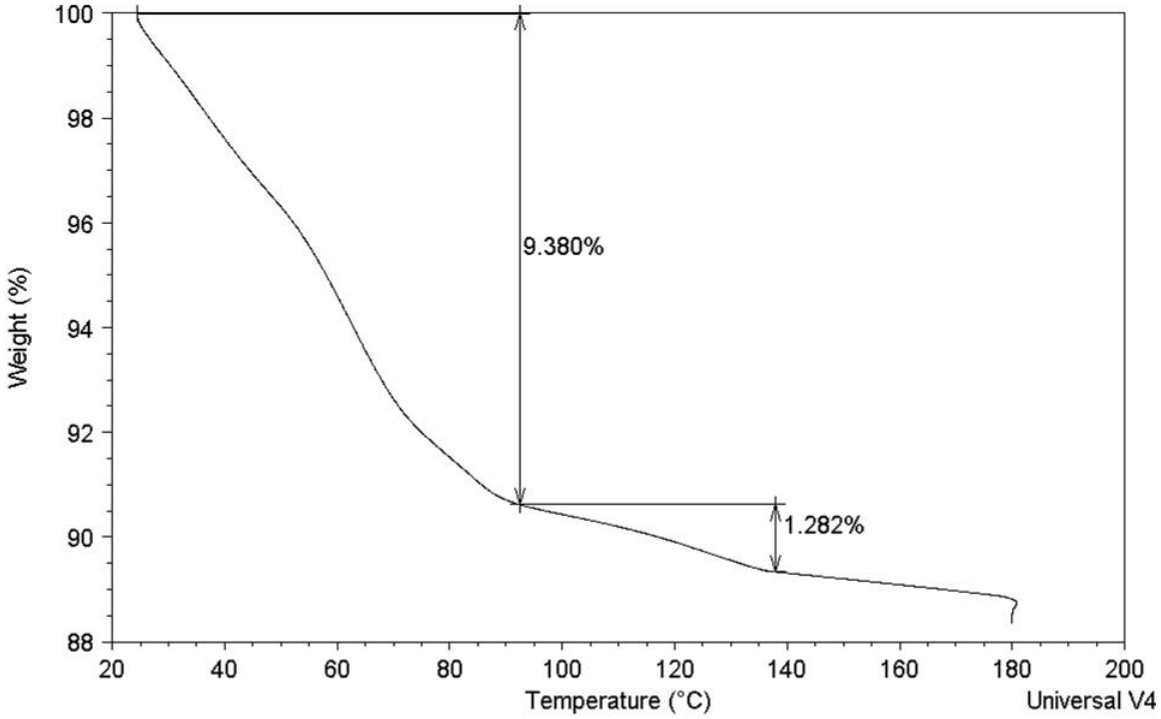

1. Dehydrated powder materials of compound 4.4 are soaked in benzene and evaporated to dryness.

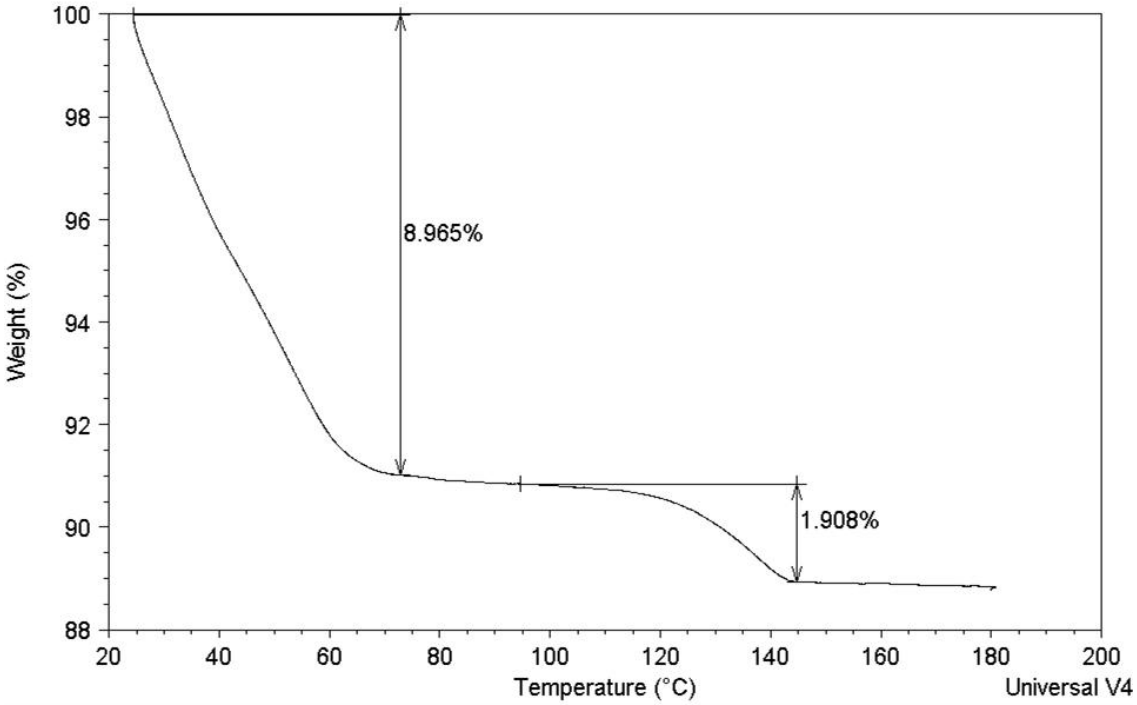

2. Dehydrated powder materials of compound 4.4 are soaked in 2-propanol and evaporated to dryness.

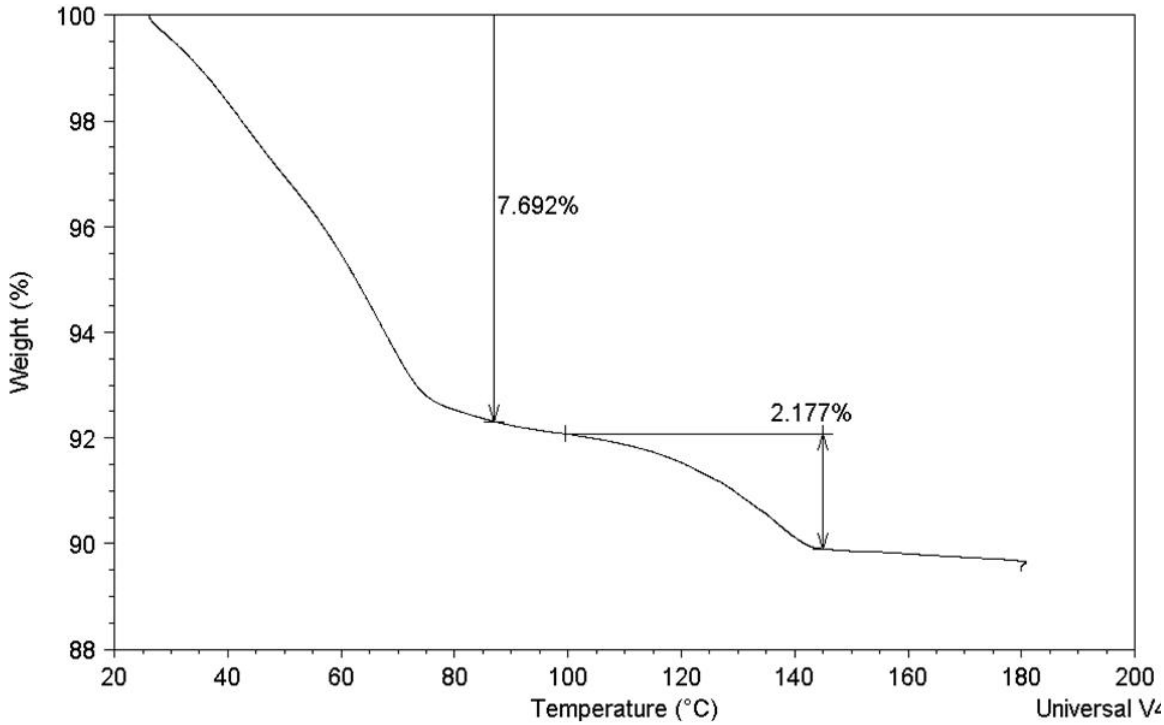

3. Dehydrated powder materials of compound 4.4 are soaked in ethanol and evaporated to dryness.

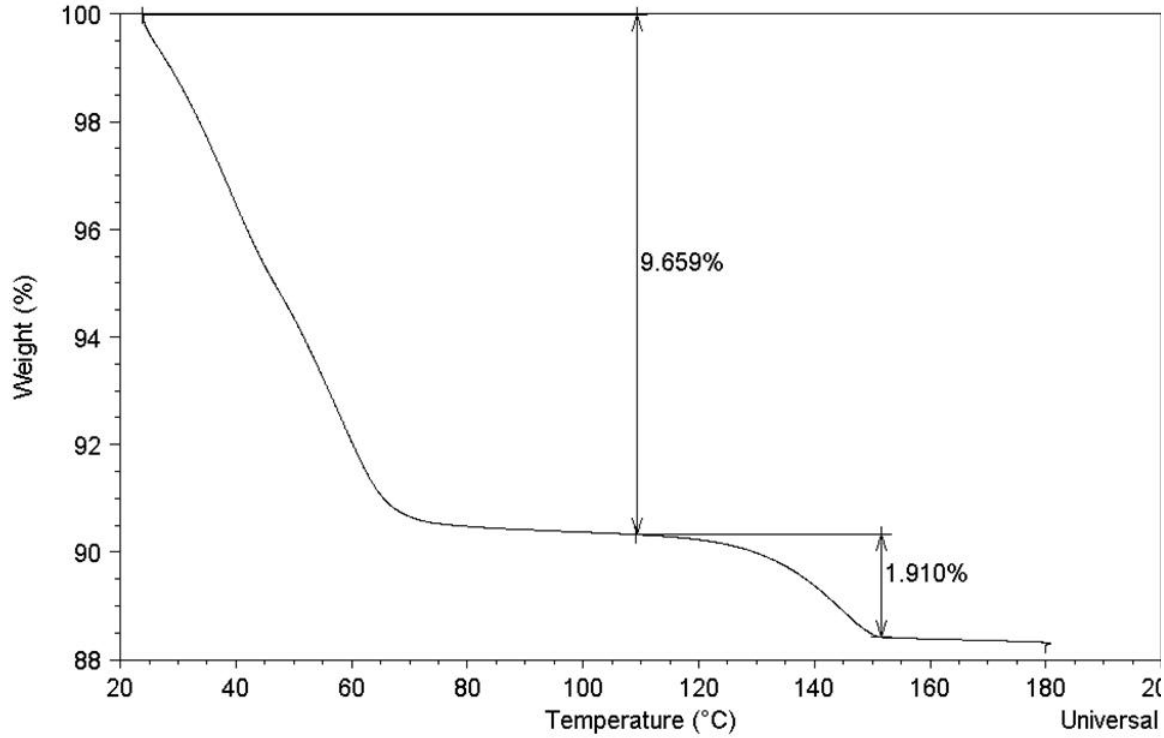

4. Dehydrated powder materials of compound 4.4 are soaked in methanol and evaporated to dryness.

Appendix E: Copyright

Manuscript 1 (Chapter 2)

Obtain Permission

2010/08/18

Jones, Jennifer (ELS-OXF)

宛先: hmotegi@vt.edu

差出人が差出人セーフ リストに追加されました。この差出人からのメッセージは常に表示されます。

Dear Hirofumi Motegi

Thank you for your online request.

As author of the requested article, you do not need to seek Elsevier's permission to include it in your thesis (including it being placed on your university website) as it is part of the rights you retain as an Elsevier journal author.
For further information on the rights you retain as an Elsevier journal author, please visit our web page athttp://www.elsevier.com/wps/find/authorsview.authors/copyright.

Yours sincerely
Jennifer Jones
Rights Assistant
Global Rights Department

Elsevier Ltd
PO Box 800
Oxford OX5 1GB
UK